UNIVERSITÉ DE MONTRÉAL

DESIGN, FABRICATION AND CHARACTERIZATION OF DWDM BY SOL-GEL

SHAHRAM ALAVIAN
DÉPARTEMENT DE GÉNIE ÉLECTRIQUE
ET DE GÉNIE INFORMATIQUE
ÉCOLE POLYTECHNIQUE DE MONTRÉAL

THÈSE PRÉSENTÉE EN VUE DE L'OBTENTION DU DIPLÔME DE
PHILOSOPHIAE DOCTOR (PhD.)
(GÉNIE ÉLECTRIQUE)
DECEMBER 2001

© Shahram Alavian, 2001.

National Library of Canada
Bibliothèque nationale du Canada

Acquisitions and Bibliographic Services
Acquisitions et services bibliographiques

395 Wellington Street
Ottawa ON K1A 0N4
Canada

395, rue Wellington
Ottawa ON K1A 0N4
Canada

Your file Votre référence

Our file Notre référence

The author has granted a non-exclusive licence allowing the National Library of Canada to reproduce, loan, distribute or sell copies of this thesis in microform, paper or electronic formats.

L'auteur a accordé une licence non exclusive permettant à la Bibliothèque nationale du Canada de reproduire, prêter, distribuer ou vendre des copies de cette thèse sous la forme de microfiche/film, de reproduction sur papier ou sur format électronique.

The author retains ownership of the copyright in this thesis. Neither the thesis nor substantial extracts from it may be printed or otherwise reproduced without the author's permission.

L'auteur conserve la propriété du droit d'auteur qui protège cette thèse. Ni la thèse ni des extraits substantiels de celle-ci ne doivent être imprimés ou autrement reproduits sans son autorisation.

0-612-65534-2

Canada

UNIVERSITÉ DE MONTRÉAL

ÉCOLE POLYTECHNIQUE DE MONTRÉAL

Cette thèse intitulée:

DESIGN, FABRICATION AND CHARACTERIZATION OF DWDM BY SOL-GEL

Présentée par: ALAVIAN Shahram

en vue de l'obtention du diplôme de: Philosophiae Doctor
a été dûment acceptée par le jury d'examen constitué de:

Mr. K. Wu, PhD., président
Mr. S. Iraj Najafi, PhD., membre et director de recherche
Mr. Fadhel Ghannouchi, PhD., membre et co-director de recherche
Mr. Jean-Jacque Laurin, PhD., membre
Mr. Godehard Hilfer, PhD., membre

To my mother

Acknowledgments

I would like to express my deepest thanks towards Dr. S. I. Najafi, my director, and Dr. Fadhel Ghannouchi, my co-director. Their guidance and encouragement were indispensable in the completion of this thesis.

Special thanks to Dr. Lei Wang for his tremendous help during transcription of this thesis. Thanks are due to Dr. Guo Yin for fabrication and Mr. Peyman Meshkinfam, my best buddy, for tests and measurements.

To all my academic teachers and professors, starting from my aunt who taught me the first grade, twice, to those who spent sleepless nights to transcribe their lectures from Chinese to English just to be able to teach me: my everlasting, immeasurable and unforgetable gratitude.

Finally and most importantly, I would like to thank my parents and my brother for their love, patience and support, *just keep'em a'coming!*

Resumé

Des simulations permettent de produire la réponse spectrale. Celle ci est fonction des paramtres suivants: indices de réfraction du matériau, dimensions du guide d'onde, distance spectrale , nombre de canaux et la fréquence du canal central.

Le matériau est préparé en utilisant la technique du sol-gel. Le processus implique deux matériaux avec deux indices de réfraction différents. Des gaufres de silicium seront utilisées comme substrat pour leur compatibilité avec la technologie des semi-conducteurs et l'optique intégrée.

La méthode du réseau de phase (PAG) est choisie pour la conception de la puce photonique. La méthode de l'indice effectif est utilisée pour analyser le dispositif optique et ainsi réduire le probléme de trois deux dimensions. La réponse spectrale du dispositif est simulée en utilisant la transformée de Fourier plutot q'un algorithme de propagation, car cette méthode est plus rapide. Les dimensions des guides d'onde canal sont choisis pour permettre un bon confinement optique de la lumiére et une réduction des pertes dues au couplage avec les fibres d'entrée et de sortie ainsi que dans les régions courbées du circuit. Le couplage entre deux sorties adjacentes est calculé en utilisant la méthode de la propagation d'onde (WPM). Les différentes étapes de la conception sont les suivantes :

- Calcul des modes optiques et leurs indices effectifs.

- Calcul de la différence du chemin optique entre les canaux dans la région du réseau afin de déterminer la différence de phase nécessaire et la longueur du guide planaire.

- Utilisation de la transformée de Fourier pour focaliser différentes longueurs d'onde dans différents canaux et analyse de leurs interférences.

La distance spectrale du dispositif est de 2.25 nm. Les pertes d'isolation de deux canaux adjacents ("cross talk"), sont inférieures -25 dB. Les pertes d'insertion dues

la conception sont inférieures -3dB. La différence en termes de pertes entre le canal central et un canal situé une extrémité, appelée uniformité du réseau de phase, est inférieures -3dB. La réponse spectrale du dispositif devrait etre indépendante au changement de la température.

Abstract

Sol-gel method of hybrid glass fabrication is investigated. A systematic method is presented and applied towards fabricating an arrayed waveguide grating (AWG). The method includes the production of a photo-mask for obtaining the resolution of waveguide fabrication and a novel method of calculation in prism coupling method.

After a detailed review of the theory behind the design of AWGs, the parameters obtained from the sol-gel method are used towards a design of an AWG. Using the limits and variations in the sol-gel method a perturbation analysis is done to predict the output response of the device under these variations.

Before designing the layout of the photo-mask, losses due to the mode coupling between two adjacent channels, fiber to channel, bending, cross talk and star-couplers are analyzed to obtain the best geometry possible in order to produce the optimum response.

It is found that the thickness variation affects greatly the crosstalk parameter. In cases where the thickness varies gradually over the grating region, the effect is to broaden the bandwidth. However, in cases where thickness varies stochastically, the effect is to raise the background noise level.

Variations of the channel dimensions , when they occur globally, cause a shift in the output response. This shift depends on the difference in dimensions of the designed and fabricated channel.

Any change in the sol-gel method causes a change in the refractive index of the material. If such a change is the same for both guiding and the cladding material, the effect is also a shift depending on the difference between the expected refractive indices expected and the actual refractive indices of both materials.

The refractive index of the sol-gel hybrid materials depends greatly on temperature. This characteristic may be exploited to tune the device to the exact central

wavelength, by changing the temperature and hence fixing the refractive indices.

The dependence of the output response to all the variations are presented.

The photo-mask of an AWG layout is designed. Using the sol-gel method, the actual device is fabricated and then tested.

The measured results of the fabricated AWG are within the expected and predicted range. Good insertion loss and channel isolations have been achieved.

Moreover, a novel propagation method is presented and applied to extract propagation constants and the output profiles of integrated photonics devices without neither solving the wave equation nor using the paraxial approximation. By approximating the variation of the field to 4th order, this method is applied to the case of a sol-gel multimode planar waveguide. Propagation constants and output profiles are extracted and are in good agreement with the values obtained from the analytical method. The case of a full π circular rotation of a single mode planar waveguide is also illustrated.

Furthermore, a novel, low temperature, sol-gel method of fabrication for inorganic transparent films is proposed. Using this method, single-layer, crack free and transparent silica based films were fabricated. Fabrication of a silica sol-gel film with no doping produced single layer films with an average roughness of about 0.5 nm, for a surface area of 10 μm^2 was obtained. Titanium doped films for the purpose of the refractive index increase is also considered. The refractive index and the loss measurements for silica-titania films was 1.510 ± 0.001. The infrared absorption spectra for both silica and silica-titania films are presented. The results suggest that the densification between 100^oC and 150^oC produces little change in quality of the material.

Condensé en français

Les multiplexeurs en longueur d'onde dense (les DWDM) sont des dispositifs optiques qui transmettent les fréquences provenant de sources séparées et les combinent en une seule fibre optique ou bien qui divisent un signal optique en plusieurs signaux différents. Les bandes passantes d'exploitation des DWDM sont majoritairement composées de longueurs d'onde semi-continues à l'intérieur d'une zone de bande passante donnée.

Le multiplexage dense par longueur d'onde est une technologie qui a fait une entrée tout récemment dans l'industrie de la photonique. Le premier dispositif DWDM a été produit en 1991. À ce moment, un guide d'onde matriciel a été utilisé pour produire un dispositif à 32 canaux tridimensionnel avec espacement de 1 nm.

Toutefois, ces dispositifs sont difficiles à produire puisque l'assemblage des composants exige une grande précision et parce qu'ils sont sensibles aux instabilités mécaniques et de température.

Les DWDM à matrice à réseau phasé (Phased array grating based DWDM ou 'PHASAR') ont été proposés pour la première fois en 1988. Le premier dispositif a été utilisé pour multiplexer et démultiplexer les états polarisés d'une longueur d'onde et, plus tard au courant de la même année, le premier multiplexeur/démultiplexeur de longueur d'onde a été conçu.

Un grand nombre de développements ont été faits en ce qui a trait à la longue fenêtre de longueur d'onde et à un plus grand nombre de canaux.

Dans le domaine de la réactivité à la polarization, des guides d'onde non-birefringents ont été développés. Une approche au développement de dispositifs non-réactifs à la polarization a été le «order matching». Différentes méthodes de compensation par polarization ont été employées. Un dispositif, indépendant de la polarization, a été fabriqué en utilisant le plateau 'halfwave'.

Afin d'obtenir une réponse «plate», des canaux multimodes ont été façonnés aux zones extrantes du dispositif. Une réponse 'plate' a aussi été provoquée par la division de la matrice en deux sous-matrices. En utilisant une conicité parabolique à l'intrant un effet 'plat' a été créé sans l'usage d'une sous-matrice.

Un colloïde est un système de petites particules suspendues dans un médium qui se conforme au mouvement Brownien. Un «sol» est une suspension colloïdale de particules solides dans un liquide qui peut être densifiée en utilisant le procédé sol-gel. En optique, la méthode sol-gel est une solution à basse température pour la préparation de verre basée sur la polymérisation d'alkoxydes métalliques hydrolysés. Les alkoxydes métalliques sont des molécules où un atome métallique est lié à un carbone via un atome d'oxygène. Un exemple d'un précurseur d'alkoxyde métallique utilisé dans les applications optiques est le méthacryloxypropyltriméthoxysilane (MAPTMS).

Les alkoxydes métalliques réagissent dans l'eau. La réaction laisse l'atome métallique attaché à un ion hydroxyle (OH^-). Pour cette raison, cette réaction est nommée hydrolyse.

Le procédé de densification comporte deux volets : l'hydrolyse et la condensation. La condensation est le procédé qui relie les particules «sol» via des liens hydroxyles afin de former un réseau. Ce processus de polymérisation continue à créer un réseau jusqu'à ce que tout le système devienne un seul réseau. En optique, une fois que ce réseau est sec, un médium transparent en résulte, dans la plupart des cas, du verre. La polymérisation est un procédé par lequel des molécules plus grandes sont fabriquées à partir de molécules plus petites qui peuvent former au moins deux liens.

Depuis quelques années, le procédé sol-gel a été un sujet d'intérêt considérable puisqu'il contrôle les propriétés intrinsèques du matériau, le coût de fabrication, l'aisance de l'application et une bonne stabilité chimique et physique du produit final.

Parmi les méthodes conventionnelles de déposition de matériaux optiques – métallisation par pulvérisation cathodique sous vide, dépôt en phase vapeur, hydrolyse à la flamme – la

technologie sol-gel est une des méthodes à privilégier pour la fabrication de couches transparentes minces ayant d'excellentes qualités optiques. Un de ses avantages dans les dispositifs optiques intégrés, tel que mentionné plus haut, est sa puissance de manipulation par rapport aux propriétés optiques des matériaux pour dispositifs actifs et passifs. Un tel changement inné dans le matériau est généralement obtenu en utilisant les précurseurs appropriés ou des dopants, la densification au laser et l'induction par photosynthèse.

Le fait d'incorporer des précurseurs organiques et inorganiques dans les matériaux hybrides sol-gel a fait progresser l'optique intégrée. Des rapports récents sur les dispositifs intégrés optiques conçus par induction par photosynthèse et densification au laser ont été publiés, mais, tel que mentionné plus haut, ces matériaux ont aussi un fort taux de perte par absorption dans la région 1550 nm et, de plus, la fluorescence à cette longueur d'onde n'a toujours pas été accomplie.

Afin d'avoir un effet de guidage dans un dispositif optique, la structure doit être fabriquée en utilisant des indices de réfraction différents. Dans le procédé de fabrication du sol-gel, un tel changement d'index de réfraction signifie une différente concentration de dopant dans le matériau-hôte. Les dérivés des groupes métalliques de transition comme le titane et le zirconium sont ordinairement utilisés pour augmenter l'indice de réfraction. De ce fait, deux solutions sont employées pour fabriquer une structure optique : une solution pour la couche de guidage et une autre pour les couches tampon et de gainage.

Le précurseur pour le sol-gel utilisé dans cette dissertation est le méthacryloxypropyltriméthoxysilane (MAPTMS). Les deux principaux constituants de cette molécule sont le triméthoxysilane [$Si(CH_3O)_3$] et le méthacrylate [$C_4H_5O_2$]. Le triméthoxysilane rend possible la gélification (sol-gelability) du MAPTMS. Ce sont les liens méthoxy qui sont hydrolysés et liés à leur tour à d'autres molécules via la condensation et la polymérisation inorganique. La condensation est le plus affectée par la température et sa propre condensation tandis que celle-ci réduit la distance entre deux monomères, ce qui augmente la probabilité de liens entre deux monomères. L'atome de silicium, qui agit comme un métal dans le gabarit des alkoxydes métalliques du précurseur du sol-gel, assure la compatibilité de l'indice de réfraction avec l'oxyde de silicium.

Le lien double dans le méthacrylate est responsable de la sensibilité UV du MAPTMS. C'est ce double lien qui fait qu'un MAPTMS se lie à un autre. Puisque la chaleur risque de ne pas être localisée de la même façon que par l'exposition à l'UV, on note que la polymérisation inorganique se manifeste globalement à travers la couche tandis que la polymérisation organique semi-localisée du matériau est exploitée pour imprimer l'image d'un dispositif optique. Le terme 'semi-localisé' est utilisé dans le sens suivant : une fois que le photon est présent aux environs du double lien entre les deux atomes de carbone, la polymérisation est entamée et se propage à partir du point initial. Par contre, l'effet est amorti et se dissipe. Ce qui veut dire que, dépendant du dosage UV, la polymérisation peut être plus grande ou plus petite selon la surface affectée.

Le procédé de fabrication de la structure optique débute avec la déposition d'une couche tampon. Une méthode traditionnelle de déposition est celle du revêtement par centrifugation (spin-coating). Cette méthode est ordinairement utilisée pour déposer des couches minces de résine photosensible et de polymère dans les industries des semi-conducteurs et de l'optique. Dans cette méthode, une fois le substrat recouvert par la solution, le mandrin de serrage sous le centre du substrat tourne à une vélocité angulaire prédéterminée et pour une période de temps prédéterminée.

Une fois la rotation terminée, une couche visqueuse recouvre le substrat. Cette couche est maintenant traitée à la chaleur et inondée d'UV pour densification et stabilisation. L'exposition à la chaleur et à l'UV comporte trois étapes: la pré-cuisson, l'inondation à l'UV et l'après-cuisson. Après le revêtement par centrifugation, la couche est encore visqueuse et susceptible aux déformations en surface et à la contamination par des particules en suspension dans l'air. Pour éviter ces complications, la couche est placée dans un four à température moyenne afin que la surface durcisse. La couche n'est pas menée à sa solidification finale, par contre, puisque ceci minimiserait les chances de mouvement et de rotation requis pour que les liens organiques se tracent. Une fois la pré-cuisson terminée, la couche est 'localisée' sous une source UV dont la longueur d'onde et l'intensité sont connues. La surface subit une exposition à l'UV dosée afin qu'un réseau organique soit créé et pour finaliser la polymérisation organique. Après l'inondation à

l'UV, la couche est mise au four pour une différente sorte de traitement à la chaleur. Cette fois, l'objectif est de solidifier la couche et de compléter la polymérisation inorganique. Le produit final est du verre ayant l'indice de réfraction du tampon désiré.

Après avoir terminé ce processus pour la couche tampon, le substrat est recouvert de la solution de guidage en utilisant la même méthode de déposition. Puisque la vitesse et le temps de déposition du revêtement par centrifugation pour cette solution pourrait résulter en une épaisseur et une viscosité différente, le revêtement par centrifugation, dans ce cas, pourrait exiger des valeurs différentes quant à la vélocité angulaire et à la vitesse de rotation. Après le revêtement par centrifugation, le substrat est mis au four pour une pré-cuisson. Une fois la pré-cuisson terminée, la couche de guidage est prête pour l'étape principale de la fabrication du dispositif. Un masque photographique est apposé sur la couche. Ce masque est un 'négatif' puisque la surface du masque, là où les guides d'ondes sont, est gravée. Ces gravures permettent à l'UV de passer et entame la polymérisation dans cette région de la couche. Une fois le masque apposé sur la couche, la couche est exposée à l'UV. Encore une fois, le dosage de l'UV est prédéterminé. La région non-polymérisée peut être dissoute à l'alcool tandis que les régions polymérisées ne peuvent pas être dissoutes. Pour cette raison, un alcool spécial est employé dans le développement, sinon, la région non-exposée serait dissoute. Après le développement, le substrat est localisé sous une source UV pour saturation UV et pour une après-cuisson qui solidifiera sa structure. Après l'application de la couche de guidage, une solution tampon, maintenant appellée 'gainage' est appliquée par revêtement par centrifugation et est saturée à l'UV et à la chaleur pour compléter la structure finale.

Comme tout autre procédé, la méthode de fabrication du sol-gel à ses limitations. D'un côté, on peut améliorer le procédé pour réduire ses limitations et, d'un autre côté, on peut utiliser la flexibilité du design pour corriger certaines erreurs, variations ou autre limitation de la méthode de fabrication. La seule façon de faire ceci est d'établir les paramètres au préalable.

Un des obstacles principaux pour la microfabrication est la limitation qu'impose la photolithographie. Cette limitation se manifeste dans la résolution de l'impression et dans

le développement des canaux. Par exemple, la région polymérisée peut être plus grande que la région exposée. Dans le cas où un dosage UV minimum est requis pour une partie du dispositif, il pourrait être excessif pour une autre section. Ceci devient un problème lorsque, par exemple, un canal large de 6 microns wide et un de 20 microns reçoivent la même exposition UV pour le même montant de temps. La différence de largeur implique une différence de surface, c'est-à-dire un dosage UV différent. Le résultat est que les deux canaux à 20 microns doivent être placés à une distance minimum. Toute distance inférieure fait que les canaux se rejoignent et forment une dalle plus large que 40 microns.

Un autre point à considérer est le développement. Dans le procédé sol-gel, le développement est fait par immersion de la puce dans l'alcool. Quelque soit la vitesse du passage de l'alcool sur la surface, il y a toujours une distance minimum entre deux canaux non-exposés où l'alcool ne peut pas pénétrer pour dissoudre la région non-exposée.

Pour cette raison, afin d'établir les paramètres de l'effet, on doit connaître la distance minimum entre deux canaux, ce qui produit deux guides d'onde bien définis quant à leur largeur et leur hauteur. Pour ce faire, un masque a été conçu avec des colonnes de canaux longs de 500 microns avec des largeurs de 2 à 30 microns. Pour chaque largeur, il y a des colonnes de séparations différentes entre deux canaux de 1 à 10 microns. Une fois que le masque est imprimé sur le film et développé, les distances minimums pour les différentes largeurs de canaux sont obtenues. Pour les fins de cette dissertation, les deux seules largeurs de canaux qui ont été utilisées dans le dispositif optique sont de 21 et 6 microns. Après avoir employé le masque et avoir fabriqué les canaux, la distance minimum pour obtenir deux canaux isolés était de 3 microns pour les canaux de 6 and 21 microns.

On peut établir les paramètres d'une couche optique par son épaisseur et son indice de réfraction. La couche optique la plus simple serait une couche avec un indice de réfraction homogène et isotropique. Les deux paramètres peuvent être obtenus par la méthode du couplage de prisme. L'idée derrière la méthode de couplage de prisme est qu'un guide d'onde multimode à des états d'excitations indépendents de ses modes. Ces états ont deux paramètres en commun: l'épaisseur et l'index de réfraction de la couche. Pour cette raison, un minimum de deux états d'excitation est suffisant pour obtenir ces deux

paramètres. Ces excitations peuvent être provoquées en 'couplant' de la lumière dans une couche multimode film via un prisme.

Une fois que l'indice de réfraction et l'épaisseur de la couche sont mesurés, il est important de savoir la tolérance de ces mesures sur la tranche entière. Ceci est important parce que l'épaisseur et l'indice de réfraction affectent l'indice effectif du mode guidé. Dans les dispositifs optiques, où la différence de phase joue un role important, des indices effectifs non-constants causent une différence aléatoire de phase qui interrompt la réponse.

Afin d'obtenir la variation de l'épaisseur et de l'indice de réfraction de la couche sur la tranche, des mesures sont faites tel qu'illustré dans la figure (3.5) le nombre de boîtes indique l'épaisseur en microns. Puisque le matériel réparti sur la tranche est le même, on peut s'attendre à une plus grande sensibilité dans l'épaisseur que dans l'indice de réfraction. La variation de % 0.027 pour l'indice de réfraction est assez petit pour croire que la variation de % 7.34 est fiable.

Un dispositif DWDM est été conçu, fabriqué et mis à l'essai. Les charactérisques attendues et mesurées du dispositifs sont indiquées dans les tableaux 7.1 et 7.2, respectivement.

L'affaiblissement excessif du dispositif après le calcul de l'affaiblissement estimé du couplage et de la conception (3 dB) est d'environ 8 dB. Cet affaiblissement excessif est du en partie à la perte par propagation de la structure. L'affaiblissement de couplage entre fibre et canal est calculé à 0.75 dB, ce qui est consideré élévé. Cette perte est due principalement au couplage de modes mal assortis entre fibres et canaux. La raison principale de cet affaiblissement est du au plus faible dégré de liberté. Initialement, il y a deux conditions pour le guide d'onde à canaux et un paramètre ouvert qui est la largeur du canal w. La première condition est que le guide d'onde ne doit pas être capable de guider plus de deux modes. La deuxième condition est que l'affaiblissement par modes mal assortis entre fibres et canaux soit au minimum. Une fois que w est déterminé pour satisfaire la première condition, la deuxième condition ne sera pas optimisée, comme on peut le voir. La solution à ce problème est d'exploiter un des avantages de la technologie

sol-gel qui est sa flexibilité par rapport au changement de l'indice de réfraction du matériau. Un tel avantage produit un dégré de liberté qui peut être utilisé pour trouver le guide d'onde à canaux qui non seulement supporte pas plus que deux modes mais qui a un affaiblissement de couplage minimum avec la fibre.

Tel qu'expliqué dans le chapitre précédent, les indices de réfraction des matériaux de gainage et de guidage ont été estimés en mesurant les indices de réfraction à 1.55 et à 0.632 microns. La différence constante entre les indices de réfraction actuels et ceux mesurés est la cause du décalage dans la réponse. Le décalage de 6.57 nanomètres correspond à une différence de 0.008 entre les indices de réfraction estimés et actuels.

Les longueurs d'onde, tant à 1 qu'à 3 dB, sont de meilleure qualité qu'anticipé puisque le procédé de déposition était de meilleur qualité. La diaphonie est aussi à peu près 4 dB de plus qu'anticipé à cause de la qualité de la fabrication des canaux, particulièrement dans la région de la matrice.

Toutes les spécifications du dispositif sont acceptables sauf le décalage du dispositif qui est considéré plus que petit. Même s'il a été expliqué que le décalage peut être compensé avec le contrôle de la température, afin de mettre au point le canal central de ce dispositif à 1300.00 nanomètres, il est mieux de garder le dispositif à 85.7 °C! Par contre, le problème sera résolu pour les prochains dispositifs puisque les indices de réfraction actuels sont maintenant connus.

Un aspect du DWDM qui n'a jamais été utilisé comme une condition est la largeur de bande des canaux. Cette caractéristique est essentielle dans les dispositifs commerciaux. Une variation de puissance prédéterminée à même la portée d'une largeur de bande est importante puisque ceci permet de manœuvrer la portée de la bande si la source ou le dispositif se décale pour quelque raison que ce soit.

La figure \ref figure:conclusion:compareloss (conclusion : Comparaison de l'affaiblissement) est l'intersection de deux graphique pour fins de comparaison visuelle. L'intersection a été faite en bougeant la réponse théorique en longueur d'onde de 6.57 nm et en baissant la puissance à 9.3 dB. Il est possible de voir que l'espacement entre canaux et les largeurs de bande à 1 et à 3 dB sont à l'intérieur de la portée anticipée. En ce qui a trait aux travaux futurs sur ce produit, le prochain masque photographique devrait être conçu avec l'objectif de décaler les longueurs d'ondes vers les longueurs d'ondes appropriées pour chaque canal. Alors, il est important de mesurer le présent dispositif à une température mesurée. Ceci est le cas parce que le prochain dispositif doit aussi être mesuré à cette température.

Contents

Dedications iv
Acknowledgments v
Resumé vi
Abstract viii
Condensé en francias x
List of Tables xxii
List of Figures xxiii
List of Abbreviations xxxi
List of Appendices xxxii

1 Introduction **1**

2 Solgel Method of Glass Fabrication for Integrated Optics **5**

2.1 Sol-gel 5
2.2 Hybrid sol-gel method of device fabrication 11

3 Extracting fabrication parameters **16**

3.1 Material parameters and fabrication resolution 17
3.2 Refractive indices and film thicknesses 18
3.3 Fabrication variations 23

4 Theory **25**

4.1 Design Procedure 30

4.1.1 *AWG* Parameters 31

Material parameters 31

Device specification parameters 31

Design parameters 31

Step One: Analysis of the channel and the channel dimension, w 32

Step Two: Grating order, m 33

Step three: Slab length, R 34

Step four: Length increment ΔL 35

4.1.2 Simulation 35

4.1.3 Physical layout of the device 38

5 Designing a DWDM **44**

5.1 Specifications 44

5.2 Parameters 44

5.2.1 Material parameters 44

5.2.2 Channel dimension 45

5.2.3 Mode mismatch loss 46

5.2.4 Grating order m 47

5.2.5 Length difference ΔL 48

5.2.6 Length of the slab, R 48

5.2.7 Number of gratings, M 49

5.2.8 Return Loss 49

5.3 Simulation 52

5.4 Design tolerance 55

5.4.1 Shift 55

5.4.2 Film thickness variation 57
5.5 Design:Physical layout 59

6 Test and characterization **63**
6.1 Measurement steps 64
6.2 Results 65

7 Discussion **69**

8 Conclusion **73**

A Inorganic, single-layer and crack free films for integrated optical devices using sol-gel method of fabrication. **76**
A.1 Abstract 76
A.2 Introduction 77
A.3 Silica films 79
A.4 Silica-titania films 80
A.5 Results 81
A.6 Conclusion 86

B Analysis of integrated photonics devices by a new propagation method **87**
B.1 Introduction 87
B.2 Wave propagation method 89
B.3 Analysis of a planar sol-gel multimode waveguide as a simple photonics device 92
B.4 Application of a WPM to a full pi circular rotation of a single mode slab waveguide 94
B.5 Conclusion 99

List of Tables

3.1 Summary of the fabrication and material parameters. 23

5.1 Specification of a DWDM to be designed 44

5.2 Refractive indices of the guiding and cladding/buffer material. . . . 45

5.3 Effective indices of m=0 for the channel and slab waveguide. The above parameters belong to a channel of $5 \times 5\mu$m with inside refractive index of 1.520 and the outside refractive index of 1.502, both at 1300 nm. 47

5.4 Theoretical specifications of the designed DWDM. 54

5.5 Predicted specifications of the designed DWDM. 59

6.1 Detailed characteristics of measured DWDM. 66

7.1 Expected specifications of the DWDM 71

7.2 Specifications of the measured DWDM. 71

B.1 comparing the propagation constants averaged over the first 2400 microns and their corresponding incident angles, obtained by WPM method, with the same values obtained by solving the wave equation on the cross-section of the slab. The values are rounded to equal decimals. 94

List of Figures

1-1 Different sections of the an Arrayed Waveguide Grating Dense Wavelength Division Multiplexer 3

2-1 Hydrolysis of the MAPTMS. Solid links are identical. Dotted lines represent the organic link 6

2-2 Condensation stage of the hydrolyzed MAPTMS. Solid links are identical. Dotted lines represent the organic link 6

2-3 The hydrolyzed links form a bond at higher temperature which leads to condensation of the gel to form a glass. The gray vector specifies the new link that connects the two hydrolyzed MAPTMS. 8

2-4 The MAPTMS molecule is composed of three constituents. *Trimethoxysilane* is the inorganic component which will be responsible for the glass properties. *Methacrylate* component is responsible for the UV sensitivity and organic polymerization 9

2-5 One of many possible routes of organic polymerization is a) a UV-sensitive link is broken into two radicals. b) one of the radicals is attached to a molecule resulting a bigger molecule with a un-bonded electron and c) the molecule grows as it is attached to other smaller molecules. 10

2-6 Once the substrate is covered by the solution, the rotating chuck under the center of the substrate rotates with a predetermined angular velocity and for a predetermined length of time. At the end, the substrate is covered by a thin film. 12

2-7 After the spin coating the film has to be prebaked to dry the surface. The surface dryness prohibits the dust particles to contaminate the film and also, for guiding layer, it prohabits the film from sticking to the mask surface. 13

2-8 The process of fabricating the optical devices is composed of three parts: 1-buffer deposition and saturation, 2-guiding deposition, prebake, UV-imprint, development and saturation, and, 3-cladding deposition and saturation. 14

2-9 A microscopic picture of a square ridge fabricated using sol-gel method of glass fabrication. 15

3-1 As the separation between two waveguide distances reduces, the resolution of the development reduces accordingly. 17

3-2 To obtain the minimum distance between two channels required in order to isolate two adjacent channels, a series of waveguides are made with different separation distances. After the development process, the minimum distance that isolates two channels is considered to be the minimum separation between two channels. 18

3-3 Only the discrete values of θ_i can excite the corresponding modes. The parameter θ_i depends on the refractive index of the film and its thickness. Since there is an independent dispersive equation for each mode, at least two modes are required to be excited in order solve the two unknowns: refractive index and the film thickness. 19

3-4 measuring the film refractive index, n_f, In cases where a single measurement is subject to higher error, by eliminating the isolated graph the total result is much more accurate. The difference in error can be seen in the dotted line and solid lie boxes. 22

3-5 In order to obtain the variation of the refractive index and the film thickness due to fabrication variations, a wafer was divided into small sections and each section was measured by prism coupling method. The small deviation in refractive index confirms the standard variation of thickness variation. The value underlined is the average of the neighboring values. 24

4-1 When a tilted coherent light travels through the slits of a distance d apart, far from the slits the interference pattern forms. Different wavelength would have their first maxima at different location. . . . 26

4-2 A three dimensional interference experiment maybe *approximated* to a two dimensional planar device. The image plane and the plane of slits both form a circle whose center is located on the circumference of the other circle. 29

4-3 Starting from the refractive indices of both, the guiding and the buffer materials , one can set the dimension of the channel to obtain the field profile close to that of single mode fiber. 32

4-4 The first step of the effective index method for finding the effective index of the mode of a single mode channel is first to consider the a symmetric slab whose height is equal to the height of the channel. 33

4-5 After calculating the effective modal index of the single mode slab, the perpendicular slab will be analyzed with the slab refractive index equal to that of effective modal index of the previous slab. The effective modal index of this channel is then approximated to be the effective modal index of the channel. 34

4-6 Knowing the response function of the star coupler and the profile of the input field at the input channel-slab junction is sufficient to obtain the total field at the output channel. The overlap integral of this total field and the profile of the output channel provides the output power for that wavelength in dB. 35

4-7 The simulation algorithm is applied to an 8 channel wavelength demultiplexer AWG with .8 nanometer channel spacing resolution, 1550 nanometer fixed at the central output channel. The bold graph corresponds to the central channel. Note that the simulation produces the 1550 nanometer for the central channel wavelength, confirming the design parameters. 39

4-8 Different sections of the an Arrayed Waveguide Grating Dense Wavelength Division Multiplexer 40

4-9 Since the radius of the slab, taper extension and any extra extension after the taper are going to be constant for all the grating channels, l_0 is denoted as a constant value for all the gratings. 41

4-10 Using the condition of fixed ΔL and physical layout, one obtains two equations. These two equations are sufficient to find the two unknown for each grating. 41

4-11 A phtoto-mask design of an 8-channel AWG is produced in AutoCAD format using the algorithm discussed in this section for a straight-arc-straight template. 43

5-1 width=0.9 of given refractive indices, as the dimension of a symmetrical channel increases, the number of guided modes also increase. The y axis represents the number of modes. Note that for 5 microns width, the channel carries two modes and it is well below cut-off for the third mode. This allows lower sensitivity to index variations. . 46

5-2 For 1 5 × 5μm channel waveguide the fiber to channel transition of power has 0.75 dB loss 47

5-3 Total number of gratings effects the insertion loss and the cross talk. Lower number of the gratings causes the light to be collected at the first slab and the field profile to be wider at the output channel than the channels mode profile. This will lead more coupling to the adjacent output channels leading to higher crosstalk. For number of gratings above 45, the insertion loss is about 0.6 dB and a crosstalk less than -60 dB. 50

5-4 Return loss in fiber depends strongly on the refractive index of the channel waveguide. For the refractive index of the 1.513 the return loss is -32.17 dB. 51

5-5 The simulated output response of a 4 channel DWDM. Design parameters in this section were supposed to produce a device with following specifications: Channel spacing of 2.25 nm and the central wavelength of 1300.00 nm. As seen, the central wavelength is exactly 1300.00 and the the grids on the graph are set at 2.25 nm. The insertion loss of the channels from left to right are: 1.54, 1.29, 1.28 (central channel), 1.52 dB. This leads to non-uniformity of 0.24 dB. The crosstalk for the central channel at 0 dB is 65 dB 53

5-6 The theoretical expected bandwidth for the central channel to be expected at 1 dB and at 3 dB are 0.75 nm and 1.3 nm, respectively. 54

5-7 Variation of $1 \times 10^{-4} nm/1^{o}C$ for refractive index means a shift of $0.1\text{nm}/1^{o}C$ in channel output wavelength. This effect can be used to tune the device to fall exactly on the specification grid. To do that, the chip is mounted on a planar heater whose responsibility is not only to heat the device to a desired temperature, but also the maintain the device to such a temperature in case the ambient temperature changes. Maintaining the device at a certain temperature insures the thermal stability of the device. 56

5-8 The gradual thickness variation from first grating to 51th grating in a linear fashion is shown. dn=0 corresponds to no variation. dn=0.00002 corresponds to variation of 5 to 6 microns from the first grating to the last. finally, dn=0.00008 corresponds to variation of 5 to 8 microns 57

5-9 A random thickness variation from one grating to another produces no shift. However, the noise level increases greatly, which results lower crosstalk level. The above results are from the variations of 0.1 microns. 58

5-10 Bending loss of the $6\mu m$ and $5\mu m$ channels are presented against different bending radii. To make sure that the bending loss is the least sensitive the minimum radius of 3 mm is chosen. 60

5-11 Power transfer from one channel to to its adjacent is calculated. The importance of this calculation is due to crosstalk parameter. A 0.05 dB/cm coupling loss will produce a 19.4 dB/cm crosstalk. 61

5-12 Second slab at the output 62

5-13 Second slab at the grating 62

5-14 Full layout of the device 62

6-1 Measurement setup. Using HeNe laser the coupling of the fiber to the device at the input and the output is optimized. By using the switch, the broadband is sent to the DWDM device and by using the OSA the response is measured for all the wavelengths. The tunable laser and the polarization scrambler is used for the polarization loss. 64

6-2 Output response of the DWDM measured. The fourth channel has a higher insertion loss which is due to difference in coupling of the output channel with the output fiber. 66

6-3 The output response of the measured DWDM with an emphasis on the bandwidths. 67

6-4 A view of the output junction. 68

7-1 A relative overlap of the theoretical and measured output response of the DWDM. 72

A-1 By creating an airflow during the solution state a great deal of the solvent is evaporated before gellation. 79

A-2 The IR absorption of both glasses are almost the same except for the 1100 cm^{-1} and 3400cm^{-1} region. 81

A-3 The double-pick is the evidence of the Si-O and Ti-O bonds. 82

A-4 The cyclic silicate structure is untouched after titanium doping of the TEOS. 83

A-5 In the 3400cm^{-1} region titanium doped sol-gel has higher absorption, which is unusual. 84

A-6 a $10 \times 10\mu m$ of surface of the silica-titania film had a variation of the surface equal to 0.53 nm. 85

B-1 Since the field moves along the incrementing z, the chosen input plane wave field is projected on the plane of cross-section (dashed line). 92

B-2 A plane wave entering a 6 microns slab waveguide perpendicular to the incident excites all possible modes. Far from the perturbations at the entry, the total field is analyzed between the 70-100 microns (a). By varying the incident angle the average mode number within the same 70-100 microns region, becomes an integer for first (b), second (c) and the third mode (d). 95

B-3 By varying the angle at the input different modes are excited (a). At $\theta = \theta_m$ the average mode number within the first 70-100 microns becomes a constant integer. The average propagation constant $< \beta_m >$ is measured for the first 2400 microns for first (b), second (c) and the thirs mode by entering a plane wave with the corresponding incident angle. The average $< \beta_m >$ is then found to be 5.988, 5.942 and 5.875 $(\mu m)^{-1}$, respectively. 96

B-4 When more than one mode are propagating, the total intensity along the waveguide is optical path dependent. The different intensity profiles of the slab waveguide at 81 and 85 microns is shown. 97

B-5 along the curviture of the waveguide, the displacement vector **l** makes a non-zero angle with the propagation vector, **k**, of the local field. . 98

B-6 For the same [plane wave] input profile, different output intensity profiles are illustrated for different radii for the case of a full π circular roatation of a single mode slab waveguide of 3 microns. The center of the circle is towards the decreasing r for each case of r_0. 99

List of Abbreviations

AWG = Arrayed Waveguide Grating

BPM = Beam Propagation Method

dB = Decibel

DWDM = Dense Wavelength Division Multiplexer

FPR = Free Propagation Region

FSR = Free Spectral Range

MAPTMS = Trimethoxysilane

OSA = Optical Spectral Analysis

PHASAR = Phased Arrayed Grating

SOL-GEL = Solution to Gelation

UV = Ultraviolet

WPM = Wave Propagation Method

List of Appendices

Appendix A = Inorganic, single layer and crack free film for integrated optical devices using sol-gel method of fabrication.

Appendix B = Analysis of Integrated Photonic Devices by a New Propagation Method.

Chapter 1

Introduction

Experimental discovery of the electromagnetic waves by Heinrich Hertz (1857 to 1894) lead to radio, television, radar and a meaning to the word "telecommunication". Today, telecommunication process is based on the propagation of electromagnetic waves. These waves are modulated from the primary sources, transmitted over the medium and finally de-modulated into the signal of other nature while the integrity of the signal throughout the process is maintained.

With each wave there exists a frequency and a corresponding wavelength that is unique. The absence of direct interaction between two electromagnetic waves allows one to feed many different signals each with a different wavelength into the same transporting medium without loosing information from one wavelength into another.

Regardless of the modulation algorithms, wavelength, or the frequency, is mainly used to separate and identify different signals. This means that the channel capacity of a telecommunication system is essentially the number of transmitted wavelengths over the system.

One of the most important specifications of the transporting medium in telecom-

munications, therefore, is bandwidth. It is the length in wavelength or frequency domain in which the medium is to maintain the entire requirements. The larger the operating bandwidth the larger this region may be divided to different wavelengths or, on the other hand, different channels.

The recent overwhelming development in the worldwide connectivity of computers has increased the need for the amount of information available and the ease of access to it.

The capacity of a telecommunication device has a direct relationship with the absolute operating frequency range. Therefore, it becomes clear why optics, due to higher frequency operating range, compared to microwave for example, has become the center of attention in the world of telecommunications.

The lowest insertion loss of optical fibers, and the recent developments in Erbium doped fiber amplifier (EDFA) devices that can amplify signals up to 75 nm of operating bandwidth has increased the support for 1550 nm wavelength as the standard wavelength for the telecommunications.

Dense wavelength division multiplexor (DWDM), are the optical devices that feed different neighboring wavelengths coming from different routes into one single fiber optic and vise versa. Their operating bandwidths are mostly of semi-continuous wavelengths within a given bandwidth region.

DWDMs have become a technology that has recently entered the industry. The first DWDM devices goes back to 1988 where a grating was used to fabricate a three dimensional device with 32 channel with 1 nm channel spacing [1].
However, these devices are very difficult to fabricate due to the precision required in order to assemble the components and their sensitivity to mechanical and temperature stability.

Phased array grating based (PHASAR) DWDMs were first proposed in 1988 [2]. The first device was used to multiplex and de-multiplex the polarization states for

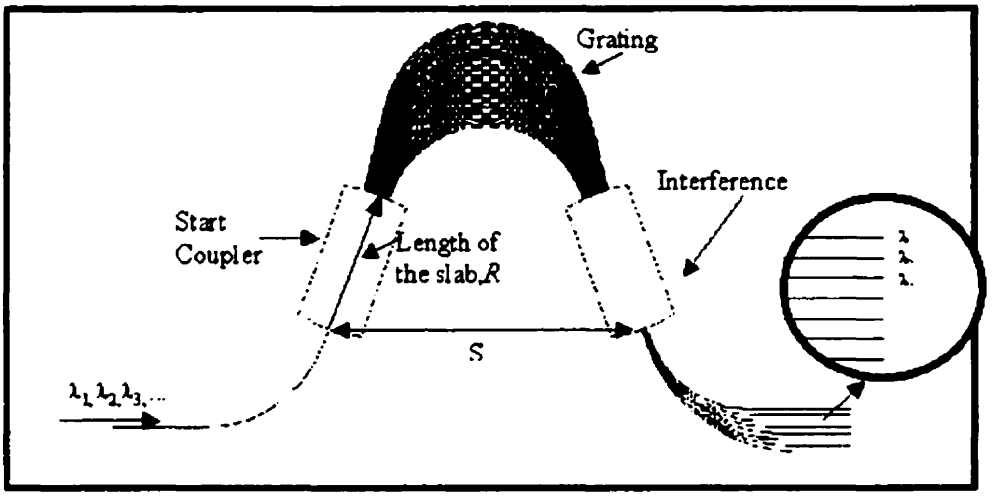

Figure 1-1: Different sections of the an Arrayed Waveguide Grating Dense Wavelength Division Multiplexer

one wavelength [3] following with the first wavelength multiplexer de-multiplexer in the same year [4]

Great number of developments have achieved in terms of the long wavelength window and greater number of channels ([5],[6] and [7]).

In terms of polarization sensitivity, [8] and [9] used non-birefringent waveguides. One approach towards the polarization insensitive device was through order matching [10]. Different polarization compensating methods were employed in [11],[12] and [13]. One method of polarization independent device was applied using the halfwave plate [14], [15].

To obtain the flat response, [16] fabricated multimode channels at the output sections of the device. Breaking the grating into two sub-gratings [17] has also lead to flat response. By using a parabolic taper at the input [18] were able to achieve the same flatness without the usage of sub-grating.

Recent demands in AWG market has increased greatly. The manufacturers of

AWG are trying to produce this device as cheap and as much as possible. Hybrid sol-gel method of glass fabrication is very much adapted for these purposes. It allows fabrication of optical chips in large numbers. Most of other methods of waveguide fabrication use either wet-etching with acid solution or reactive ion etching that has a very small chamber allowing small number of devices. Hybrid sol-gel method, thanks to its photo-printable capability, permits large number of wafers to be exposed under a photo-mask with ease.

The purpose of this thesis is to fabricate an AWG, DWDM, using sol-gel method from sol-gel materials. Chapter 2 describes the concept behind sol-gel method of glass fabrication and its application in integrated optics. In chapter 3 the parameters that are used for design and simulation is extracted. Chapter 4 represents the theory and the concept underlying the AWG. As an example a device given a specific set of properties is designed and its tolerances are simulated. The fabricated device is tested and measured in chapter 5. finally, the results of measured device and its theoretical expectation is compared in chapter 7.

Chapter 2

Solgel Method of Glass Fabrication for Integrated Optics

2.1 Sol-gel

A *colloid* is a suspended particle system in a medium that follows a Brownian motion. A *sol* is a colloidal suspension of a solid particle in a liquid, which can be densified using sol-gel process. In optics, the *sol-gel* method is a low-temperature solution for glass preparation based on polymerization of hydrolyzed metal alkoxides [19], [20]. *Metalalkoxides* are molecules in which the metal atom is linked to a carbon through an oxygen atom. Polymerization is the process of making larger molecules from small units, called *monomers*, that can form at least two bonds [21]. An example of a metal alkoxide precursor commonly used in optics applications is methacryloxypropyltrimethoxysilane (MAPTMS) where the silicon atom is the metal in the metal alkoxide template explained above.

Metal alkoxides readily react with water. The reaction leaves the metal atom attached to a hydroxyl ion (OH^-) . For this reason this reaction is called *hydrolysis*.

A formulation of this hydrolysis for MAPTMS is shown in figure 2-1.

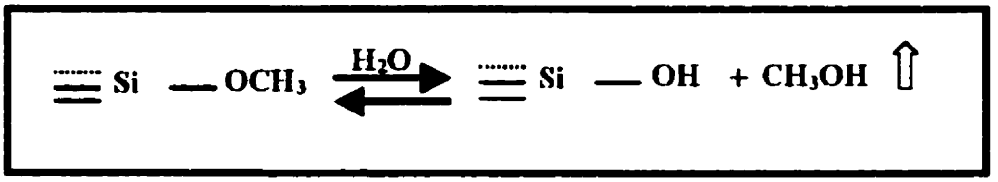

Figure 2-1: Hydrolysis of the MAPTMS. Solid links are identical. Dotted lines represent the organic link

The transformation of MAPTMS solution to a solid glass requires a great deal of densification process. Such densification is composed of two stages: hydrolysis and condensation. *Condensation* is the process of linking the sol particles together by their hydroxyl links to form a network.

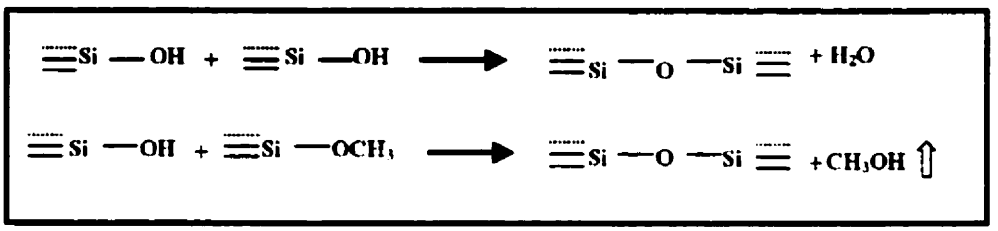

Figure 2-2: Condensation stage of the hydrolyzed MAPTMS. Solid links are identical. Dotted lines represent the organic link

The process of condensation through the inorganic links continues to interconnect the sub networks until the whole system becomes one single network. In sol-gel optics, once this network is dried, the result will be a transparent medium, in most cases it becomes glass. Hydrolysis and condensation process should be controlled extensively. As an example to appreciate the importance of the condensation process, consider the case of a poorly controlled condensation where alcohol remains

trapped inside the network and that this alcohol absorbs greatly the transmitted light. The result would be a power drop across the optical device. On the other hand, consider the case of most inorganic sol-gel films where the water produced during an un-optimized condensation evaporates during the heat treatment and leaves the fragile network hollow.

Precursors with both organic and inorganic links to silicon atom lead to *hybrid* sol-gel glasses. Therefore, as defined, sol-gel glasses are considered inorganic if silicon atom has no direct link to carbon.

In recent years, sol-gel process for making hybrid glasses has been the subject of considerable interest due to its control over the intrinsic properties of the material, low cost of fabrication, ease of application and good chemical and physical stability of the final product.

Among conventional methods of depositing optical materials, sol-gel technology in general has become one of the rapidly maturing methods to fabricate thin transparent films with good optical qualities. One of its advantages in optical integrated devices, as mentioned above, is its power of manipulation over the optical properties of the material for both active and passive devices [22], [23]. Such an intrinsic change in the material is commonly achieved by the use of the proper precursors [24], [25] or dopants [26], laser densification [27] and photo-polymerization [28].

There have been recent reports on integrated optical devices [29] where photo-induction and laser densification have been used. However, these materials have low heat tolerance. They oxidize in sub 200^0 C, which is less than the temperature required for evaporation of water.

As shown in figure 2-4 The precursor for the sol-gel used in this thesis is MAPTMS. Two of three constituents of this molecule are trimethoxysilane [$Si(CH_3O)_3$] and methacrylate [$C_4H_5O_2$]. Trimethoxysilane is responsible for the sol-gel*ability* of MAPTMS. It is the methoxy linkage that is hydrolyzed and linked to other

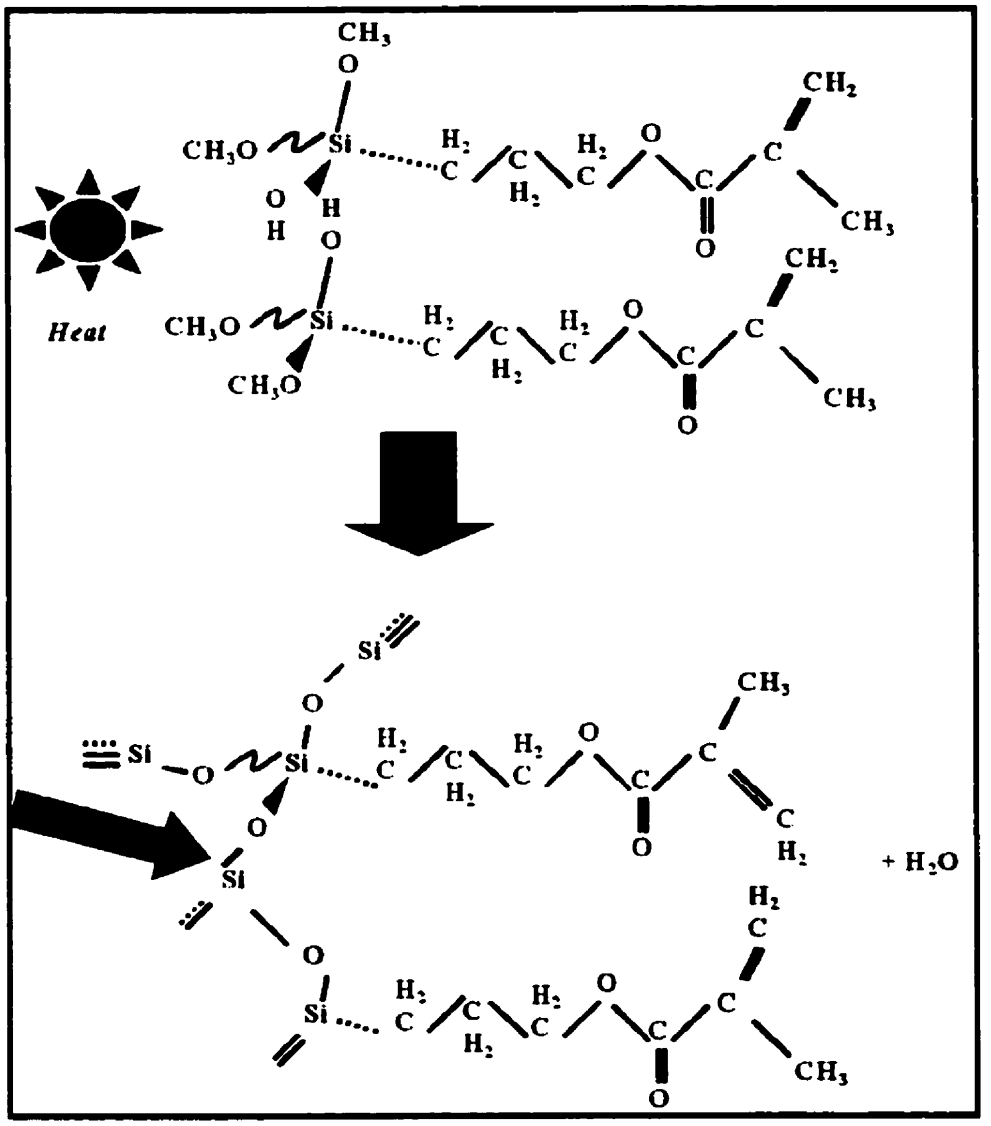

Figure 2-3: The hydrolyzed links form a bond at higher temperature which leads to condensation of the gel to form a glass. The gray vector specifies the new link that connects the two hydrolyzed MAPTMS.

molecules through condensation and the inorganic poly-condensation. The condensation is mostly effected by temperature and its own condensation, since the latter decreases the distance between two monomers, hence increasing the probability of linkage between two monomers. The silicon atom, which acts as the metal in the metal alkoxide template of the sol-gel precursor, insures the compatibility of the refractive index with that of silica.

The double bond in carbon-carbon methacrylate link, in conjunction with C-O bond, is responsible for UV sensitivity of the MAPTMS. It is this double bond that causes the MAPTMS molecules to link to another.

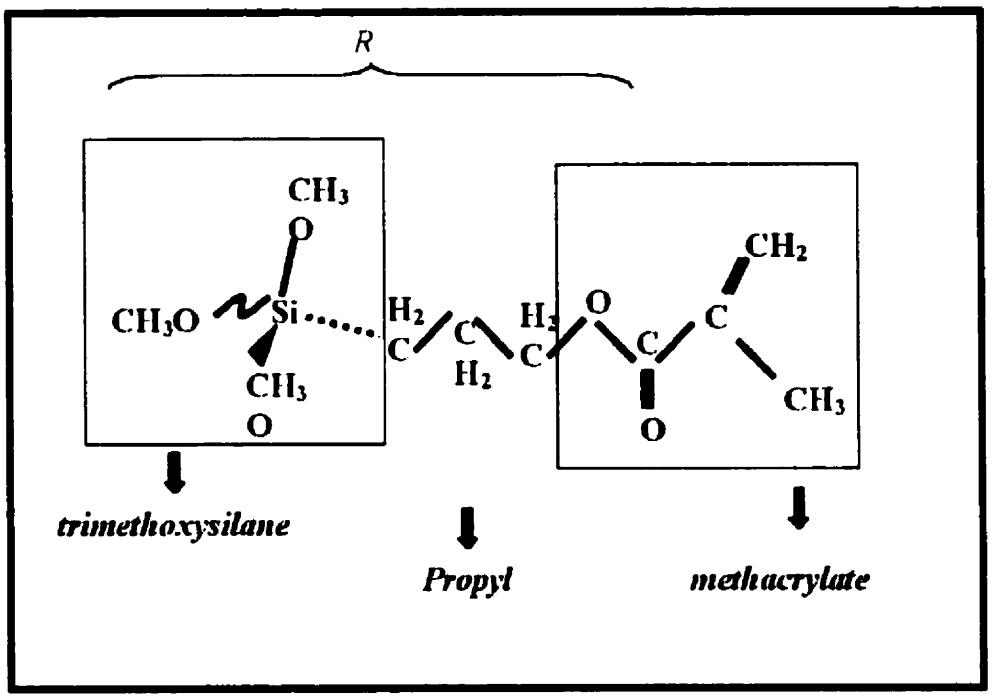

Figure 2-4: The MAPTMS molecule is composed of three constituents. *Trimethoxysilane* is the inorganic component which will be responsible for the glass properties. *Methacrylate* component is responsible for the UV sensitivity and organic polymerization

Since heat may not be localized the same way that UV can, it is easy to note that the inorganic condensation happens globally through out the film while the organic polymerization may be semi-localized by localizing the UV light. It is this semi-local organic polymerization of the hybrid sol-gel material that is exploited to print the image of the optical device. The term "semi-localized" is used in the following sense: once the photon is present at the vicinity of the double bond between two carbon atoms, the polymerization is "initiated" and propagated away from the initial point. However, the effect is damped and dissipated. Therefore, depending on the UV dosage the polymerization maybe larger or smaller than the exposed surface.

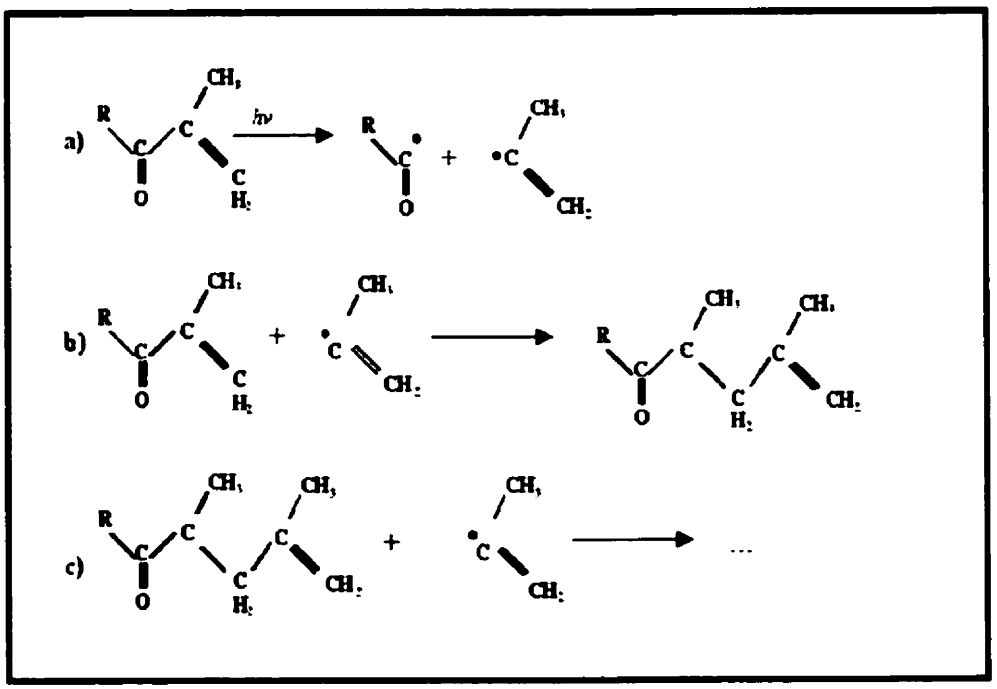

Figure 2-5: One of many possible routes of organic polymerization is a) a UV-sensitive link is broken into two radicals. b) one of the radicals is attached to a molecule resulting a bigger molecule with a un-bonded electron and c) the molecule grows as it is attached to other smaller molecules.

2.2 Hybrid sol-gel method of device fabrication

In order to have guiding effect in an optical device, the structure should be fabricated using different refractive indices. In sol-gel method of fabrication such a change of refractive index means different concentration of dopant in the host. Derivatives of early transition metal groups like titanium and zirconium, in higher concentrations, are commonly used to increase the refractive index. Therefore, two solutions may be used for fabricating an optical structure: one solution with higher dopant concentration for guiding layer and one with lower dopant concentration for the buffer and the cladding for higher and lower refractive index respectively.

The process of making the optical structure starts with depositing the buffer layer. A traditional method of deposition is spin coating. This method is commonly used to deposit photo-resist and polymer thin films in semiconductor and optical industry. In this method, as shown in figure 2-6, once the substrate is covered by the solution, the rotating chuck under the center of the substrate rotates with a predetermined angular velocity and for a predetermined length of time.

Once the rotation is ended, a thin and viscous film is formed over the substrate. This film is subsequently treated with heat and UV flood for densification and stability. By *stability* is meant that any further UV and heat treatments would cause no change to refractive index. The heat and UV flood are divided into three steps: Prebake, UV flood and postbake. After the spin coating, the film is still viscous and sensitive to surface deformation and particle contaminations. To avoid these effects, the film is placed in an oven with a moderate temperature just to harden or dry the surface. Note that the film is not driven into its final solidification since it would minimize any portability required for the organic bonds to interconnect. Steps are shown in figure 2-7. Once the prebake treatment is finished the film is put under a UV source whose wavelength and intensity is known.

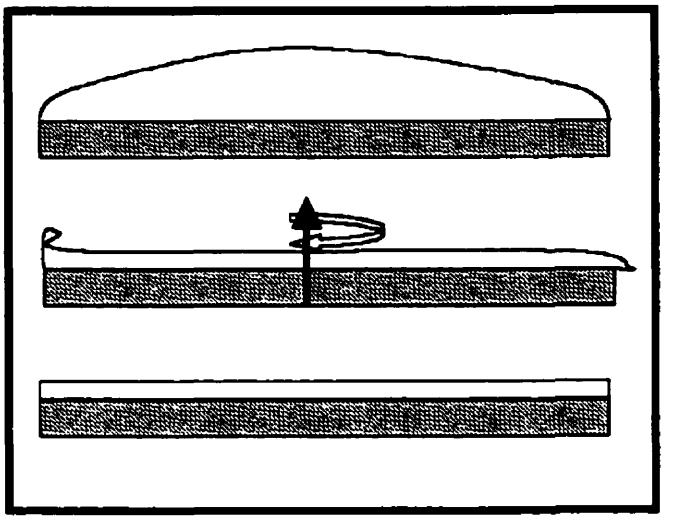

Figure 2-6: Once the substrate is covered by the solution, the rotating chuck under the center of the substrate rotates with a predetermined angular velocity and for a predetermined length of time. At the end, the substrate is covered by a thin film.

Subsequently, the surface undergoes a preset dose of UV shine in order to create the organic network and finalize the organic polymerization. After the UV flood, the film is put in the oven for a different heat treatment. At this time, the objective is to solidify the film and complete the inorganic condensation. The final product is a glass with a constant and stable refractive index of the desired buffer.

After completing the process for the buffer layer, the substrate is then covered with the guiding solution for the spin deposition; the same way mentioned before. Since the speed and the deposition time of the spin coating will result in different thickness and that the viscosity of the guiding solution may be different, the spin coating at this time may require different values for its angular velocity and the spin time. After the spin coating, as shown in figure 2-8 the substrate is put into the oven for prebake treatment. Once the prebake treatment is finished, the guiding film is now ready for UV imprinting where pattern of the optical device

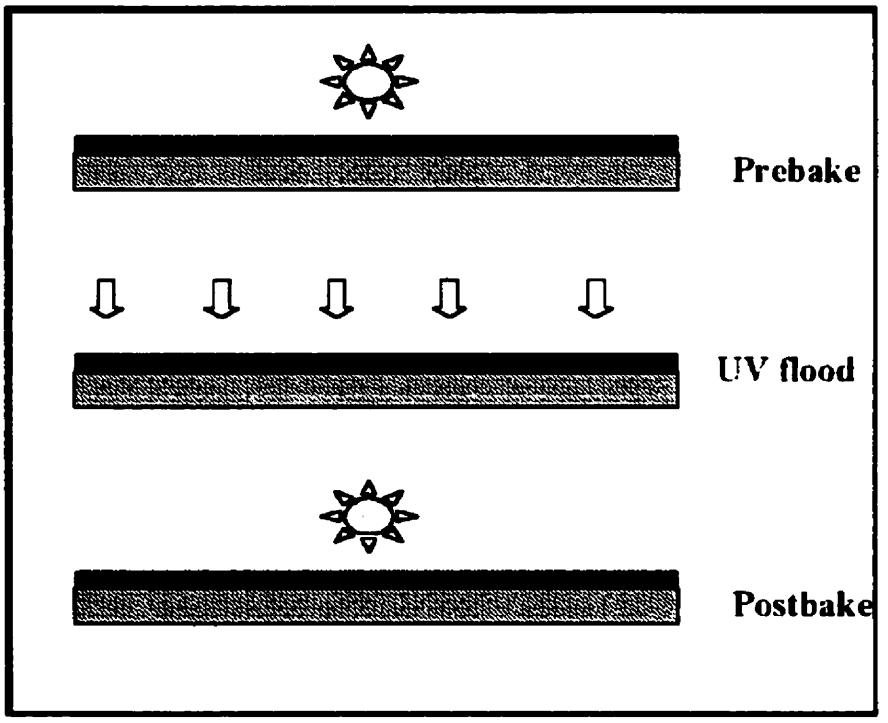

Figure 2-7: After the spin coating the film has to be prebaked to dry the surface. The surface dryness prohibits the dust particles to contaminate the film and also, for guiding layer, it prohabits the film from sticking to the mask surface.

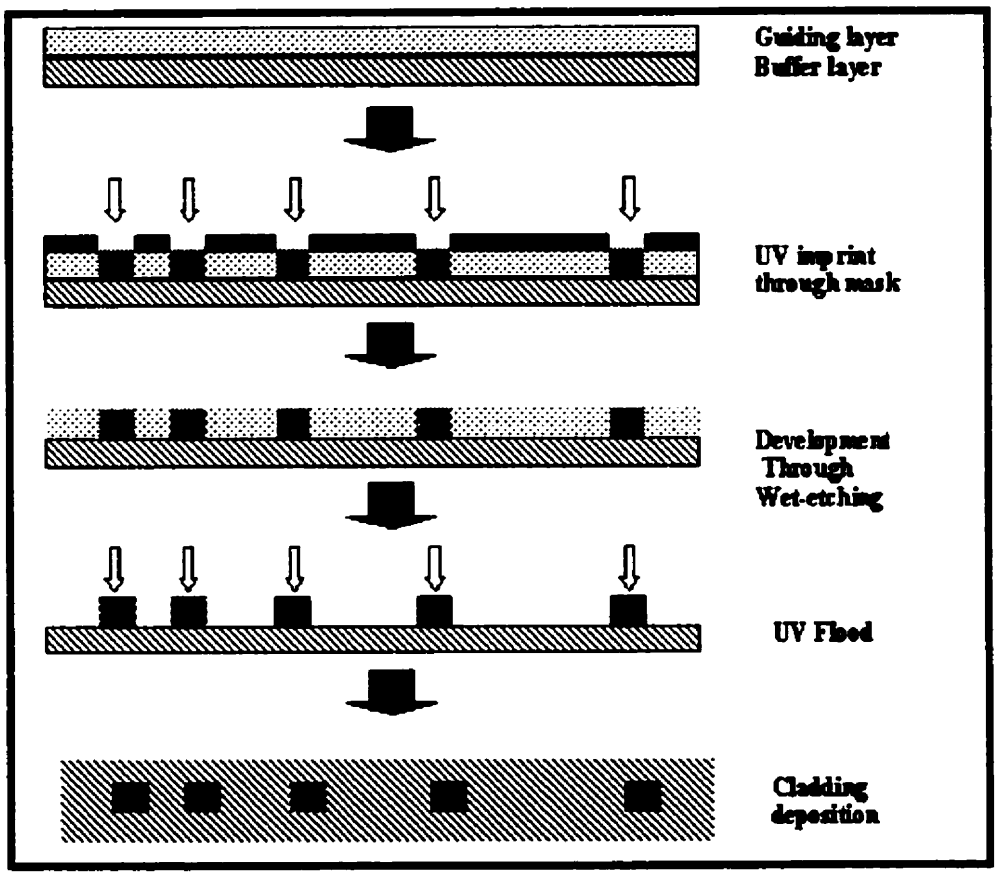

Figure 2-8: The process of fabricating the optical devices is composed of three parts: 1-buffer deposition and saturation, 2-guiding deposition, prebake, UV-imprint, development and saturation, and, 3-cladding deposition and saturation.

is formed. For this process, a prefabricated photo-mask is put on the surface of the film. The photo-mask is defined negative since the surface of the mask at the location of the optical waveguides is etched away. This opening allows the UV light to pass through the opening and semi-locally polymerize the region. After depositing the mask over the guiding layer, UV is shined. Again, the dosage of the UV is predetermined. The non-polymerized region can be dissolved in alcohol while the polymerized regions may not. Therefore, a suitable alcohol is used in order to develop, other words, remove the non-exposed region. After the development, the substrate is then located under the UV source for UV-saturation and postbake is applied to solidify the structure. After the guiding layer , the buffer solution, now called cladding is spin coated, UV and heat saturated to obtain the final structure.

The figure 2-9 shows the image of a square 6 × 6 microns channel before cladding deposition.

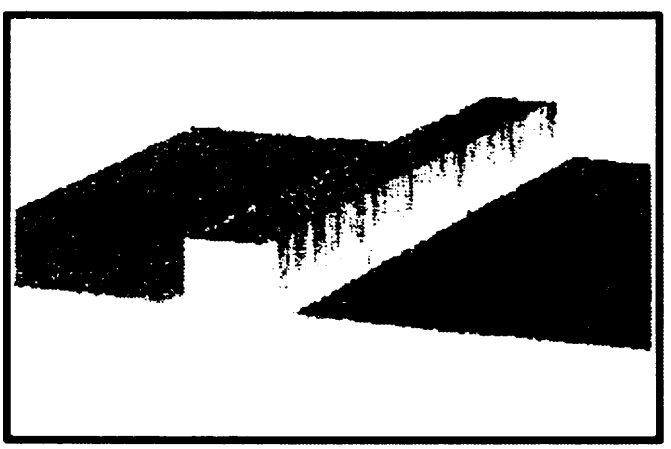

Figure 2-9: A microscopic picture of a square ridge fabricated using sol-gel method of glass fabrication.

Chapter 3

Extracting fabrication parameters

Like any other processes, sol-gel method has its own limits [30]. Though from one hand one can improve the process to reduce these limitations, however, on the other hand, one can also use the flexibility of the design to offset the errors, variation, or any other limits of the fabrication, as much as possible. The only way to achieve this is by parameterizing the limits first, one way or another.

One of the main obstacles for micro-fabrication is the limit of the photo lithography. These limitations appear in resolution of printing and in developing the channels. For example, the polymerized region may end up being greater than the exposed region; causing *broadening effect.* Consider the case where the minimum UV dosage required for one part of the device is excessive for another section. This indeed is an issue where, for example, the channel of 6 microns wide and a taper of 21 microns wide receive the same UV exposure in the same configuration. The difference in width would mean the difference in surface area and hence different UV dosage. In this case if the configuration undergoes the minimum UV-dosage designated for 21 microns, the 6 microns will undergo an over exposure which leads to unpredictable width.

Another point to consider is development. In sol-gel process, development is done by immersion of exposed chip in alcohol. No matter how fast is the current of the alcohol flow over the surface, there is always a minimum distance between two un-exposed channels where the alcohol is not able to dissolve the un-exposed region (see figure 3-1) .

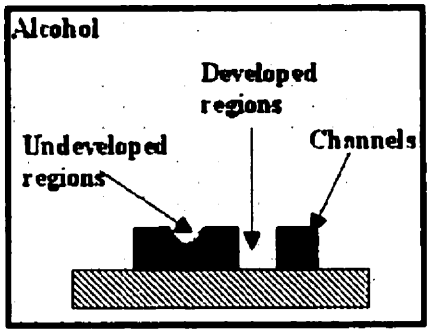

Figure 3-1: As the separation between two waveguide distances reduces, the resolution of the development reduces accordingly.

3.1 Material parameters and fabrication resolution

In order to parameterize all fabrication limits, may it be UV-exposure or development, one needs to know the minimum distance between two channels, which produces two well defined waveguides, as the function of their width and their height, by the time the device is fabricated. For this purpose a mask was designed with rows of 500 microns long each with widths ranging from 2 to 30 microns as shown in figure 3-2. For each row of given width there are columns of different separations between two channels ranging from 1 to 10 microns. Once this mask is

printed over the film and developed, the minimum distances for different channel widths are obtained. For this thesis, the only two channels widths used in the optical device are 21 and 6 microns. After employing the mask and fabricating the channels, and inspecting them under the microscope, the minimum distance for obtaining to isolated channels was found to be 3 microns, for both 6 and 21 microns.

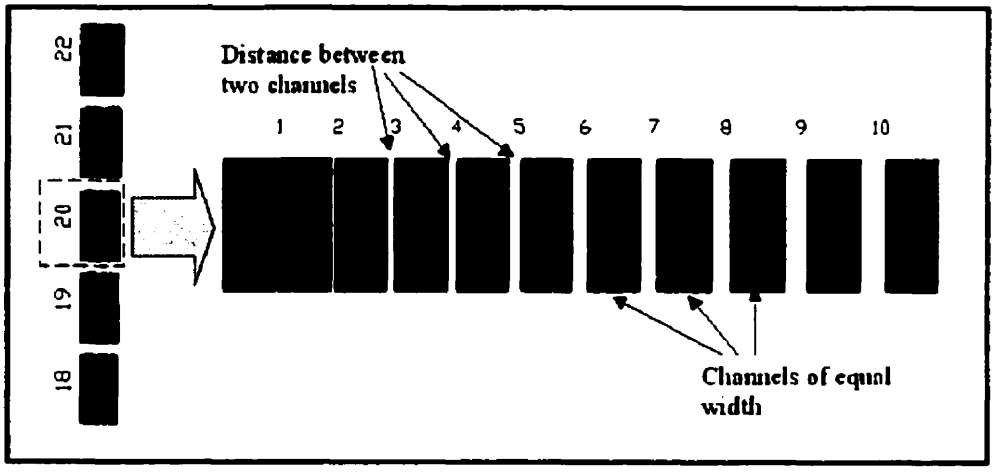

Figure 3-2: To obtain the minimum distance between two channels required in order to isolate two adjacent channels, a series of waveguides are made with different separation distances. After the development process, the minimum distance that isolates two channels is considered to be the minimum separation between two channels.

3.2 Refractive indices and film thicknesses

In general, the parameters of an optical structure are the refractive indices and dimensions. Figure 3-2 helps to find the horizontal dimensions. As for the vertical dimension (the film thickness),and the refractive index one only needs to study the

material in its film state.

As described above, an optical film may be parameterized by its thickness and refractive index. The simplest case of an optical film is a film with homogeneous and isotropic refractive index. Both parameters may be obtained by the method of prism coupling [31],[32] and[33]. The idea behind the prism coupling method is that a multimode waveguide has independent states of excitations corresponding to its modes. These states have two parameters in common: thickness and the refractive index of the film. Therefore, a minimum of two states of excitations is sufficient in order to obtain these two parameters. These excitations may be achieved by coupling light into a multimode film through a prism (see figure 3-3).

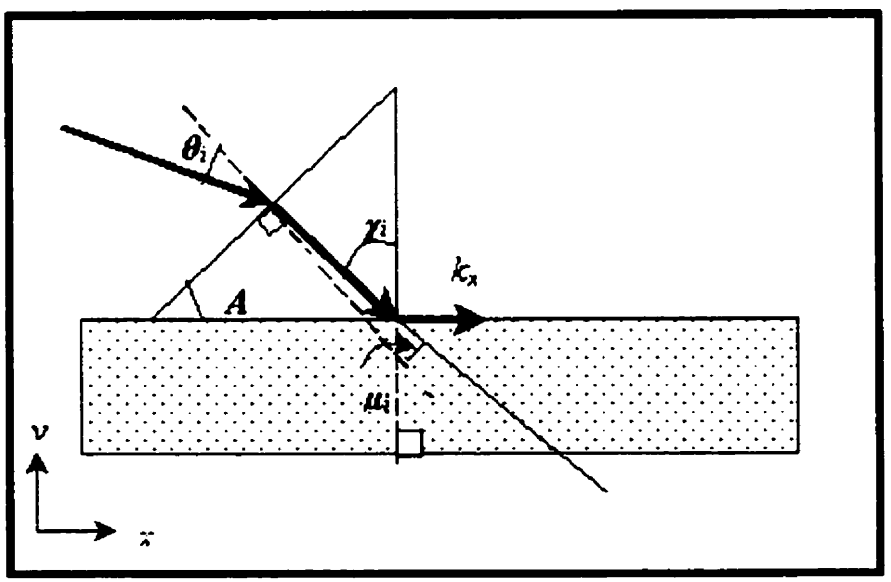

Figure 3-3: Only the discrete values of θ_i can excite the corresponding modes. The parameter θ_i depends on the refractive index of the film and its thickness. Since there is an independent dispersive equation for each mode, at least two modes are required to be excited in order solve the two unknowns: refractive index and the film thickness.

As the launching angle, θ_i, varies k_x will change. Once k_x matches the modal

constant of one of the modes of the film, coupling occurs. This coupling is detected by placing a detector at the end of the film where the guided light exits. Since the values for modal constants are discrete, there are discrete values of i for launching angle $\theta_i$that excites the modes. Using Snell's law and the geometry of the schematic shown above one can start with the following two equations:

$$n_{eff}^{m} = n_p \quad \sin \chi^m \tag{3.1}$$

and

$$\chi^m + \frac{\pi}{2} - A + \frac{\pi}{2} - \mu^m = \pi \tag{3.2}$$

where n_p is the refractive index of the prism. By applying the sin function on both sides of the above equation and using Snell's law at the interface of the prism and the film

$$\sin \chi^i = \sin \left(A + \mu^i\right) \tag{3.3}$$

According to Snell's law at the first input face,

$$\mu^i = \arcsin \left(\frac{\sin \theta^i}{n_p}\right) \tag{3.4}$$

and the final equation is obtained

$$n_{eff}^{i} = n_p \sin \left(A + \arcsin \left(\frac{\sin \theta^i}{n_p}\right)\right) \tag{3.5}$$

However, Note that n_{eff} relates to the effective mode of the slab. In order to calculate the refractive index and the thickness of the film one should solve the dispersion equation for an asymmetric slab waveguide [34] with n_s defining the

refractive index of the substrate.

$$V\sqrt{1-b^i} - m\pi + \arctan(\frac{1}{c^\epsilon}\sqrt{\frac{b^i}{1-b^i}}) + \arctan(\frac{1}{d^\epsilon}\sqrt{\frac{b^i}{1-b^i}}) = 0 \tag{3.6}$$

which can also be written as

$$h \equiv \tag{3.7}$$

$$h(n_s) = \frac{m\pi - \arctan\left(\frac{1}{c^\epsilon}\sqrt{\frac{b^i}{1-b^i}}\right) - \arctan\left(\frac{1}{d^\epsilon}\sqrt{\frac{b^i}{1-b^i}}\right)}{k_0\sqrt{\left(n_f^2 - n_s^2\right)(1-b^i)}} \tag{3.8}$$

with

$$V = k_0 h\sqrt{n_f^2 - n_s^2} \tag{3.9}$$

$$a = \frac{n_s^2}{n_f^2 - n_s^2} \tag{3.10}$$

$$b^i = \frac{\left(n_{eff}^i\right)^2 - n_s^2}{n_f^2 - n_s^2} \tag{3.11}$$

$$c = \frac{n_s^2}{n_f^2} \tag{3.12}$$

$$d = \frac{1}{n_f^2} \tag{3.13}$$

and Equation

$$\epsilon = \begin{cases} 1 & for\ \ TM \\ 0 & for\ \ TE \end{cases} \tag{3.14}$$

Where n_f and h are the refractive index and the film thickness respectively. Once n_{eff} for each m is known in (3.11), there would be an independent equation for the corresponding m given by (3.6). Common solution for all equations would be the constants n_s and h.

However, the problem occurs where measurement of the angle θ_i is subject to error. In this case, the best way instead of finding the solution that can be close to all equations, would be to eliminate the equation located furthest away from the common region on the h-n_s plane. To be able to achieve this one can use equation (3.8) were the thickness h is a function of n_f. Since n_f is the same for all modes, all functions h would intercept at one point (h,n_f) as the solution.(See figure 3-4)

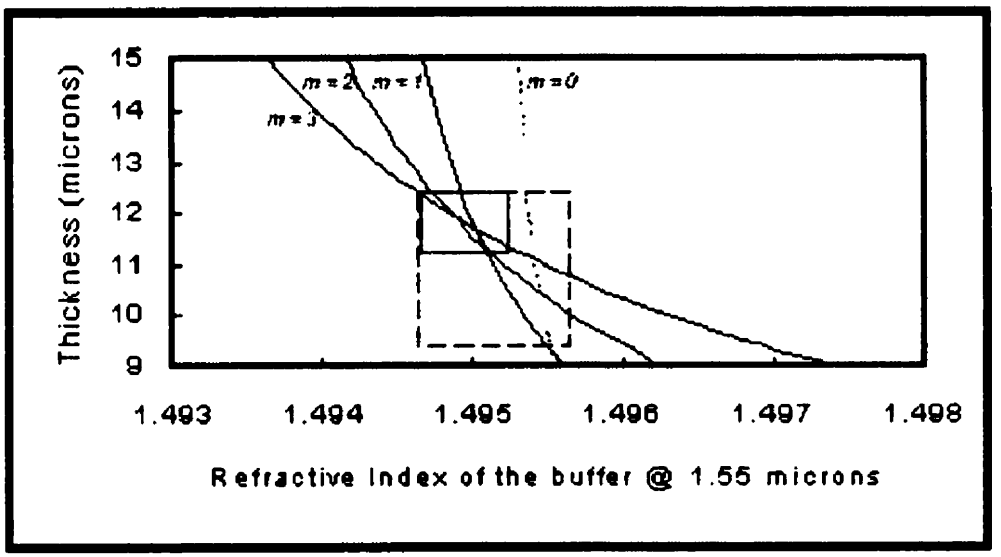

Figure 3-4: measuring the film refractive index, n_f, In cases where a single measurement is subject to higher error, by eliminating the isolated graph the total result is much more accurate. The difference in error can be seen in the dotted line and solid lie boxes.

Note that by eliminating the most isolated equation uncertainty is decreased by almost half.

Once the refractive index and the film thickness is measured it is important to know the tolerance of these measurements over the whole wafer. This importance is because of the fact that thickness and the refractive index both affect the effective index of the guided mode. In optical devices, where difference in phase plays

Refractive index @ 1.3 μm (buffer material)	1.502
Refractive index @ 1.3 μm (guiding material)	1.520
Resolution of isolation between two channels (μm)	3
Index variation	0.027%
Thickness variation	7 %

Table 3.1: Summary of the fabrication and material parameters.

an important role, non-constant effective indices will cause a randomized phase difference leading to a disrupted response.

3.3 Fabrication variations

To obtain the variation of the thickness and the refractive index of the film over the wafer, a series of the measurement is made over the wafer, as shown in figure 3-5, the number in the boxes refer to the thickness in microns. The variation of refractive index (0.027%) for refractive index is small enough to believe that the variation of the thickness (7.34%) is reliable.

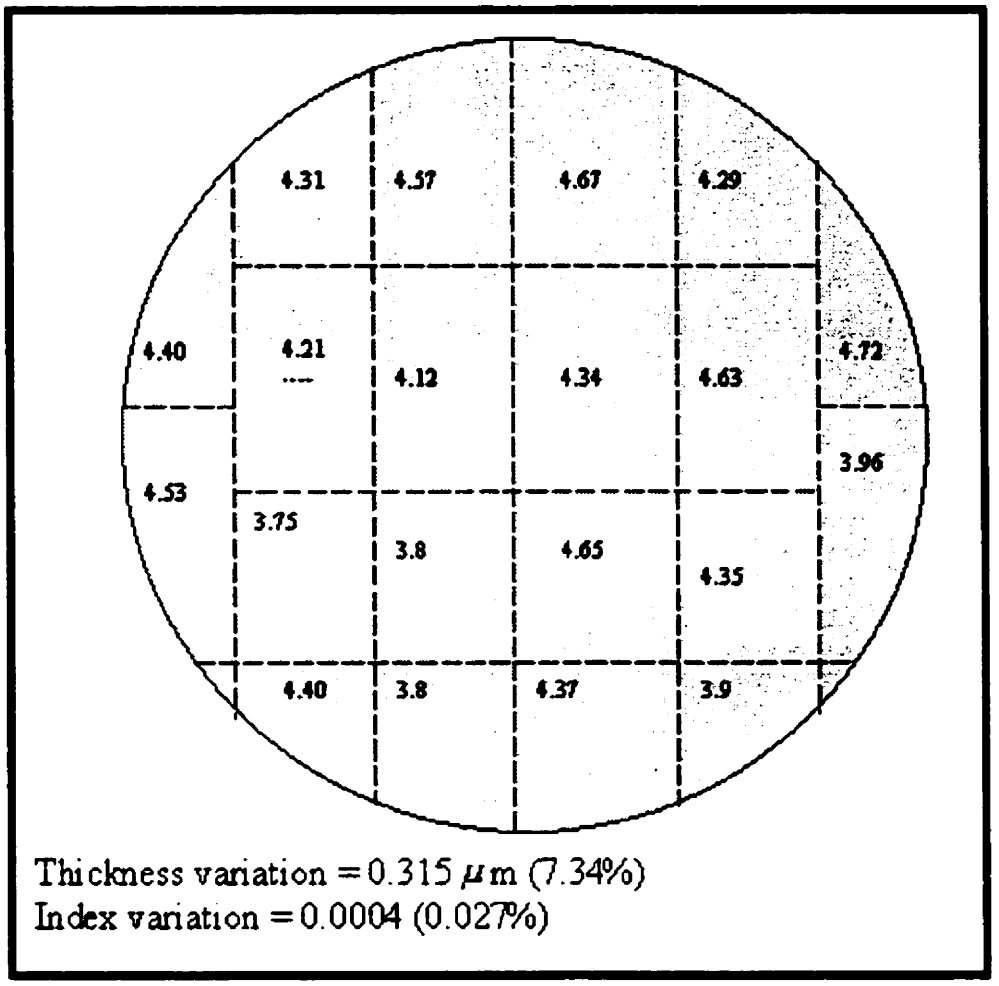

Figure 3-5: In order to obtain the variation of the refractive index and the film thickness due to fabrication variations, a wafer was divided into small sections and each section was measured by prism coupling method. The small deviation in refractive index confirms the standard variation of thickness variation. The value underlined is the average of the neighboring values.

Chapter 4

Theory

Arrayed Waveguided Grating's, $AWG's$, main functionality is very much based on grating interference. A grating consists of a large number of equally spaced slits with spacing d with an image line far from the plane of slits [35] . Once a coherent and monochromatic wave hits the plane of slits with an inclination angle with respect to the slit plane, each slit will act as a source with a constant initial phase difference from the adjacent slit (see figure 4-1). The phase difference caused by the initial tilt of the plane wave and the different path distances taken from each slit creates interference on the image line. The dispersion equation for such grating is [36]

$$n_c \tag{4.1}$$

$$\Delta L + n_s \tag{4.2}$$

$$dk \tag{4.3}$$

$$\sin\theta = 2\pi m\,(k) \tag{4.4}$$

$$m = ..., -1, 0, 1, ... \tag{4.5}$$

$$k = \frac{2\pi}{\lambda} \tag{4.6}$$

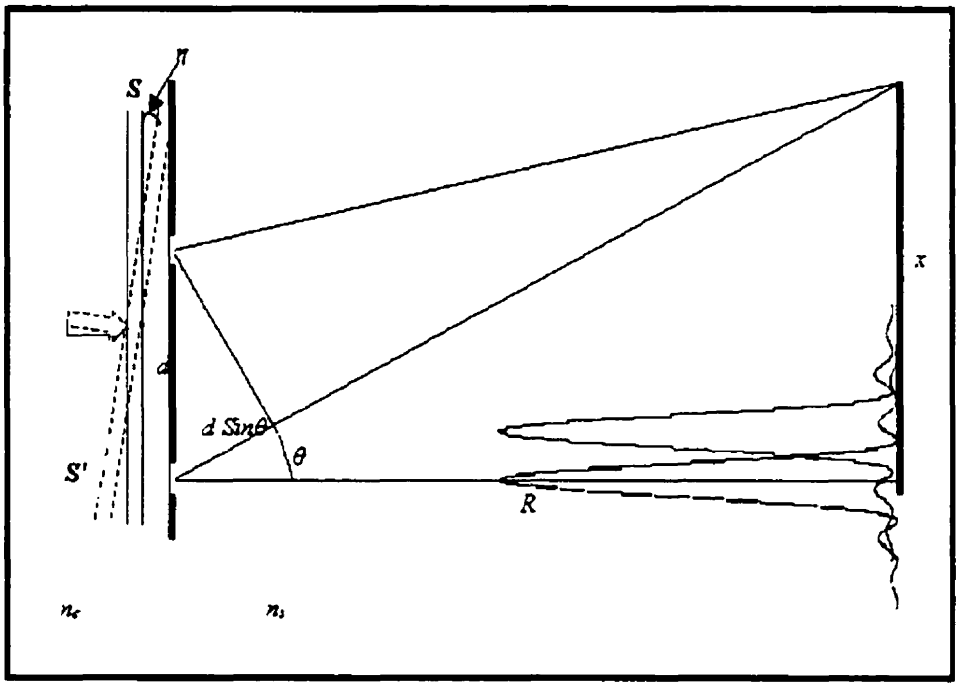

Figure 4-1: When a tilted coherent light travels through the slits of a distance d apart, far from the slits the interference pattern forms. Different wavelength would have their first maxima at different location.

Where ΔL is the physical length difference that the wave front takes to reach two different slits. The indices n_c and n_s are the refractive indices of the before and after the slits, respectively. The parameter θ defines the angular position on the image screen.

The reason why the wavefront should make an angle η is as following: If the

initial wavefront reaches the slits with no tilt($\eta = \Delta L = 0$), the most intense spot will be at $m = 0$ for all wavelengths. This means that the grating is not able to separate the wavelengths for $m = 0$. However, as η increases, the location for m = 0 for two different wavelengths differs.

For $\theta = 0$, and a given ΔL,

$$n_c \Delta L = m\lambda_0 \tag{4.7}$$

Where λ_0 is the wavelength focusing at $\theta = 0$. By varying λ at $\theta = 0$ in the above equation, one can have periodic occurring intensities as the grating goes through different orders.

$$n_c \Delta L = m_0 \lambda_0 \tag{4.8}$$

$$n_c \Delta L = \ldots = (m_0 - 1)(\lambda_0 + FSR) = m_0\lambda_0 = (m_0 + 1)(\lambda_0 - FSR) = \ldots \tag{4.9}$$

Free spectral range (FSR) is the period of the output response in wavelength. To the above equation, at $\theta = 0$ for order $m_0 - 1$, the wavelength would be $\lambda_0 + FSR$. The lower wavelength focused would be $\lambda_0 - FSR$ corresponding to $m_0 + 1$ and so on. In order to find the order of the grating

$$(m_0 - 1)(\lambda_0 + FSR) = (m_0 + 1)(\lambda_0 - FSR) \tag{4.10}$$

$$m_0 = \frac{\lambda_0 + FSR}{FSR} \tag{4.11}$$

Since m_0 is to be an integer

$$m_0 = int\left(\frac{\lambda_0 + FSR}{FSR}\right) \tag{4.12}$$

Based on (4.4), as the wavelength for the input wavefront changes the output response also varies, since it is a function of the wavelength. The variation of the device to the gradual change of the wavelength will be

$$n_c \Delta L + n_s d \sin\theta = m\lambda \tag{4.13}$$

$$\frac{\Delta\left(n_c \Delta L\right)}{\Delta\lambda} + \frac{\Delta\left(n_s d \sin\theta\right)}{\Delta\lambda} = m \tag{4.14}$$

Since ΔL and d are physical lengths, therefore, they are independent of the wavelength. Further more if $\delta\lambda$ be of the order of nanometers,

$$\frac{\Delta n_c}{\Delta\lambda} \approx \frac{\Delta n_s}{\Delta\lambda} \approx 0. \tag{4.15}$$

Therefore, (4.14) becomes

$$d n_s \frac{\Delta\theta}{\Delta\lambda} \approx m. \tag{4.16}$$

In the above equation, $\cos\theta$ is approximated to 1 since $\tan\theta \approx \sin\theta$.

Up to now, the theory described a three dimensional free space interference experiment. In the case of integrated optics, Figure 4-1 becomes two dimensional, where the plane of traveling wave is parallel to the substrate. The parameters n_c and n_s would then represent the effective index of the fundamental mode of the channel and the slab waveguide, respectively. Each slit would also be the junction region of the input channels (at the left of the slits) with the slab (at the right of the slits).

In this case, in order to separate different wavelengths, at each first-order maxima, there would be a channel to guide the wavelength out at the output region.

For focusing purpose, the input region and output region would form a circle with their center located at the circumference of the other as shown in figure 4-2

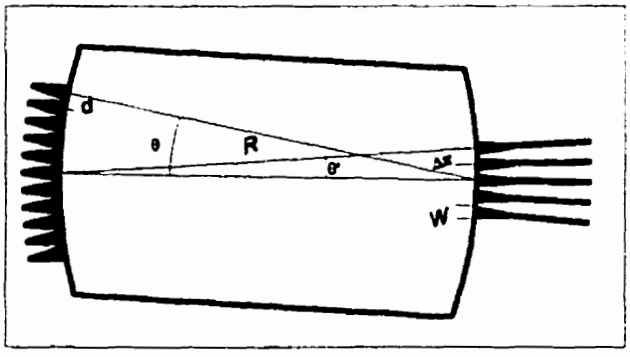

Figure 4-2: A three dimensional interference experiment maybe *approximated* to a two dimensional planar device. The image plane and the plane of slits both form a circle whose center is located on the circumference of the other circle.

$$\Delta\theta = \frac{\Delta x}{R}. \tag{4.17}$$

This means (4.18) can written as

$$R = \frac{dn_s \Delta x}{m\Delta\lambda} \tag{4.18}$$

The most relaxed parameters of the arrayed waveguide grating are usually R and ΔL. The parameter ΔL may be found by the boundary equation for the differential equation in the Equation (4.14). Equation (4.4) Would then be the solution to this differential equation. An industry standard parameter is central wavelength, which defines the wavelength dedicated to the central output channel (ie. at $\theta = 0$). This condition can be used to fix the boundary equation

$$n_c \Delta L = m\lambda_0 \tag{4.19}$$

Where λ_0 is the central wavelength.

4.1 Design Procedure

The design of the AWG has two aspects: dynamics and physical. The dynamic aspect of the design corresponds to obtaining R, ΔL, Δx and d. The physical aspect of the design is related to the physical layout.

4.1.1 *AWG* Parameters

Material parameters

- n_{in}, n_{out} = Refractive indices of the channel and the surrounding buffer, respectively.

Device specification parameters

- $\Delta\lambda$ Channel spacing. It is the resolution of the grating in wavelength
- N=Number of channels
- λ_0=Central wavelength

Design parameters

- Δx=Separation between the centers of the receiving channels.
- d=Separation between the centers of the transmitting channels.
- N_s=Effective index of the slab.
- N_c=Effective index of the channel.
- M=Number of grating.
- m=order of grating.
- R=Radius of the slab.
- ΔL= Length difference between two adjacent grating channels.

Step One: Analysis of the channel and the channel dimension, w

The channel should be symmetric for two reasons. The fundamental mode profile of the channel would resemble the mode of the fiber, which means lower coupling loss at both input and the output facets. Also, a symmetric channel is independent of the polarization of the input profile, which in turn, leads to no polarization dependent loss.

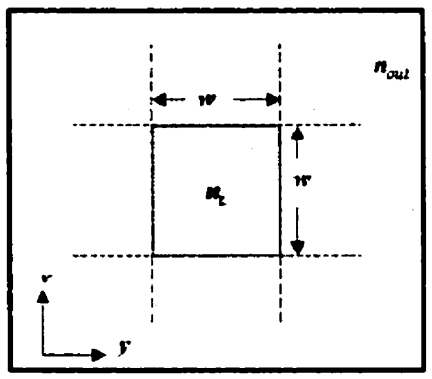

Figure 4-3: Starting from the refractive indices of both, the guiding and the buffer materials , one can set the dimension of the channel to obtain the field profile close to that of single mode fiber.

Since the fiber is considered to support one mode, odd modes of the channels will automatically vanish at the coupling point. This is the reason why one should find the channel dimension, w, for which the channel supports no more than two modes. furthermore, though channels may support two modes, the design is set the way, as will be seen later, that the second mode is not excited.

The effective index for the fundamental mode along x axis will be n_s. Next, consider another slab with a direction perpendicular to the previous one and the thickness w except that the refractive index of the inside channel is now replaced with n_s. The effective index of the fundamental mode along the y-axis can now

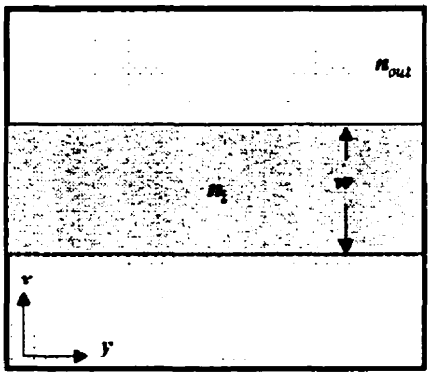

Figure 4-4: The first step of the effective index method for finding the effective index of the mode of a single mode channel is first to consider the a symmetric slab whose height is equal to the height of the channel.

be *approximated* to n_c. The main advantage of effective index is to reduce the structure from three-dimensional to a two-dimensional problem. Therefore, from here on, a channel *effectively* is a vertical slab with the same outside refractive index and an inside refractive index equal to the effective index of the fundamental mode of a horizontal slab.

Step Two: Grating order, m

As mentioned above, free spectral range, FSR, is the period of the output response in wavelength.

$$FSR \geq |\lambda_{LastChannel} - \lambda_{FirstChannel}| \tag{4.20}$$

It is important to note that in (4.19), the higher is the FSR, the smaller the length increment, ΔL, which would make an stress later on the creating the layout for which such a length increment can be achieved. On the other hand, with an FSR too low, there is the possibility of the channel overlapping due to small fabrication

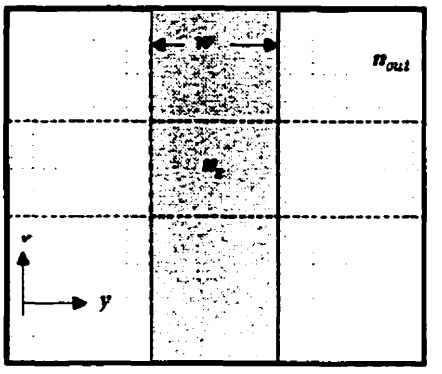

Figure 4-5: After calculating the effective modal index of the single mode slab, the perpendicular slab will be analyzed with the slab refractive index equal to that of effective modal index of the previous slab. The effective modal index of this channel is then approximated to be the effective modal index of the channel.

variations. Once FSR is set, the grating order, m is found by (4.12)

$$m = int\left(\frac{\lambda_0 + FSR}{FSR}\right) \tag{4.21}$$

Step three: Slab length, R

The channel separation, Δx, and the grating separation, d, are usually set in order to obtain the slab length (4.18)

$$R = \frac{dn_s\Delta x}{m\Delta\lambda} \tag{4.22}$$

large enough to obtain the far field approximation in the slab as will be explained later.

$$\frac{\Delta x^2}{\lambda R} \ll 1 \tag{4.23}$$

Step four: Length increment ΔL

Using the central wavelength, λ_0, n_c and (4.19) the grating order, m the length increment ΔL

$$\Delta L = \frac{m\lambda_0}{n_c} \tag{4.24}$$

is found.

4.1.2 Simulation

Consider the geometry of figure 4-6 involving two circles of radius R, each of which passes through the center of the other, and consider on the two circles, two points P and P' with coordinates θ and θ', respectively. For small θ and θ' the distance between the two points is given by [37]

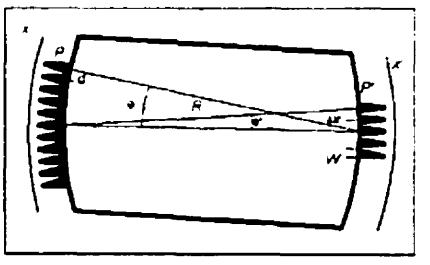

Figure 4-6: Knowing the response function of the star coupler and the profile of the input field at the input channel-slab junction is sufficient to obtain the total field at the output channel. The overlap integral of this total field and the profile of the output channel provides the output power for that wavelength in dB.

$$D = R\,(1 - \sin\theta \sin\theta') \tag{4.25}$$

As a consequence by placing at P a point source of unit amplitude, the resulting

response obtained at P' is

$$U = \frac{e^{jkD}}{\sqrt{j\lambda R}} = \frac{e^{jkR}}{\sqrt{j\lambda R}} e^{jkR\sin\theta\sin\theta'} \tag{4.26}$$

Noting that

$$\sin\theta = \frac{x}{R} \tag{4.27}$$

and

$$\sin\theta' = \frac{x'}{R} \tag{4.28}$$

Respectively.

The term

$$kR\sin\theta\sin\theta' \tag{4.29}$$

can be re-written as

$$2\pi w'u = 2\pi wu' \tag{4.30}$$

where

$$w = \frac{d\sin\theta}{2\lambda}, \tag{4.31}$$

$$w' = \frac{\Delta x\sin\theta'}{2\lambda}, \tag{4.32}$$

$$u = \frac{2x}{d}, \tag{4.33}$$

and

$$u' = \frac{2x'}{\Delta x}. \tag{4.34}$$

Therefore, U maybe written as

$$U = \frac{e^{jkR}}{\sqrt{\lambda R}} e^{2\pi ju'w} \tag{4.35}$$

The Fourier transform of the total field resulting from a distribution source,

$$E = A\psi(x) \tag{4.36}$$

on the receiving circle is the net multiplication of the response by the Fourier transform of the source. Where the normalization factor A is found by

$$A^2 = \frac{1}{\int_{\infty}^{\infty} |\psi(x)|^2 dx} \tag{4.37}$$

$$= \frac{2}{d\int_{\infty}^{\infty} |\psi(u)|^2 du} \tag{4.38}$$

So the Fourier transform of the total field is:

$$\overline{G}(u', u) = U(u')\,\overline{E}(u') \tag{4.39}$$

where the over-line defines the Fourier transform of the field. The transfer coefficient of the field is calculated by

$$\alpha = \int \overline{G}(u')\,E'(u'))du' \tag{4.40}$$

$$= \frac{1}{\sqrt{\lambda R}} \int e^{2\pi j w u'} \overline{E}(w')\,E'(u')du' \tag{4.41}$$

$$= \frac{1}{\sqrt{\lambda R}} \overline{E'}(w')\,\overline{E'}(w) \tag{4.42}$$

where prime defines the receiver aperture.

The power transfer T from a transmitter P to the receiver P' would then be

$$T = \frac{1}{\lambda R} |\overline{E}(w')|^2 |\overline{E'}(w)|^2 \tag{4.43}$$

The above equation is called Friis equation. Re-writing the equation in more detail:

$$T = \frac{d\Delta x}{\lambda R}\eta\left(w'\right)\eta'\left(w\right) \tag{4.44}$$

$$\begin{aligned}
\eta\left(w'\right) &= \frac{1}{2}\frac{\left|\overline{\psi}'\left(w'\right)\right|^2}{\int_{-\infty}^{+\infty}\left|\psi'\left(u'\right)\right|^2 du'} & \eta'\left(w\right) &= \frac{1}{2}\frac{\left|\overline{\psi}\left(w\right)\right|^2}{\int_{-\infty}^{\infty}\left|\psi\left(u\right)\right|^2 du} \\
\overline{\psi}\left(w\right) &= \int_{-1}^{+1}\psi\left(u'\right)e^{2\pi jwu'}du' & \overline{\psi}'\left(w'\right) &= \int_{-1}^{+1}\psi'\left(u\right)e^{2\pi jw'u}du \\
w &= \frac{d\sin\theta}{2\lambda} & w' &= \frac{\Delta x\sin\theta'}{2\lambda} \\
u &= \frac{2x}{\Delta x} & u' &= \frac{2x'}{d}
\end{aligned} \tag{4.45}$$

Since the fiber is taken single mode, the only mode of the channel to consider will be the fundamental mode. Therefore, regardless of how wide is Δx only the profile of the fundamental mode is considered for both ψ and ψ'. As an example, an 8-channel AWG is parameterized to produce a channel spacing of .8 nanometer and the central channel of 1550 nanometer. The above simulation algorithm produces the output response of the device in figure 4-7. It is important to note that the simulated central wavelength is 1550 as designed.

4.1.3 Physical layout of the device

The fundamental idea behind all AWG,DWDM templates is different geometrical ways of creating the length difference ΔL. The layout in figure 4-9 describes the slab and the grating section of the AWG template called straight-arc-straight. Each grating is labelled as i. The parameter S is the distance between two points defining the point of contact between the central input/output channel and the slab for both slabs. Note that these points also the centers of the circles for which gratings are

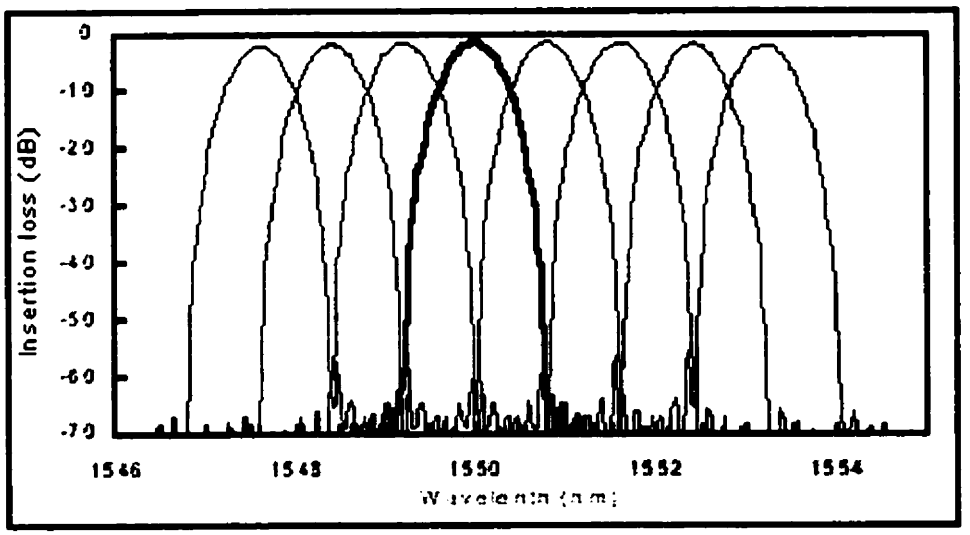

Figure 4-7: The simulation algorithm is applied to an 8 channel wavelength demultiplexer *AWG* with .8 nanometer channel spacing resolution, 1550 nanometer fixed at the central output channel. The bold graph corresponds to the central channel. Note that the simulation produces the 1550 nanometer for the central channel wavelength, confirming the design parameters.

located on. In this figure, the first slab, the *ith* grating and the corresponding radius r_i and extension l_i are shown, respectively.

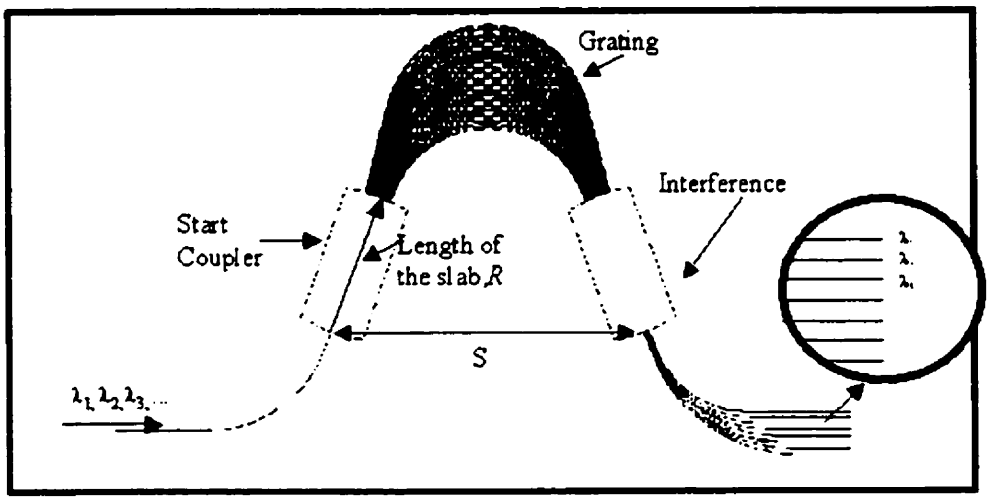

Figure 4-8: Different sections of the an Arrayed Waveguide Grating Dense Wavelength Division Multiplexer

There are two conditions that fix the two degrees of freedom r_i and l_i.

$$(l_0 + l_i)\cos\alpha_i + r_i \sin\alpha_i = S/2 \tag{4.46}$$

$$l_{i+1} - l_i + r_{i+1}\alpha_{i+1} - r_i\alpha_i = \Delta L/2 \tag{4.47}$$

$$\alpha_i = (i-1)\,\alpha + \alpha_0 \tag{4.48}$$

$$i = 1, 2, 3, \ldots \tag{4.49}$$

- l_0: Includes the radius of the slab, length of the taper l and any other constant extension after the tapers.
- l_i: An extra extension whose length depends on the grating number.

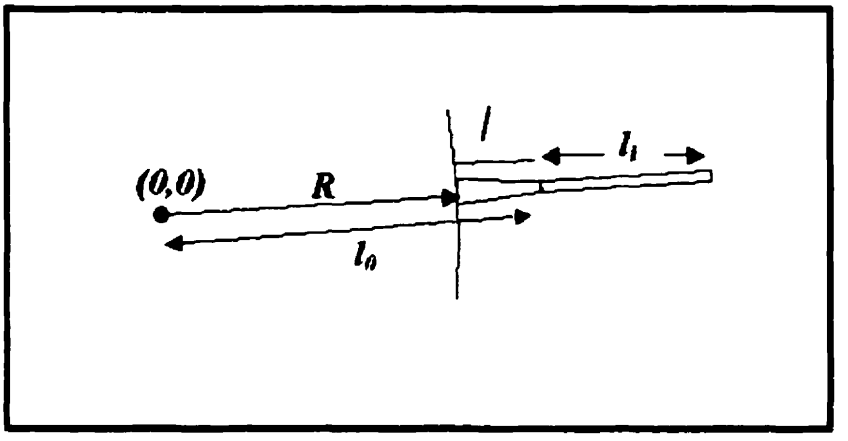

Figure 4-9: Since the radius of the slab, taper extension and any extra extension after the taper are going to be constant for all the grating channels, l_0 is denoted as a constant value for all the gratings.

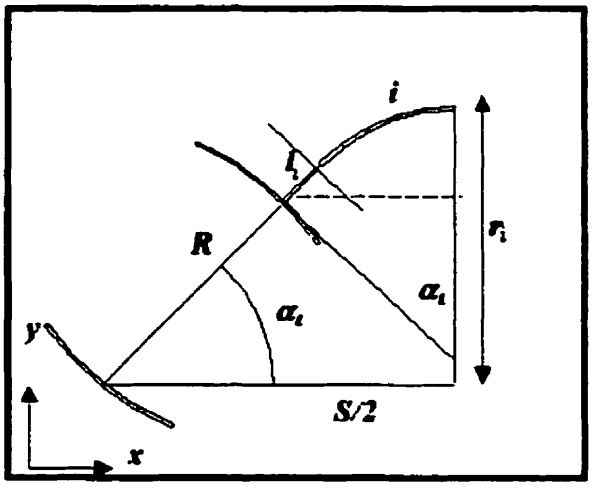

Figure 4-10: Using the condition of fixed ΔL and physical layout, one obtains two equations. These two equations are sufficient to find the two unknown for each grating.

- α_i: is the angle between x-axis and the line joining the center to the *ith* grating.
- r_i: Radius of the *ith* grating .
- α_0: Initial angle that the first grating makes with x-axis at the slab junction.
- S: the distance between the two centers of the upper circles of the two slabs.

The above equations may be re-written as

$$(l_o + l_i)\cos\alpha_i + r_i \sin\alpha_i = S/2 \quad (4.50)$$

$$l_{i+1} - l_i + [\frac{S/2 - (l_0 + l_{i+1})\cos\alpha_{i+1}}{\sin\alpha_{i+1}}]\alpha_{i+1} - r_i\alpha_i = \Delta L/2 \quad (4.51)$$

$$\alpha_i = (i-1)\,\alpha + \alpha_0 \quad (4.52)$$

$$i = 1, 2, 3, ... \quad (4.53)$$

The procedure to draw the layout is as follows: consider $l_1 = 0$. The radius for the first grating would be found in (4.50). Use r_1 and l_1 in (4.51), l_2 would be found. l_2 in (4.50) would give r_2 and the process continues through iteration of all gratings. The main conditions that evaluate the layout are the physical size and the minimum radius, which in turn corresponds to bending loss. Using S and α_m both may be achieved. However, once the length difference ΔL becomes too small other templates should be considered. As an example of the above algorithm, the layout of an 8-channel *AWG* is obtained (see figure 4-11) to produce the response presented in figure 4-7.

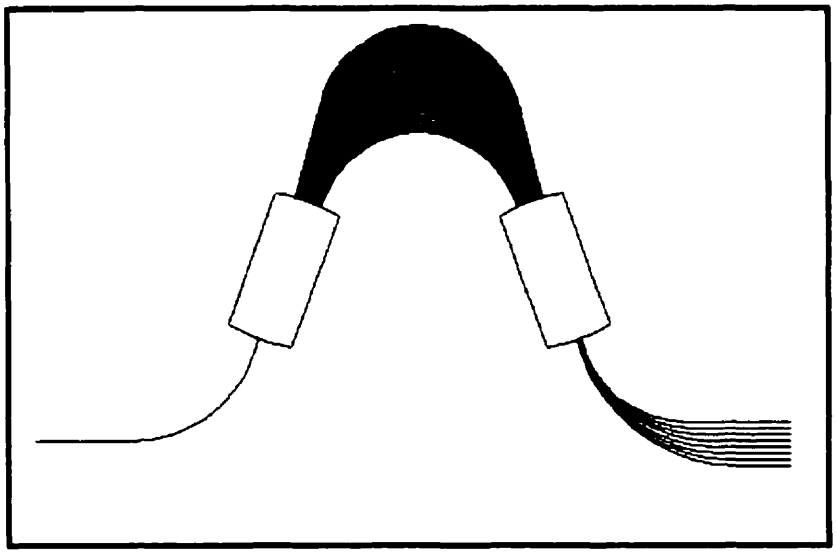

Figure 4-11: A phtoto-mask design of an 8-channel *AWG* is produced in AutoCAD format using the algorithm discussed in this section for a straight-arc-straight template.

Chapter 5

Designing a DWDM

The design procedure explained in previous sections is now going to be applied towards making an actual device. The procedure starts from the design specification and the material refractive indices.

The design specification is described in table 5.1.

5.1 Specifications

5.2 Parameters

5.2.1 Material parameters

The refractive indices are obtained by measuring the films using prism coupling method in 1.523 microns wavelength and approximated for 1.3 microns by applying

Channel spacing (nm)	2.25
Number of channels	4
Central wavelength (nm)	1300.00

Table 5.1: Specification of a DWDM to be designed

Refractive index of the guiding layer@1.3	1.520
Refractive index of the buffer layer @1.3	1.502

Table 5.2: Refractive indices of the guiding and cladding/buffer material.

the same difference that exists in silica between the two wavelength. The results are given in table 5.2.1. With fixed refractive indices of the buffer and guiding material, the dimensions of the channel waveguide is parameterized independently from the type of device being designed. Before selecting the actual numerical dimensions, due to symmetry considerations for both TE and TM polarization, the width of the channel and its height should be equal. In order to find the width of the channel waveguide, the first issue is the number of modes that the symmetrical channel waveguide with this dimension carries. Second, is the coupling efficiency between the channel and the fiber at the input and the output section of the device.

5.2.2 Channel dimension

For the first issue, since the fiber is chosen single mode, the channel waveguide can carry two modes. It is important to note that the input fiber will not transfer any power into second mode since the second mode is an odd mode and the overlapping integral from the mode of the fiber to the second mode of the channel vanishes. Choosing two modes instead of a single mode inside the channel allows the fundamental mode to be more confined, which leads to less sensitivity to side wall non-uniformities and bending loss. In order to make sure that the variation in refractive indices during the fabrication process does not excite the third mode, the dimension of the channel is selected to be half way between the second and the third mode. Figure 5-1 shows the number of modes the symmetrical waveguide carries for different widths. Note that 5×5 microns channel provides two modes and it is well below cut-off for the third mode. Therefore, slight variation of the

refractive index will not excite the third mode.

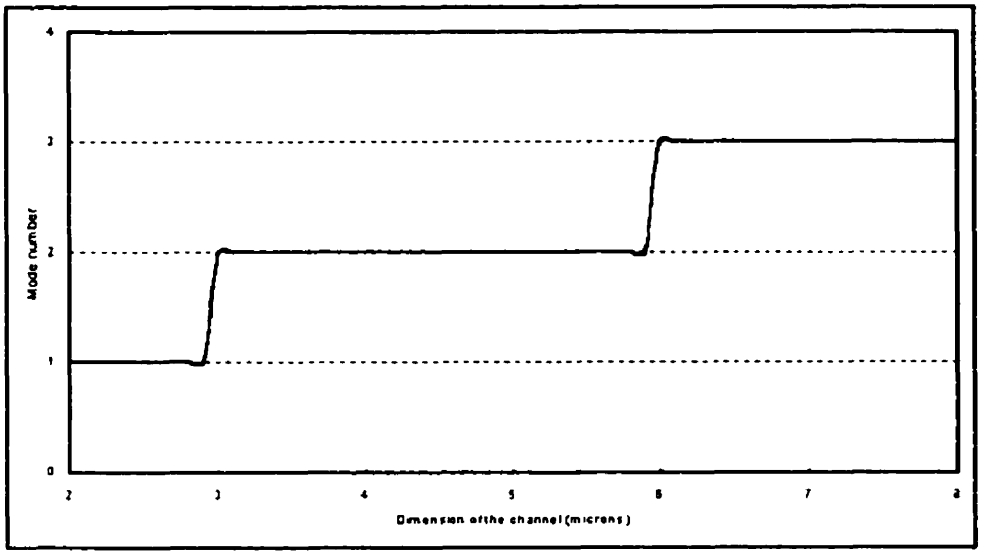

Figure 5-1: width=0.9 of given refractive indices, as the dimension of a symmetrical channel increases, the number of guided modes also increase. The y axis represents the number of modes. Note that for 5 microns width, the channel carries two modes and it is well below cut-off for the third mode. This allows lower sensitivity to index variations.

5.2.3 Mode mismatch loss

Another factor to be considered is the loss due to mode mismatch between the fiber and the fundamental mode of the channel. figure 5-2 shows the loss due to mode miss-match between the fiber and the various channel dimensions. for a channel of $5 \times 5\mu m$ it is important that the 0.74 dB loss per facet is not small. However, though a 6 microns has 0.5 dB loss, such a dimension produces the third mode at cut-off, hence, not desirable.

Obtaining the dimensions of the channel waveguide will lead to effective index of the fundamental mode of the slab, n_s, and the channel,n_c, which are needed

Figure 5-2: For 1 5 × 5μm channel waveguide the fiber to channel transition of power has 0.75 dB loss

Effective index of the slab (n_s)	1.517721787
Effective index of the channel (n_c)	1.515536098

Table 5.3: Effective indices of m=0 for the channel and slab waveguide. The above parameters belong to a channel of $5 \times 5\mu$m with inside refractive index of 1.520 and the outside refractive index of 1.502, both at 1300 nm.

for designing the DWDM and for its simulation. The results are provided in table 5.2.3.

5.2.4 Grating order m

In order to calculate the grating order, the free spectral range, *FSR*, has to be estimated. The main philosophy behind this design is to have the potentiality to become an 8 channel device. There for the *FSR* has to cover all the channels and more. In this case, not only the device is functional for the four channels, but also,

it will work later for 8 channels by only adding the channels when designing the layout. In this case the FSR should be

$$\begin{aligned} 8 \times 2.25nm &= 18nm \\ 18nm + 2nnm &= 20nm \end{aligned} \tag{5.1}$$

where the 2 nm given is the safety margin.

Therefore, m is calculated by

$$\begin{aligned} m &= int\left(\frac{\lambda_0 + FSR}{FSR}\right) \\ &= int\left(\frac{1300 + 20}{20}\right) \\ &= 66 \end{aligned} \tag{5.2}$$

5.2.5 Length difference ΔL

$$\begin{aligned} \Delta L &= \frac{m\lambda_0}{n_c} \\ &= \frac{66 \times 1300.00}{1.514206755} \\ &= 56.663\mu m \end{aligned} \tag{5.3}$$

5.2.6 Length of the slab, R

A taper of $18\mu m$ and the resolution of $3\mu m$ that was found in parametrising the solgel fabrication would lead to the separation, d, of $21\mu m$ between two grating channels, and between two output channels, Δx. Therefore,

$$d = 21\mu m \tag{5.4}$$

$$\Delta x = 21\mu m \tag{5.5}$$

Having obtained the separations between two output and two grating channels, the slab length R can be calculated by:

$$\begin{aligned} R &= \frac{n_s \Delta x d}{m \Delta \lambda} \\ &= \frac{1.517015445 \times 21 \times 21}{66 \times 2.25} \\ &= 4505.076\mu m \end{aligned} \tag{5.6}$$

5.2.7 Number of gratings, M

Before being able to simulate the device one would need to find the number of gratings. The main parameters effecting this choice is the insertion loss and crosstalk. Though an infinite number of gratings would result the best possible insertion loss and crosstalk, however, it would put a great constraint on the physical layout of the device. So the main objective is to obtain the minimum number of the gratings that achieve the least insertion and crosstalk loss.

Figure 5-3 describes the insertion loss and crosstalk for various number of gratings by simulating each simulation with different number of gratings. To be safe, 51 gratings were selected.

5.2.8 Return Loss

The last parameter is the return loss which is related to the refractive index of the epoxy used to connect the fiber to channel waveguide. However, since the sol-gel material is UV sensitive, one way to fiber coupling process may be to use the sol-gel directly as the epoxy. The return loss due to reflection of light back into the fiber for various refractive indices are represented in in figure 5-4.

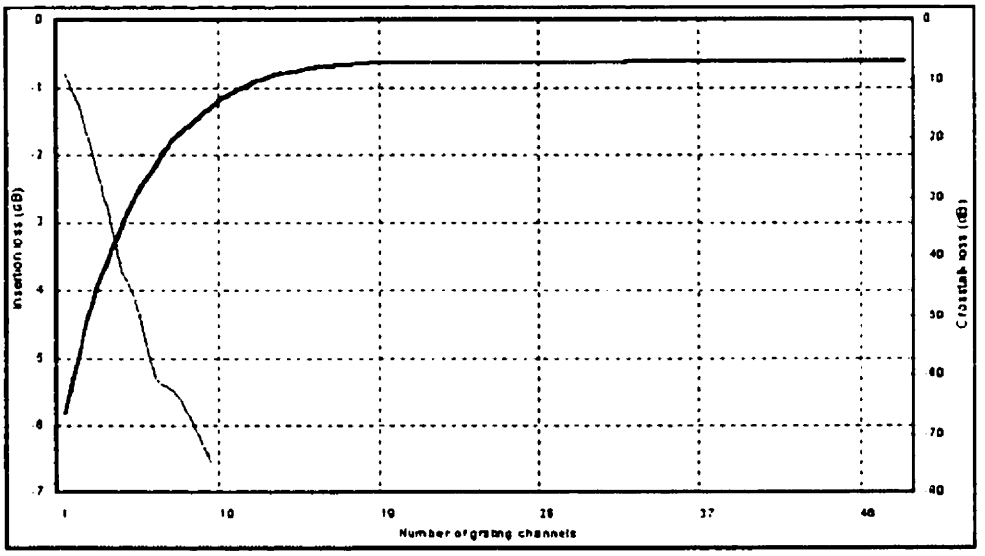

Figure 5-3: Total number of gratings effects the insertion loss and the cross talk. Lower number of the gratings causes the light to be collected at the first slab and the field profile to be wider at the output channel than the channels mode profile. This will lead more coupling to the adjacent output channels leading to higher crosstalk. For number of gratings above 45, the insertion loss is about 0.6 dB and a crosstalk less than -60 dB.

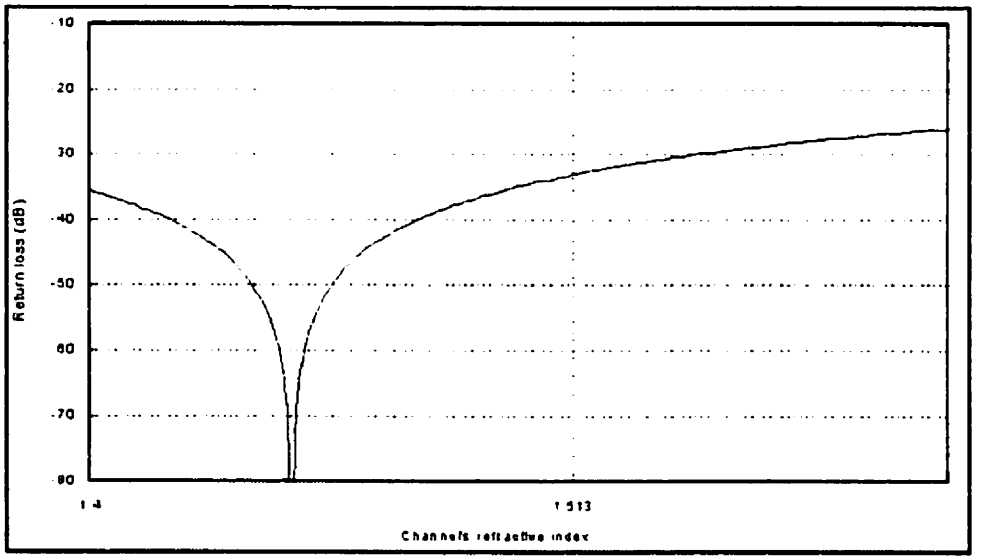

Figure 5-4: Return loss in fiber depends strongly on the refractive index of the channel waveguide. For the refractive index of the 1.513 the return loss is -32.17 dB.

5.3 Simulation

After having obtained all the physical and the optical parameters of the device one can proceed with the simulating the device under the wavelength range of the FSR. The algorithm of the simulation is as follows:

- For the wavelength $\lambda\,(1293 - 1309nm)$
  - For the channel $N\,(1-4)$
    - * For the grating i $(1-51)$
      - · Calculate T_{in}^{i} which is the power transfer between the input channel and the ith grating
      - · Assign $\sqrt{T_{in}^{i}}$ and $e^{-j(i\Delta Ln_c)}$ as the amplitude and the phase of the field of the grating channel, respectively.
      - · Calculate T_{i}^{N} which is the power transfer between the ith grating and the Nth channel.
      - · Accumulate $\left(T_{in}^{i}.T_{i}^{N}\right)$ as the contribution of total power transfer from the ith grating for the Nth channel.
    - * Next grating
    - * Print the total power transfer in dB
  - Next channel
- Next wavelength

The result of the simulation is presented in figure 5-5. Note that the target values for both the central wavelength and channel spacing is achieved. The insertion loss of the central channel is 1.28 dB, which is just more than double of the power transfer loss found in the star coupler using 51 gratings in figure 5-3. The insertion

loss variation of the device from central channel to first, *non-uniformity* is 0.24 dB. The crosstalk at 0 dB, which is the power transfer from one output channel to another at the designated wavelength of a given channel, for the central channel is 65 dB.

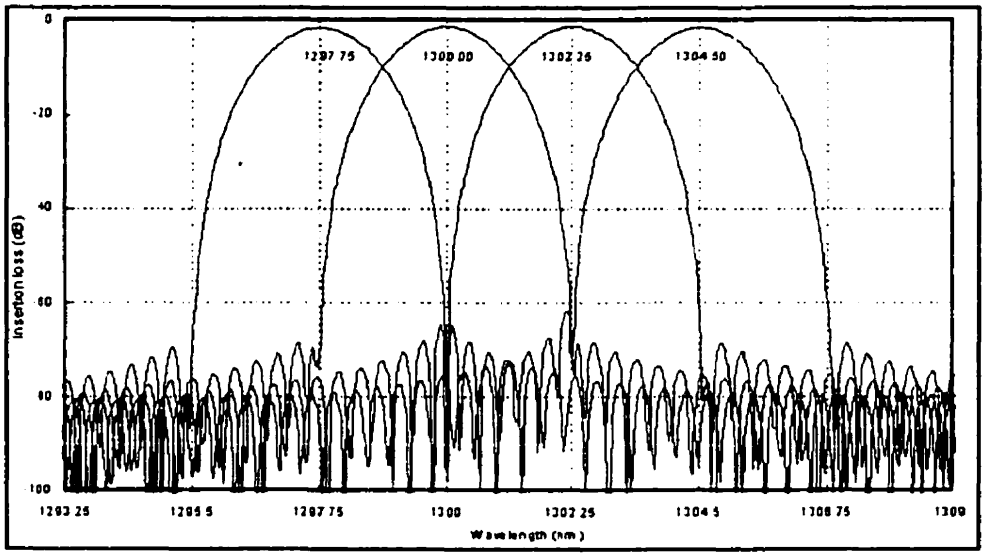

Figure 5-5: The simulated output response of a 4 channel DWDM. Design parameters in this section were supposed to produce a device with following specifications: Channel spacing of 2.25 nm and the central wavelength of 1300.00 nm. As seen, the central wavelength is exactly 1300.00 and the the grids on the graph are set at 2.25 nm. The insertion loss of the channels from left to right are: 1.54, 1.29, 1.28 (central channel), 1.52 dB. This leads to non-uniformity of 0.24 dB. The crosstalk for the central channel at 0 dB is 65 dB

One of the most important parameters of any filter or DWDM is the bandwidth. figure 5-6 shows the peak of the channels at 1 and 3 dB. The simulated bandwidths at 1 and 3 dB are 0.75 nm and 1.3 nm, respectively.

Table 5.3 presents the device specifications in the ideal case where the limitations of the fabrication played no role.

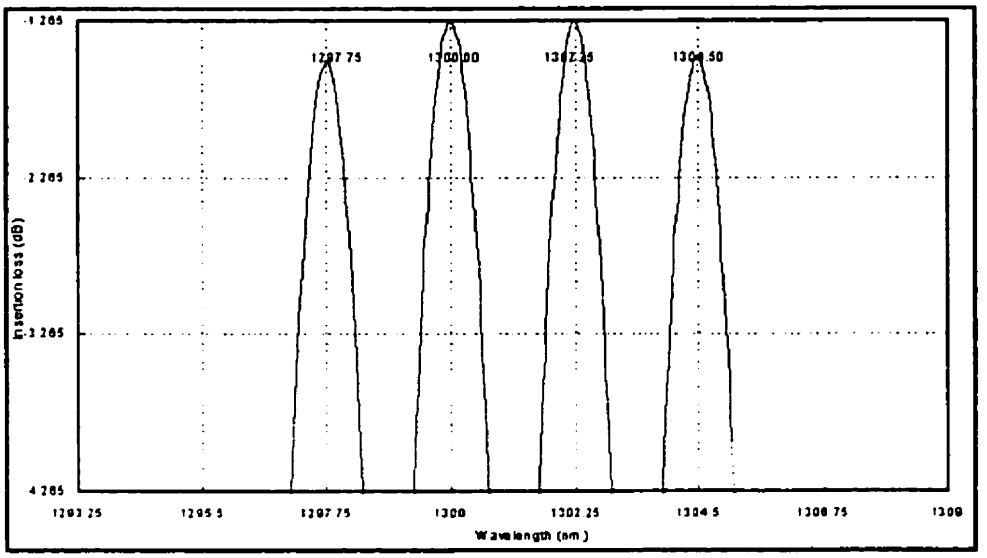

Figure 5-6: The theoretical expected bandwidth for the central channel to be expected at 1 dB and at 3 dB are 0.75 nm and 1.3 nm, respectively.

Channel	1	2	3	4
Insertion loss (dB)	-1.54	-1.28	-1.27	-1.52
Coupling loss (dB)	2 × 0.75	2 × 0.75	2 × 0.75	2 × 0.75
Central wavelength (nm)	1297.75	1300.00	1302.25	1304.50
Cross-talk 0 dB	-71.55	-66.03	-62.48	-76.50
Bandwidth 1dB	0.8	0.8	0.8	0.8
Bandwidth 3dB	1.1	1.1	1.1	1.1
Channelspacing (nm)	-	2.25	2.25	2.25
Return loss (dB)	-32.17	-32.17	-32.17	-32.17

Table 5.4: Theoretical specifications of the designed DWDM.

5.4 Design tolerance

After obtaining the theoretical specification based on ideal fabrication, it is important to understand the tolerance of the device under fabrication limits.

5.4.1 Shift

The first parameter sensitive to fabrication and measurement is the refractive index. If the error for both refractive indices are the same, that is, the contrast of the refractive index between the guiding layer and the buffer layer stays constant, the effect would be a shift in the response of the device. Such a problem exists all the time no matter how accurate is the measurement. One reason is that the refractive index of the guiding layer inside the channel is not the same of the refractive index of the guiding layer in film state measured using prism coupling, and refractive index measurement of inside the channel is not evident. However, Whatever the cause of the problem, one effective method of compensating of the shift is utilizing the dependence of the refractive index of the material on temperature. The refractive index change in sol-gel fabricated thin film from MAPTMS is measured [?] to be $1 \times 10^{-4}/1^{o}C$. To obtain this effect in terms of the shift of the response, one should calculate the central wavelength for different refractive indices, which in turn is a function of the temperature. Figure 5-7 represent the shift of the device for various temperatures. A DWDM chip has to be mounted on a planar temperature controller in order to maintain the device at a desired temperature should the ambient temperature changes, which commonly occurs. However, initially the temperature of the controller is set to shift the device to fall on the specific grid.

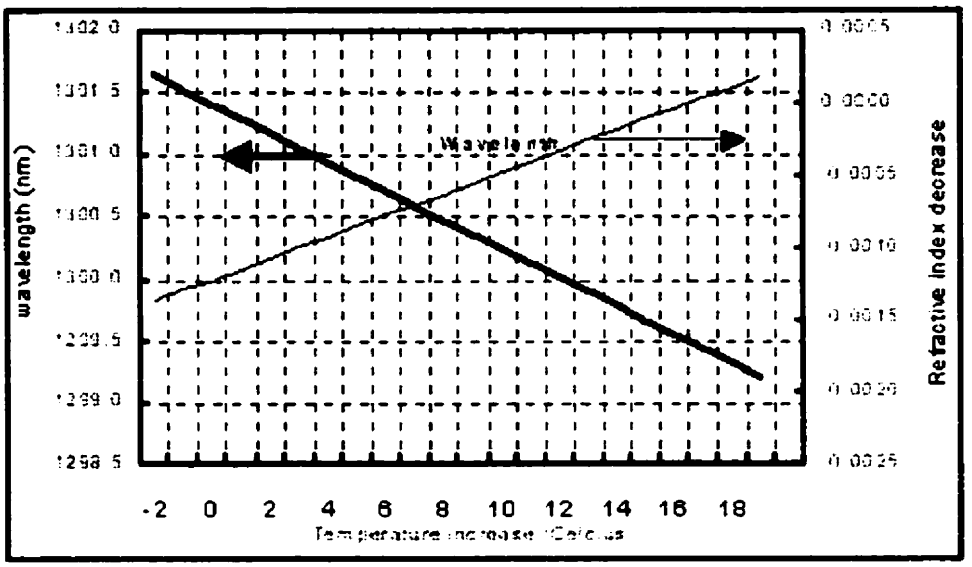

Figure 5-7: Variation of $1 \times 10^{-4} nm/1^{o}C$ for refractive index means a shift of $0.1\text{nm}/1^{o}C$ in channel output wavelength. This effect can be used to tune the device to fall exactly on the specification grid. To do that, the chip is mounted on a planar heater whose responsibility is not only to heat the device to a desired temperature, but also the maintain the device to such a temperature in case the ambient temperature changes. Maintaining the device at a certain temperature insures the thermal stability of the device.

5.4.2 Film thickness variation

Another fabrication limit is the thickness variation of the thin film. Regardless of the method of deposition, thickness of the film varies from one location of the film to another. The effect of the thickness variation in guiding layer is to change the effective index of the channel. Such a change could be gradual throughout the grating area or local, that is, from one grating to another in a random fashion.

In terms of gradual variation of the film thickness, as the figure 5-9 presents, the effect is to broaden the response of the channel and shift its central wavelength. Broadening the channel response will cause crosstalk to be effected drastically.

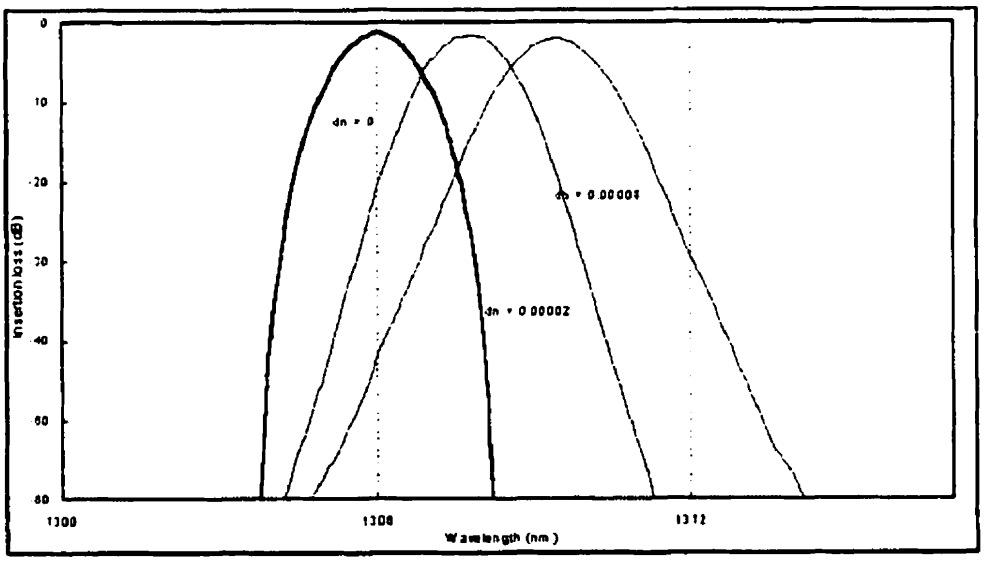

Figure 5-8: The gradual thickness variation from first grating to 51th grating in a linear fashion is shown. dn=0 corresponds to no variation. dn=0.00002 corresponds to variation of 5 to 6 microns from the first grating to the last. finally, dn=0.00008 corresponds to variation of 5 to 8 microns

Another kind of film thickness variation is taken locally. By "local" it is meant that the grating channels have different thickness one compared to another in a

random fashion. The effect is to produce no shift. However, the noise level is raised. In most cases the theoretical crosstalk from 60 to 70 dB changes to practical 20 to 30 dB respectively, just because of the noise level. Figure 5-9 shows this effect.

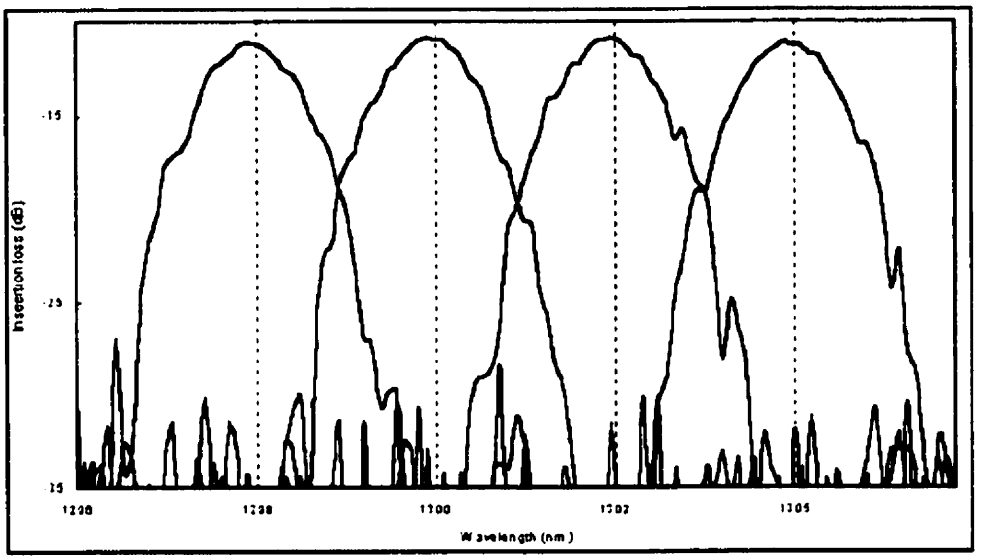

Figure 5-9: A random thickness variation from one grating to another produces no shift. However, the noise level increases greatly, which results lower crosstalk level. The above results are from the variations of 0.1 microns.

Theoretical expected specification:

Channel	1	2	3	4
Insertion loss (dB)	-1.70	-1.4	-1.36	-1.52
Coupling loss (dB)	2×0.75	2×0.75	2×0.75	2×0.75
Central wavelength (nm)	1297.7±0.1	1300.0±0.1	1302.2±0.1	1304.5±0.1
Cross-talk 0 dB	≥ -22	≥ -22	≥ -22	≥ -22
Bandwidth 1 dB	0.7 ± 0.1	0.7 ± 0.1	0.7 ± 0.1	0.7 ± 0.1
Bandwidth 3 dB	1.4 ± 0.1	1.4 ± 0.1	1.4 ± 0.1	1.4 ± 0.1
Channel spacing (nm)	-	2.25 ± 0.2	2.25 ± 0.2	2.25 ± 0.2

Table 5.5: Predicted specifications of the designed DWDM.

5.5 Design:Physical layout

The process of the design ends by making the AutoCAD computer file of the actual photomask. However, before producing all the numbers describing the geometry of the device, one should find the minimum radius allowed in bending the channel waguides. Once the property of the channel is known, the bending loss for different radii may be obtained. One point to keep in mind is that one of the objectives to have two modes inside the channel was to have a better confinement. This allows smaller bending radius. Figure 5-10 represents the loss of $6\mu m$ and $5\mu m$ channels for various radii. One of the characteristics of the bending loss is that the graph is very sharp. To make sure that the loss is the least sensitive, the minimum radius of 3 mm is chosen.

In devices where crosstalk is an important parameter, one should calculated the power transfer from one channel to another adjacent channel. This is important to note that the crosstalk level should be very low. For example a power transfer of 0.05 dB/cm produces a 19.4 dB/cm crosstalk. This calculation is done by simply assuming that 0.05 dB of unit power of one signal has coupled into another channel of power 1. Figure 5-11 represents the coupling loss per centimeter. According to this figure, if two channels are more than $10\mu m$ apart, the level of crosstalk is

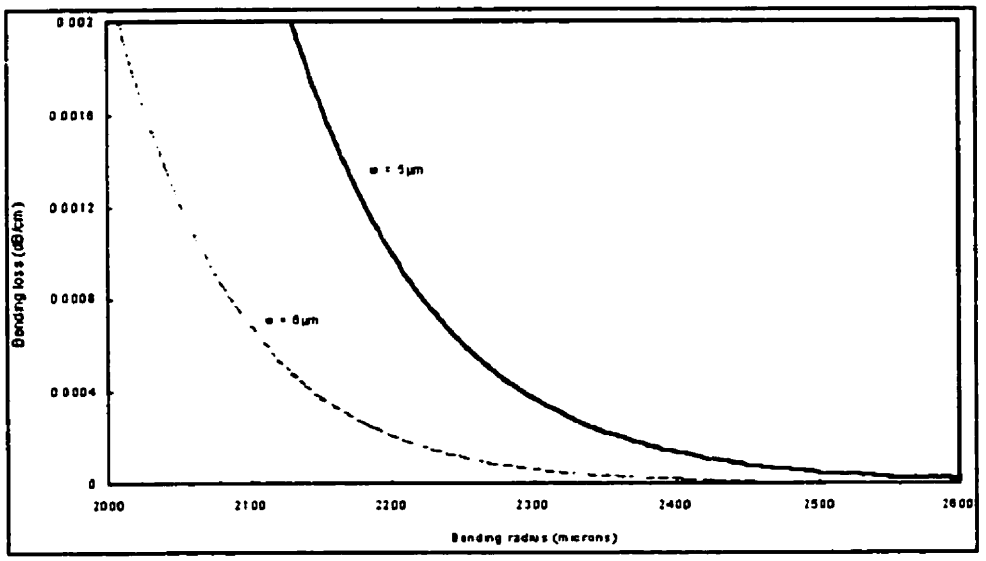

Figure 5-10: Bending loss of the $6\mu m$ and $5\mu m$ channels are presented against different bending radii. To make sure that the bending loss is the least sensitive the minimum radius of 3 mm is chosen.

negligible.

Once the minimum radius is set, the process of making the design is straightforward. By adjusting the distance between two slabs and the angle that the slab makes with the horizontal line all the geometrical parameters of the layout, to obtain the minimum radius, are calculated. Figures 5-12 to 5-14 show different views of the AutoCAD version of the DWDM layout. Note that though the design requirement was for 4 channel waveguide, originally design was made for 5 channels to correctly set the central channel.

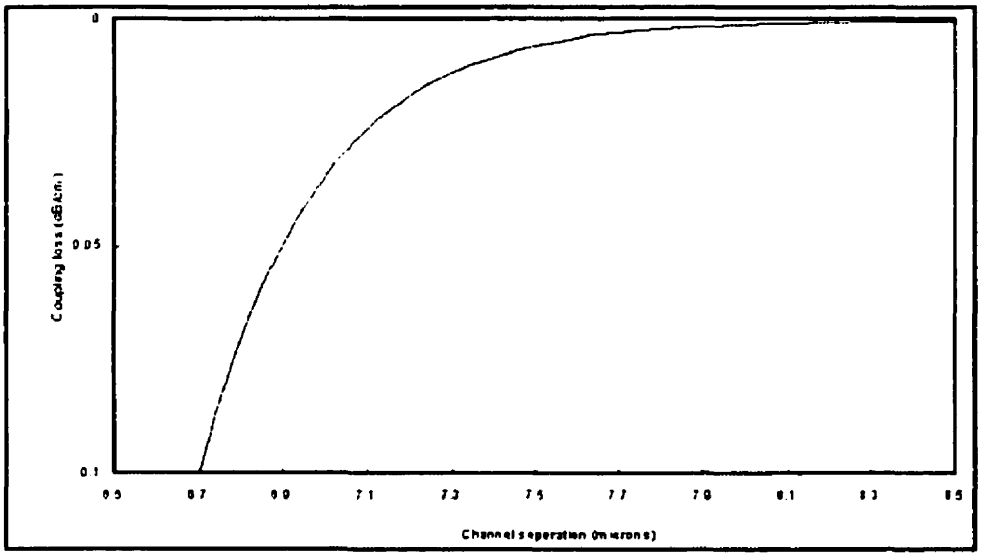

Figure 5-11: Power transfer from one channel to to its adjacent is calculated. The importance of this calculation is due to crosstalk parameter. A 0.05 dB/cm coupling loss will produce a 19.4 dB/cm crosstalk.

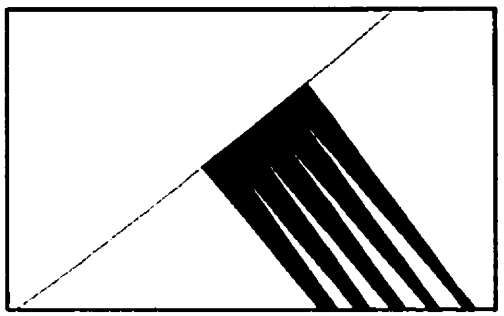

Figure 5-12: Second slab at the output

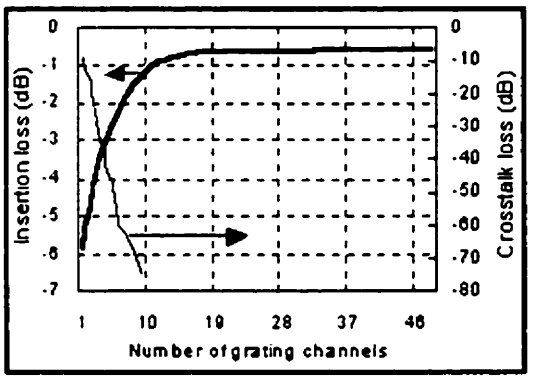

Figure 5-13: Second slab at the grating

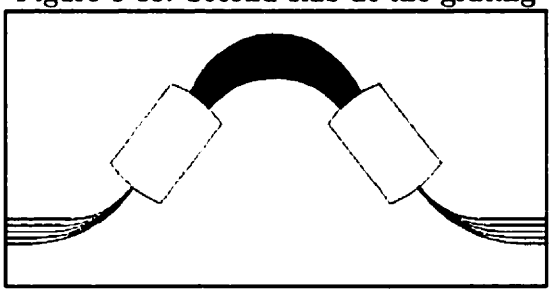

Figure 5-14: Full layout of the device

Chapter 6

Test and characterization

A complete test and measurement of a DWDM device is not a simple task. Since DWDM chip is going to be installed within a system, its characteristics affects the total characteristics of the incoming or outgoing signal.

Figure 6-1 shows the setup for measuring the DWDM response. Helium Neon (HeNe) laser is used for visual inspections and optimizing the coupling between the fiber and channel. The broadband laser which should have a constant power along the wavelength range is used for the input source. The tunable laser used here is polarized. Such a tunable laser is used for polarization independence of the device. Polarization Scrambler is used to change the state of polarization of the linearly polarized light every predetermined time. This means that the polarization remains linear for a time t and it will change to another random state and remains on that state for another elapse of time t. during each period t the Optical Spectrum Analyzer (OSA) will make a sweep and record the response for that polarization. Keeping the minimum power output and maximum power output during all the state variation at the end will provide the polarization loss.

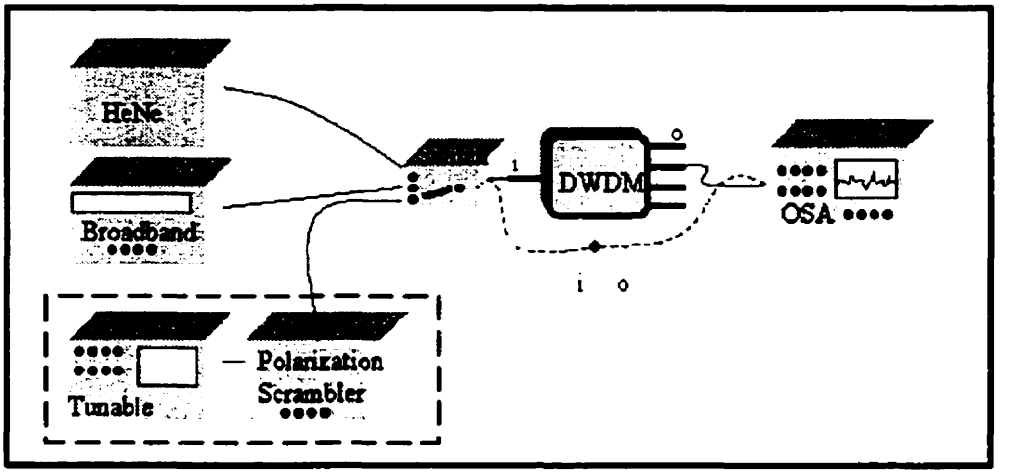

Figure 6-1: Measurement setup. Using HeNe laser the coupling of the fiber to the device at the input and the output is optimized. By using the switch, the broadband is sent to the DWDM device and by using the OSA the response is measured for all the wavelengths. The tunable laser and the polarization scrambler is used for the polarization loss.

6.1 Measurement steps

1. Locate the device on the chuck and turn on the vacuum to hold the chip solid.

2. Position the cleaved fiber labeled as i at the input channel using the positioner underneath the fiber. Maintain the visual contact during the process using the microscope focusing from the top.

3. Turn on the HeNe laser and the switch and confirm that the red light is shining on the input channel from the fiber i. Use the positioner and the microscope to maximize the intensity of the red light in the channel.

4. Connect the output fiber o to the output fiber of switch and confirm that the red light is shining on the output channel under test.

5. Use the microscope and the positioner to maximize the intensity inside the output channel.

6. Once the input and the output channels are coupled to their corresponding fiber under the red light turn the switch to broadband laser. Since the coupling for the two wavelengths are not the same, the true optimization should happen for the wavelength under test.

7. Turn the broadband laser on and turn the switch to have the infrared light going into the device. Since the infrared is invisible, turn on the OSA and connect the fiber labeled *o* to the input of OSA. Use the power in wavelength section and the "linear" option to see the power versus watt units. Use the maximum of this power to optimize the coupling of both input and the output fibers.

8. Once the input power into OSA is optimized the power response is considered as the contaminated response of the channel under test. What is meant by "contaminated" is that the measurement is terms of absolute power and not dB.

9. To obtain the loss of the channel alone, the background loss has to be measured and deducted from the response. To do this, after all the channel measurements are done, connect the input fiber *i* and output fiber *o* to optimize coupling. This power is considered to be the reference power.

6.1 Results

Figure 6-2 shows the output response of the designed and fabricated DWDM in dB. details of the results are shown in table 6.1

Channel	1	2	3	4
Insertion loss (dB)	-11	-10.7	10.8	-11.7
Central wavelength (nm)	1304.27	1306.48	1308.70	1310.84
Cross-talk 0 dB	-38.4	-37.5	-37.1	-38.9
Bandwidth 1dB	0.66	0.69	0.65	0.66
Bandwidth 3dB	0.97	0.99	0.92	1.04
Channelspacing (nm)	-	2.185	2.185	2.15

Table 6.1: Detailed characteristics of measured DWDM.

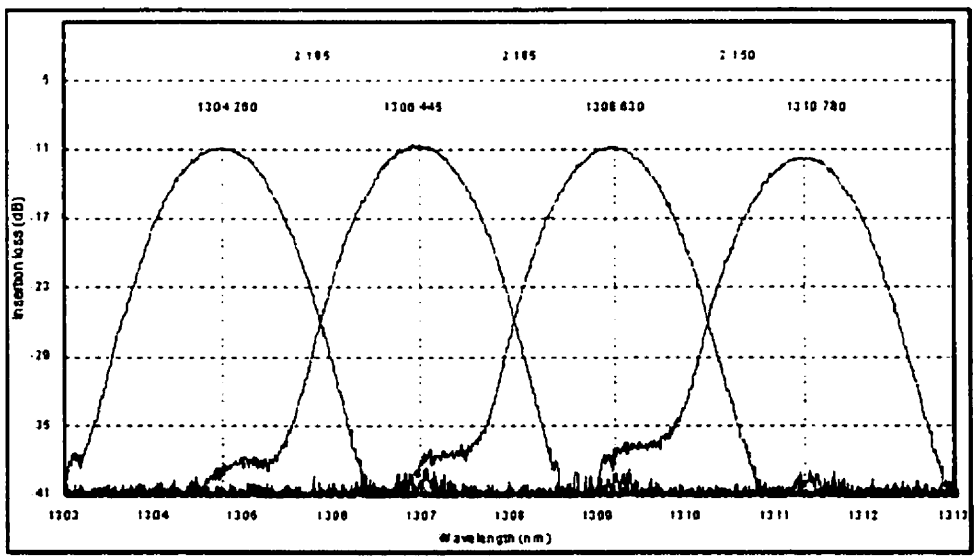

Figure 6-2: Output response of the DWDM measured. The fourth channel has a higher insertion loss which is due to difference in coupling of the output channel with the output fiber.

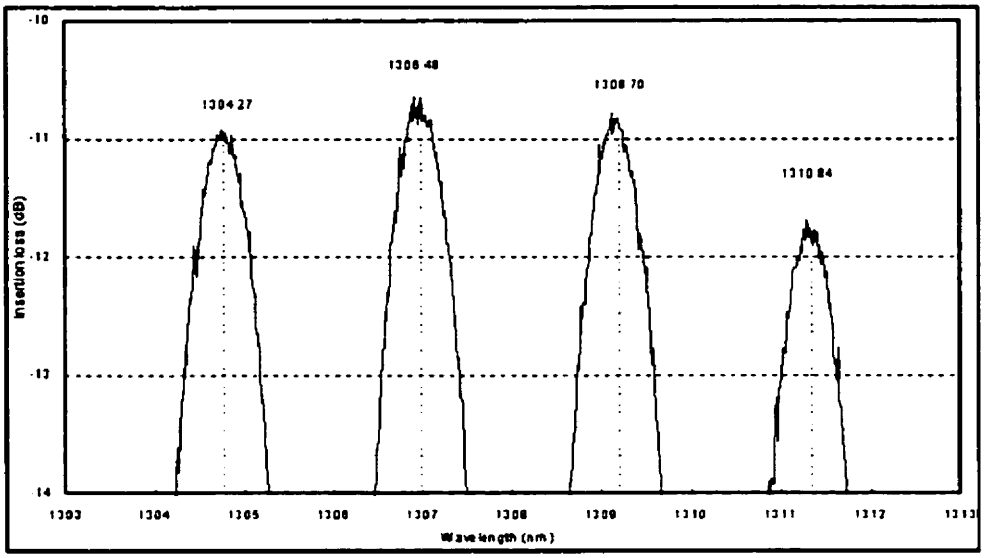

Figure 6-3: The output response of the measured DWDM with an emphasis on the bandwidths.

Figure 6-4 shows the fabrication of a DWDM at the output junction.

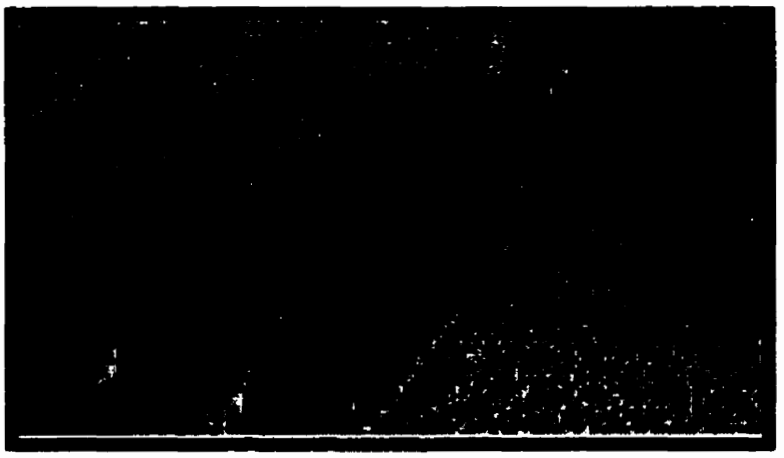

Figure 6-4: A view of the output junction.

Chapter 7

Discussion

A DWDM device was designed, fabricated and tested. The expected and the measured characteristics of the device are shown in tables 7.1 and 7.2, respectively.

The excessive insertion loss of the device after the estimated coupling and design loss of 3 dB is about 8 dB. This excessive loss is due to propagation loss of the structure. The coupling loss between fiber and the channel is calculated to be 0.75 dB, which is considered to be high. This loss is mainly due to missmatch coupling of modes between the fiber and the channel. The main reason why this loss is high is due to lower degrees of freedom. Initially, there are two conditions for the channel waveguide and one open parameter which is the channel width w. the first condition is the requirement that the waveguide should not be able to guide more than two modes. The second condition is that the mode missmatch loss between the fiber and the channel be minimum. Once w is fixed to satisfy the first requirement, the second requirement will not be optimized, as it is seen. The solution to this problem is to exploit one of the advantages of solgel technology, which is flexibility of changing the refractive index of the material. Such an advantage produces one more degree of freedom that can be used to find the channel waveguide that not

only supports no more than two modes but also has a minimum coupling loss with fiber.

As explained in previous chapter, the refractive indices of the both guiding and the cladding materials were estimated by measuring the refractive indices at 1.55 and 0.632 microns. The constant difference between the actual refractive indices and those measured causes a shift in the response. The shift of 6.57 nanometer is due to this reason. This shift corresponds to 0.008 difference between the estimated and actual refractive indices.

The bandwidths, both at 1 and 3 dB, are better than expected. This is due to a better process of film deposition than accounted for. Crosstalk is also about 4 dB better than expected, which is due to good channel fabrication specially the grating region.

All the specifications of the device is acceptable except the shift of the device which is considered more than small. Though it was explained that the shift can be compensated with temperature controller, in order to tune the central channel of this device to 1300.00 nanometer, one should maintain the device at $85.7^{o}C$! However, the problem will be solved for next devices since the actual refractive indices are now known.

One aspect of the DWDM that was never used as condition was the bandwidth of the channels. Such a characteristics is very essential in commercial devices. Predetermined power variation within a bandwidth range is important since it allows a maneuver range in wavelength if the source or the device shift in response for any reason.

Figure 7-1 is the overlap of the two graphs for a visual comparison. The overlap was made by moving the theoretical response in wavelength by 6.57 nm and shifting down in power by a 9.3 dB. It can be seen that the channel spacing and the bandwidths both at 1 and 3 dB are within the expected range. In terms of the future

Theoretical expected specification:

Channel	1	2	3	4
Insertion loss (dB)	-1.70	-1.4	-1.36	-1.52
Coupling loss (dB)	2×0.75	2×0.75	2×0.75	2×0.75
Central wavelength (nm)	1297.7±0.1	1300.0±0.1	1302.2±0.1	1304.5±0.1
Cross-talk 0 dB	≥ -22	≥ -22	≥ -22	≥ -22
Bandwidth 1 dB	0.7 ± 0.1	0.7 ± 0.1	0.7 ± 0.1	0.7 ± 0.1
Bandwidth 3 dB	1.4 ± 0.1	1.4 ± 0.1	1.4 ± 0.1	1.4 ± 0.1
Channel spacing (nm)	-	2.25 ± 0.2	2.25 ± 0.2	2.25 ± 0.2

Table 7.1: Expected specifications of the DWDM

Measured specification:

Channel	1	2	3	4
Insertion loss (dB)	-11	-10.7	10.8	-11.7
Central wavelength (nm)	1304.27	1306.48	1308.70	1310.84
Cross-talk 0 dB	-27.4	-26.3	-26.2	-27.3
Bandwidth 1 dB	0.66	0.69	0.65	0.66
Bandwidth 3 dB	0.97	0.99	0.92	1.04
Channel spacing (nm)	-	2.185	2.185	2.15

Table 7.2: Specifications of the measured DWDM.

work on this particular product. The next photo-mask should be designed with the objective of shifting the wavelengths to the right wavelength for each channel. It is important, therefore, to measure the current device at a measured temperature. This is so because the next device has to measured also at that temperature.

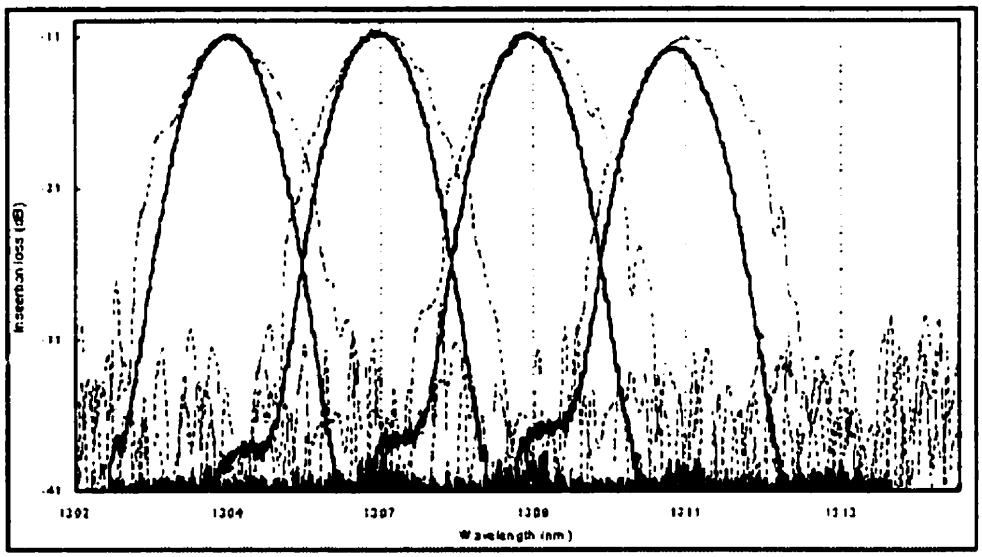

Figure 7-1: A relative overlap of the theoretical and measured output response of the DWDM.

Chapter 8

Conclusion

Sol-gel method of hybrid glass fabrication as an alternative technology for passive optical devices is proposed. A systematic method starting from the chemical solution to the final device is presented. As an illustration an arrayed waveguide grating (AWG) is fabricated using this technology. The method included the production of a photo-mask for obtaining the resolution of waveguide fabrication and a novel method of calculation in prism coupling method.

After a detailed review of the theory behind the design of AWGs, the parameters obtained from the sol-gel method are used towards a design of an AWG. Using the limits and variations in the sol-gel method a perturbation analysis is done to predict the output response of the device under these variations.

The study in tolerance of the design is performed an it is found that the thickness variation affects greatly the crosstalk parameter. In cases where the thickness varies gradually over the grating region, the effect is to broaden the bandwidth. However, in cases where thickness varies stochastically, the effect is to raise the background noise level.

Variations of the channel dimensions , when they occur globally, cause a shift

in the output response. This shift depends on the difference in dimensions of the designed and fabricated channel.

Any change in the sol-gel method causes a change in the refractive index of the material. If such a change is the same for both guiding and the cladding material, the effect is also a shift depending on the difference between the expected refractive indices expected and the actual refractive indices of both materials.

The refractive index of the sol-gel hybrid materials depends greatly on temperature. This characteristic may be exploited to tune the device to the exact central wavelength, by changing the temperature and hence fixing the refractive indices.

The dependence of the output response to all the variations are presented.

The photo-mask of an AWG layout was designed. Using the sol-gel method, the actual device was fabricated and then tested.

The measured results of the fabricated AWG are within the expected and predicted range. Good insertion loss and channel isolations have been achieved.

Moreover, a novel propagation method was presented and applied to extract propagation constants and the output profiles of integrated photonics devices without neither solving the wave equation nor using the paraxial approximation. By approximating the variation of the field to 4th order, this method was applied to the case of a sol-gel multimode planar waveguide. Propagation constants and output profiles are extracted and are in good agreement with the values obtained from the analytical method. The case of a full π circular rotation of a single mode planar waveguide was also illustrated.

Furthermore, a novel, low temperature, sol-gel method of fabrication for inorganic transparent films was proposed. Using this method, single-layer, crack free and transparent silica based films were fabricated. Fabrication of a silica sol-gel film with no doping produced single layer films with good quality. Titanium doped films for the purpose of the refractive index increase was also considered. The re-

fractive index and the loss measurements for silica-titania films was obtained. The infrared absorption spectra for both silica and silica-titania films were presented.

For future work, one is suggested try to produce these devices in more quantity to obtain a better understanding of the average responses and the standard of deviation. It is this standard of deviation that really explains the sensitivity of the device under fabrication and therefore, its fabrication yield.

Other tests involve environmental test. Operating temperature is a standard specification of any device. Operating temperature is the temperature that the device maintains the integrity of the specification. To finalize the study one should also obtain the absorbance of the material in all wavelengths.

Appendix A

Inorganic, single-layer and crack free films for integrated optical devices using sol-gel method of fabrication.

A.1 Abstract

A novel, low temperature, sol-gel method of fabrication for inorganic transparent films is proposed. Using this method, single-layer, crack free and transparent silica based films were fabricated. Fabrication of a silica sol-gel film with no doping produced single layer films with an average roughness of about 0.5 nm, for a surface area of $10\mu m^2$ was obtained. Titanium doped films for the purpose of the refractive index increase is also considered. The refractive index for silica-titania films was 1.510 ± 0.001. The infrared absorption spectra for both silica and silica-titania films are presented. The results suggest that the densification between 100^oC and 150^oC

produces little change in quality of the material.

A.2 Introduction

The sol-gel method is a low-temperature solution method for glass preparation based on polymerization of hydrolyzed metal alkoxides [38],[39]. The hydrolysis and condensation reaction driving the polymerization continues to form a porous gel extended throughout the reaction vessel. The porous gel is then dried and densified to form glass.

In recent years, sol-gel process has been the subject of considerable interest due to its control over the intrinsic properties of the material, low cost of fabrication and ease of application.

Among conventional methods of depositing optical materials like sputtering [40, 41], chemical vapor deposition [42] and flame hydrolysis [43], sol-gel technology has become one of the rapidly growing methods to fabricate thin transparent films with good optical qualities. One of its advantages in optical integrated devices is its power of manipulation over the optical properties of the material for both active [44] and passive [45] devices. Such an intrinsic change in the material is commonly achieved by the use of the proper precursors [46, 47] or dopants [48], laser densification and photo-induction.

Incorporating both the organic and inorganic precursors together in hybrid sol-gel materials has lead to significant progresses in integrated optics. There have been recent reports on integrated optical devices where photo-induction and laser densification have been used. However, as mentioned above, these materials also have high absorption loss in 1550 nm region and, furthermore, fluorescence at such wavelength region is yet to be achieved. The main problem is that hybrid materials do not survive temperatures much higher than 200°C.

Therefore, as far as the absorption loss and fluorescence is concerned, due to their high temperature tolerance, inorganic sol-gel films seem to be a good alternative to their corresponding hybrid glasses.

Much effort has been invested in production of inorganic sol-gel films with thickness above 2 microns in order to support guiding modes for 1550 nm light. One main obstacle, in development of inorganic sol-gel materials, has been the cracking effect [49]. This effect is believed to be caused mostly by the departure of water and other solvents which leaves the fragile silica network hallow locally, leading the matrix to collapse during the condensation phase. One alternative way to resolve this problem has been the multi-deposition process [50] where a film of about 0.060 to .600 μm film is deposited and subsequently annealed before the next deposition. Although such a method had lead to fabrication of film thickness higher that 10 μm [46], it does not seem to be a practical approach because of various reasons. For each time of deposition, the probability of burying dust particles into the film is increased. Since each deposition creates a certain amount of non-uniformity over the surface, the final surface is considerably non-uniform. Further more, the final refractive index is not the same as the one obtained from a single deposition due to non-linearity of condensation process [46].

As hindered above, one main reason for the crack phenomenon may be the departure of the excessive amount of solvent during the densification phase. One simple way to reduce the solvent can therefore be to extract much of initially added solvent before casting the film. With the use of solvent extraction, this paper proposes a new sol-gel method of fabrication, for inorganic silica derived and crack free materials, whose single cast can produce films with thickness more than 2 μ m.

in A.3 the method of solvent extracion is applied to create a silica based film from TEOS. Section A.4 represents the application of the same method to create

a titanium doped glass with higher refractive index. The comparative result of the infrared absorption spectrum for both glasses is given in A.5.

A.3 Silica films

The main procedure involves the fabrication of silica films derived from tetraethoxylsilane (TEOS), purchased from Hls America Inc., as the only precursor. For this process, the molar ratio of 1:4 (TEOS:water) and .098N HCl, purchased from Aldrich, was used as the source of water and H^+ catalyst. Ethyl alcohol (ethanol) 95% was chosen as the solvent with molar ratios of TEOS:ethanol equal to 1:24. At room temperature, TEOS, water and ethanol, with their corresponding molar ratios, were mixed and stirred for 5 hours under closed environment by maintaining the solution inside a vial.

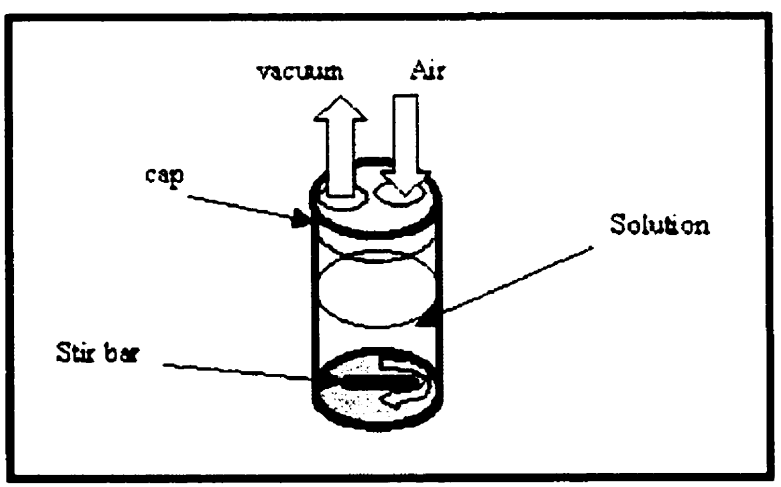

Figure A-1: By creating an airflow during the solution state a great deal of the solvent is evaporated before gellation.

Then, the vial's plastic cap was reconstructed to direct the airflow described

above by making two openings through it. One of these openings was connected to the vacuum pipeline of the laboratory while the other accommodated the inflow of air. The process of the solvent extraction required about 10 to 15 minutes. At this point, the solution was viscous and white light transparent. The final product was then filtered and spin-casted on the proper substrate. During the process of rapid extraction via airflow, due to thermodynamic properties of the solvent, the solution's temperature drops. This physical response of the solution is a welcome result as it decreases the rate of densification. Once the desired gel viscosity is attained, the solution is filtered through a 0.2 μ m filter and spin casted over the proper substrate. Using the above procedure, three silica gel films with constant thickness were prepared. All three films were casted on double polished silicon wafer, for infrared (IR) absorption measurements, and heated for 15 minutes, each one with a different temperature, namely, 50°C, 100°C and 150°C. The main purpose of the heat treatment was simply to density the film and extract the solvent without accelerating any further reaction. Since starting from 150°C, the quality of the films is altered by reduction of OH group within the silica matrix, this temperature was chosen as the maximum temperature.

A.4 Silica-titania films

By employing the procedure for silica sol-gel glasses presented above, one is now able to use metal alkoxides such as titaniumisopropoxide (TPOX), as dopant, in order to increase the refractive index. A solution of TEOS, water, ethanol with the molar ratios of 1:4:24 (TEOS: water: ethanol), as before, was made inside a vial and kept stirring for 5 hours. The precursor TPOX, purchased from Johnson Matthy Cat. Company, is then added, drop by drop while stirring, to the solution until the molar ratio of TEOS: TPOX equal to 1:0.186 was obtained. Solution was

then left stirring vigorously until the precipitated TiO2 disappeared. This period required about 5 to 10 minutes. The solution was, then, placed and kept stirring under a rapid airflow for solvent extraction, until the desired viscosity was obtained. Finally, the solution was filtered and spin-casted immediately. The solutions that aged, for even as little as 30 minutes, produced unacceptable films. Three silica-titania films were prepared using the above procedure. All three were heat treated for 15 minutes. Each film, like before, was baked at 50°C, 100°C and 150°C.

A.5 Results

There were little changes in infrared absorption spectra, for different temperatures, for both cases of silica and silica-titania films.

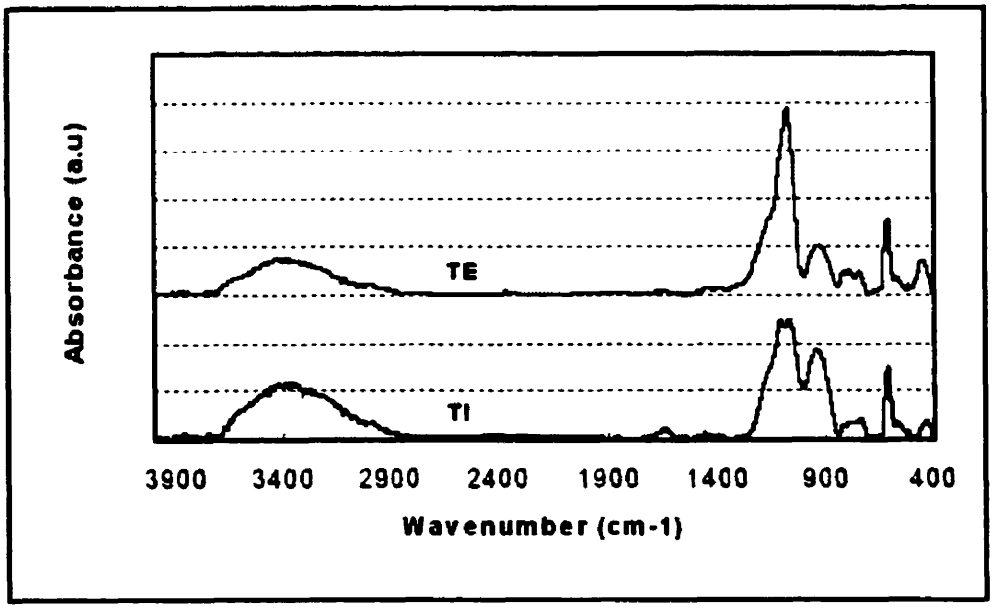

Figure A-2: The IR absorption of both glasses are almost the same except for the 1100 cm^{-1} and 3400cm^{-1} region.

Figure A-2 shows the IR absorption spectrum of the solution made only from TEOS (marked TE) and the Titanium doped films (marked TI), both heated at 100°C for 15 minutes. The main changes happen in the 850-1650 cm^{-1} region. Figure A-3 represents this region. The Si-O-Si asymmetric vibrational mode is clearly distinguishable at 1064 cm^{-1} for the case of silica film. The band around the 920-930 cm^{-1} corresponds to Si-O-Ti vibrational mode [?].

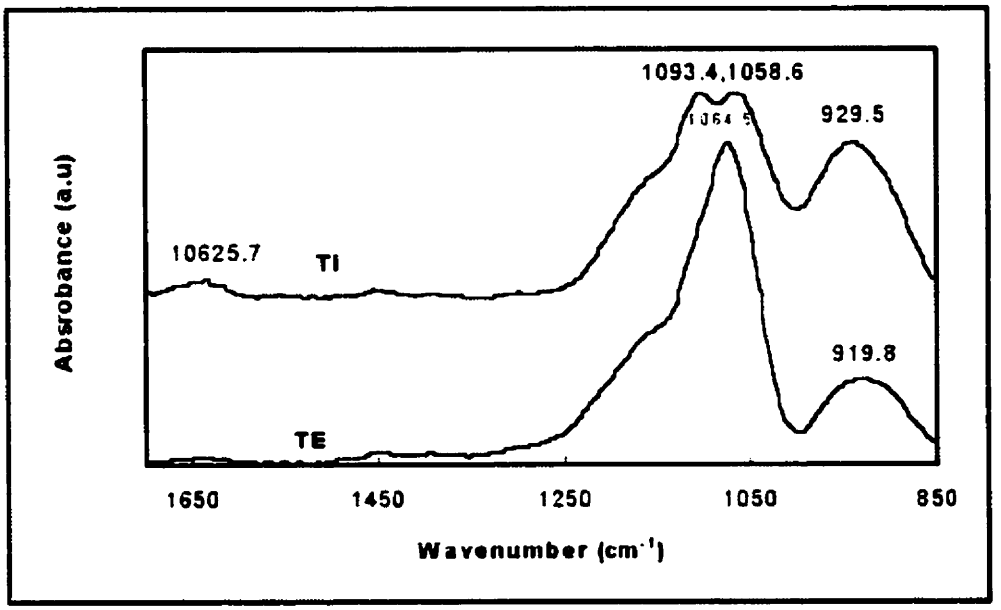

Figure A-3: The double-pick is the evidence of the Si-O and Ti-O bonds.

It maybe interesting to note that the pick for this band shifts to about the same region after the sample was heated to 400°C. The reduction of Si-O-Si in titanium film can be seen around the 1100 cm^{-1}.

It is also seen in figure A-4 around the 780 cm^{-1} band, which is the symmetric vibrational mode for SiO2, and, around the 450 cm^{-1} band, which correspond to the bending modes for SiO2. The peak at 609.4 cm^{-1} band may be assigned to vibrational mode of cyclic silicate structure [21]. The reason for such an intense

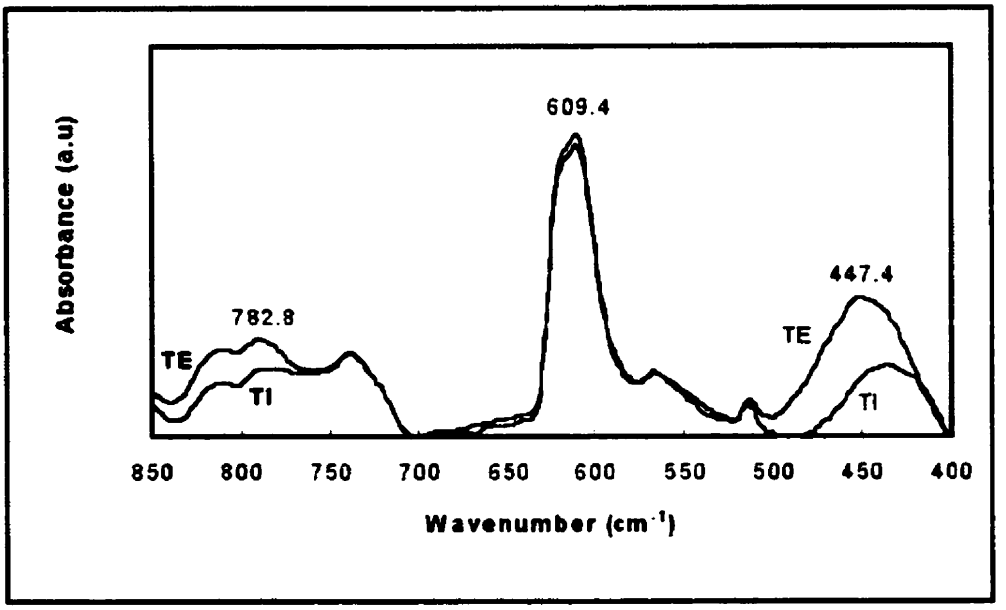

Figure A-4: The cyclic silicate structure is untouched after titanium doping of the TEOS.

peak at low temperatures of around 100°C may be the formation of these cyclic structures before the gellation, mainly during the sol phase. The almost-equal intensity of the peak for both silica and silica-titania films at 609.4 cm^{-1} may also suggest that these structures where already present in the solution before even adding the titanium. If not, addition of titanium should have altered the number of these structured. The peak around the 3400 cm^{-1} in figure A-5 corresponds to the O-H stretching mode. The difference in the peak intensity could be due to the existence of the TiO-H in the film.

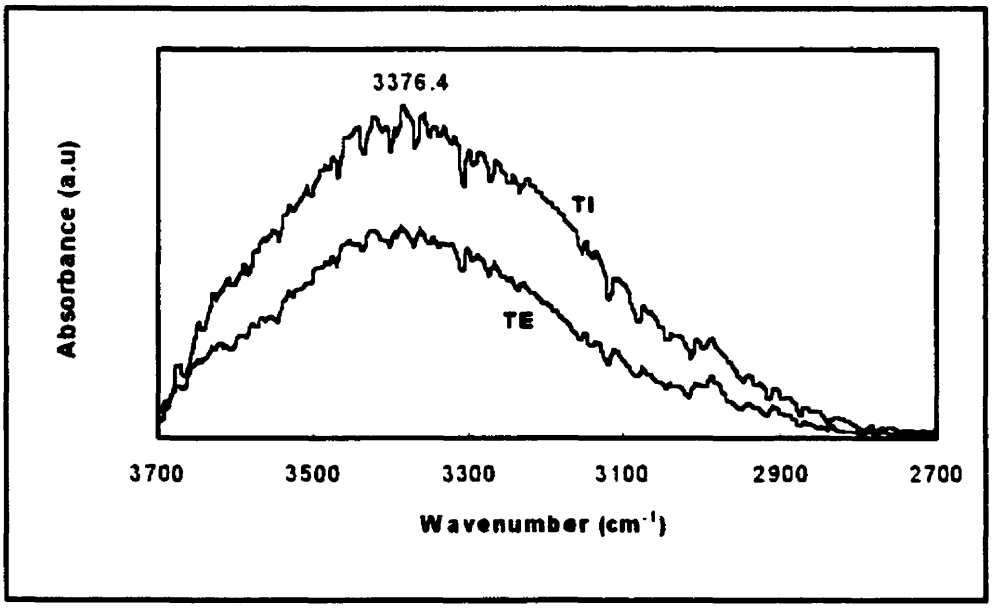

Figure A-5: In the 3400cm^{-1} region titanium doped sol-gel has higher absorption, which is unusual.

Figure A-6 shows the surface of the silica gel film spin casted on a micro slide glass, heated in 100°C for 15 minutes, using atomic force microscopy. The range of the view is 10 × 10 microns and roughness variation of the surface for this range is 0.53 nm.

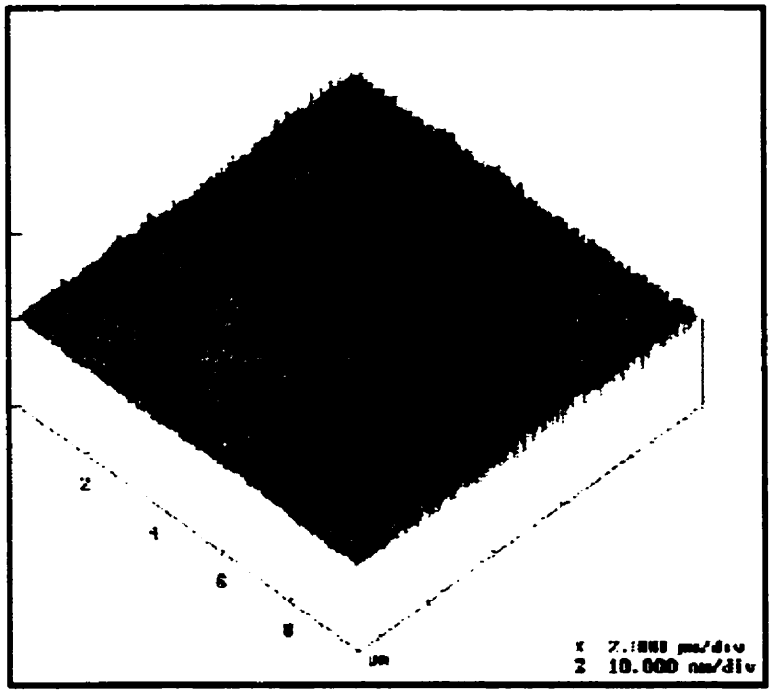

Figure A-6: a 10 × 10μm of surface of the silica-titania film had a variation of the surface equal to 0.53 nm.

A.6 Conclusion

By extracting the excessive organic solvents from the inorganic precursor solutions, before the film deposition, single layer thin films of thicker than 2 microns were obtained. The measurements of the surface roughness suggest the method to be a good starting root to produce good quality glasses for photonics devices. One main disadvantage, however, is the sensitivity of the film thickness to remaining solvent in the solution, before spin casting. The main source of this disadvantage is the way the solvent was extracted. Airflow, as it was used, seems rather incomplete unless it provides control over the quantities being extracted. For further work, therefore, one might consider the alteration of this method in order to have control over the film thickness.

Appendix B

Analysis of integrated photonics devices by a new propagation method

This appendix was published in [51]

B.1 Introduction

Presently, in order to design optical devices a common approach has so far been to solve the Maxwell's equations to obtain propagation constants and the output profiles required to define the device's performance. A simplified example of these devices is an optical waveguide whose performance is defined by the propagation constants and the output profiles. Such an approach creates few obstacles: 1) Whether the equation does not have any analytical solution or the numerical solution may require an enormous amount of time. 2) In cases where many devices are at each other's vicinity and cause mutual perturbations on each other's fields,

solving the equations separately for each device does not seem ideal since the perturbations have been omitted. And 3), In situations where only the preview of the output and not necessarily the propagation constants of the device is needed, the present method still forces one to solve the Maxwell's equations, find the propagation constants and finally obtain the output [52],[53].

Keeping the above obstacles in mind, the purpose of this paper is to present a propagation method that uses the wave equation in its differential form to describe the point wise variation of the electric field inside a device. Using this method one can consider the complete integrated system at once to include the perturbations caused by nearby devices. It also allows one to view the total intensity of the field for even a multimode waveguide without obtaining any of the propagation constants. Finally, the most important advantage would be to obtain the propagation constants by analyzing the field's variation without solving the wave equation.

The remaining of this paper is as follows. Section two reviews the fundamental principle of the second order difference using the forward and backward Taylor expansion. Furthermore, it uses the second order difference in conjunction with the wave equation to obtain the Wave Propagation Method (WPM). In section three, WPM is applied to the case of a planar multimode slab waveguide where the numerical results are compared with the values obtained from the analytical method. For section four, the application of WPM for the case of a full pi circular rotation of a slab waveguide is considered as an illustration for its capability of simulating the optical devices in polar co-ordinate system. Some possibilities for future investigations are also presented in section five.

B.2 Wave propagation method

For sufficiently small z in Cartesian co-ordinate system the forward and backward Taylor expansion of the field at (x, z) and $(x, -z)$ around $(x, 0)$ to fourth order gives

$$E(x,z) = E(x,0) + z\frac{\partial E(x,0)}{\partial z} + \frac{z^2}{2!}\frac{\partial^2 E(x,0)}{\partial z^2} + \frac{z^3}{3!}\frac{\partial^3 E(x,0)}{\partial z^3} + (0) \qquad \text{(B.1)}$$

and

$$E(x,-z) = E(x,0) - z\frac{\partial E(x,0)}{\partial z} + \frac{z^2}{2!}\frac{\partial^2 E(x,0)}{\partial z^2} - \frac{z^3}{3!}\frac{\partial^3 E(x,0)}{\partial z^3} + (0)\,, \qquad \text{(B.2)}$$

respectively. For simplicity, through out the paper, for any function f, the notation $\frac{\partial^n f(x,a)}{\partial z^n}$ implies $\frac{\partial^n f(x,z)}{\partial z^n}|_{x\to a}$. The main approximation is to neglect the terms higher than the third. Therefore, z maybe taken larger, as long as the field varies along the z-axis slowly enough, so that the product of its fourth and higher derivatives with the incrementing parameter z of the corresponding power in the expansion becomes negligible. Adding (B.1) and (B.2) and translating along the z-axis by z gives

$$(x, 2z) = 2E(x,z) - E(x,0) + z^2\frac{\partial^2 E(x,z)}{\partial z^2}. \qquad \text{(B.3)}$$

The above equation could have simply been obtained from the definition of the second derivative. However, the present approach shows limits and the approximations described above. Equation (B.3) is a second order difference which can be independently used for solving many second order differential equations such as Poisson's equation numerically [54]. As an example of a particular case of Poisson's

equation consider the co-ordinate independent wave equation

$$\left[\nabla^2 - \frac{\partial^2}{\nu^2 \partial t^2}\right] E = 0 \tag{B.4}$$

where ν is the speed of the wave. The above wave equation can be taken as the approximation of the exact differential equation obtained from the Maxwell's equations with the scalar electric field, E, in a medium with a slowly varying refractive index. The operator ∇^2 in two-dimensional Cartesian and polar co-ordinate system is defined as

$$\nabla^2(x, z) \equiv \frac{\partial^2}{\partial x^2} + \frac{\partial^2}{\partial z^2} \tag{B.5}$$

and

$$\nabla^2(r, \phi) \equiv \frac{1}{r}\frac{\partial}{\partial r}\left[r\frac{\partial}{\partial r}\right] + \frac{1}{r^2}\frac{\partial^2}{\partial \phi^2}, \tag{B.6}$$

respectively. Through out this paper, let z and ϕ be the incrementing parameter.

Replacing the second order derivative in (B.3) with its equivalent from the wave equation (B.4), one obtains the algorithm for the time dependent WPM in Cartesian co-ordinate system

$$E(x, 2z; t) = 2E(x, z; t) - E(x, 0; t) - z^2\left[\frac{\partial^2 E(x, z; t)}{\partial x^2} - \frac{\partial^2 E(x, z; t)}{\nu^2 \partial t^2}\right]. \tag{B.7}$$

For the case of polar representation, equation (B.7) becomes

$$E(r, 2\phi; t) = 2E(r, \phi; t) - E(r, 0; t) - \phi\left[r^2\frac{\partial^2 E(r, \phi; t)}{\partial r^2} + r\frac{\partial E(r, \phi; t)}{\partial r} - r^2\frac{\partial^2 E(r, \phi; t)}{\nu^2 \partial t^2}\right]. \tag{B.8}$$

Note that for both equation (B.7) and (B.8) the term inside the parenthesis satisfies

the wave equation (B.4). If the first two terms on the right hand sides are chosen so that they would also satisfy the wave equation, the linearity of above algorithm ensures that the field throughout the x-z plane is a propagating wave.

In Cartesian co-ordinate system for a sinusoidal optical wave with the wave number k propagating in an optical medium described by the refractive index, n, defined as

$$n = n\,(x, z)\,, \tag{B.9}$$

the algorithm (B.7) would then describe the variation of the time independent complex amplitude

$$\Phi(x, z) = E(x, z; t)e^{inktc}, \tag{B.10}$$

with the imaginary unity number i, in a more simplified equation of

$$\phi(x, 2z) = 2\Phi(x, z) - \Phi(x, 0) - z^2\left[\frac{\partial^2\Phi(x, z)}{\partial x^2} + k^2n^2(x, z)\Phi(x, z)\right]. \tag{B.11}$$

The irrelevance of the input profile to the propagation constants of the device for any particular wavelength means that one has the freedom to choose the input profile. For this paper the input field at the first initial two points is evaluated by

$$\phi_m = A\exp\left[-jnk(|x - \frac{w}{2}|\sin\theta_m + z\cos\theta_m)\right] \tag{B.12}$$

which describes the projection of a plane wave onto the waveguide's plane of normal cross-section figure B-1. The parameter θ is the angle between the two planes, which is equal to the angle of incident. As shown in the figure For $\theta = \theta_m$, the mth mode is excited. Parameter A is any constant and w is the width of the

waveguide.

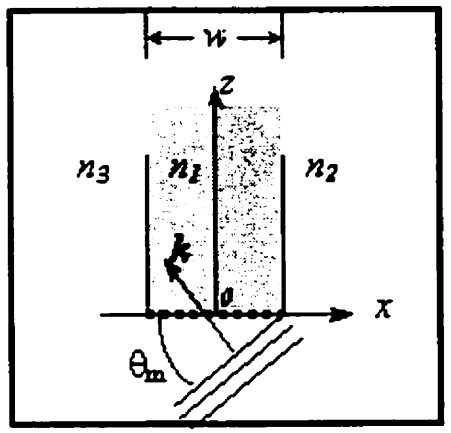

Figure B-1: Since the field moves along the incrementing z, the chosen input plane wave field is projected on the plane of cross-section (dashed line).

Once the field f at $(x, 0)$ and (x, z) is evaluate, the field at $(x, 2z)$ can be found by (B.11). Based on the same algorithm, using the field at (x, z) and at $(x, 2z)$, the filed at $(x, 3z)$ is found. This algorithm is repeated along the z-axis for all the incrementing z values until the desired distance is attained.

B.3 Analysis of a planar sol-gel multimode waveguide as a simple photonics device

After obtaining the field along the waveguide, one can easily find the propagation constants for different modes. The process of finding the propagation constants for this case is as follows. First, excite the modes separately by varying the incident angle. Then, find the distance, λ^m, for each mode m for which the field along the waveguide has the same phase. The propagation constant, β_m, for each mode m

would therefore be

$$\beta_m \equiv \frac{2\pi}{\lambda^m} \tag{B.13}$$

.

To bypass the problem of numerical instability, the simple statistical approach is applied. To identify the angle, θ_m, that excites the mode m, one can vary the incident angle and find the ratio of accumulated mode numbers to the number of samplings, (average mode number) in a certain region. Once this average becomes the integer m, the corresponding angle is the angle whose β is the propagation constant for that mode. As an example, consider the propagation of a light with 1.55 microns wavelength in an optical medium defined as

$$n(x,z) = \begin{cases} 1, & x < -3 \\ 1.481, & -3 \leq x \leq 3 \\ 1.444, & x > 3 \end{cases} \tag{B.14}$$

which is the specification of a 6 microns sol-gel film spin-coated on a silica substrate for the described light ([55],[56] and [57]). To omit the perturbation of the field at the entry the analysis region for finding the incident angle for different modes is chosen far from the input, namely at 70 to 100 microns, by advancing along z using 0.01 microns step. The x-axis is considered from -50 to +50 microns and divided into 150 grids. Figure B-2.a shows the intensity profile of the waveguide within the designated range for the zero incident angle. The incident angle is then incremented from zero by 0.01 radian steps until the mode number average becomes an integer for first (figure B-2.b), second (figure B-2.c) and the third (figure B-2.d) mode. Figure B-3.a shows the mode number average against the incident angle. When the mode average number is 0, 1 and 2, the incident angles are 0.02, 0.135 and 0.235 radian respectively. Figure B-3.b presents the propagation constants

	[WPM]	[WPM]	[Analytical]	[Analytical]
m	θ_m (rad)	$< \beta_m > (\mu m)^{-1}$	θ_m (rad)	β_m $(\mu m)^{-1}$
0	0.02	5.988	.07	5.987
1	0.135±0.015	5.942	0.149	5.937
2	0.235±0.015	5.875	0.218	5.861

Table B.1: comparing the propagation constants averaged over the first 2400 microns and their corresponding incident angles, obtained by WPM method, with the same values obtained by solving the wave equation on the cross-section of the slab. The values are rounded to equal decimals.

measured along z, by shining the light with the incident angle of first, second (figure B-3.c) and the third (figure B-3.d) mode.

Table B.1 compares the average values of the propagation constants for all three modes and their corresponding incident angle using WPM method with the results obtained by solving the equation on the cross-section of the slab waveguide for all three modes.

Figure B-4 shows the intensity profiles of the field at 81 and 85 microns from the entry. Once there are more than one modes are present, the total intensity is optical path dependent. The key for the variation of the total intensity along the waveguide lies in the fact that different modes propagate with different speed.

B.4 Application of a WPM to a full pi circular rotation of a single mode slab waveguide

For the light wave used in previous section, by using (B.8) and (B.10), the time independent WPM in polar form becomes

$$\Phi(r,2\phi) = 2\Phi(r,\phi) - \Phi(r,0) - \phi^2\left[r^2\frac{\partial^2\Phi(r,\phi)}{\partial r^2} + r\frac{\partial\Phi(r,\phi)}{\partial r} + k^2n^2(r,\phi)r^2\Phi(r,\phi)\right]. \tag{B.15}$$

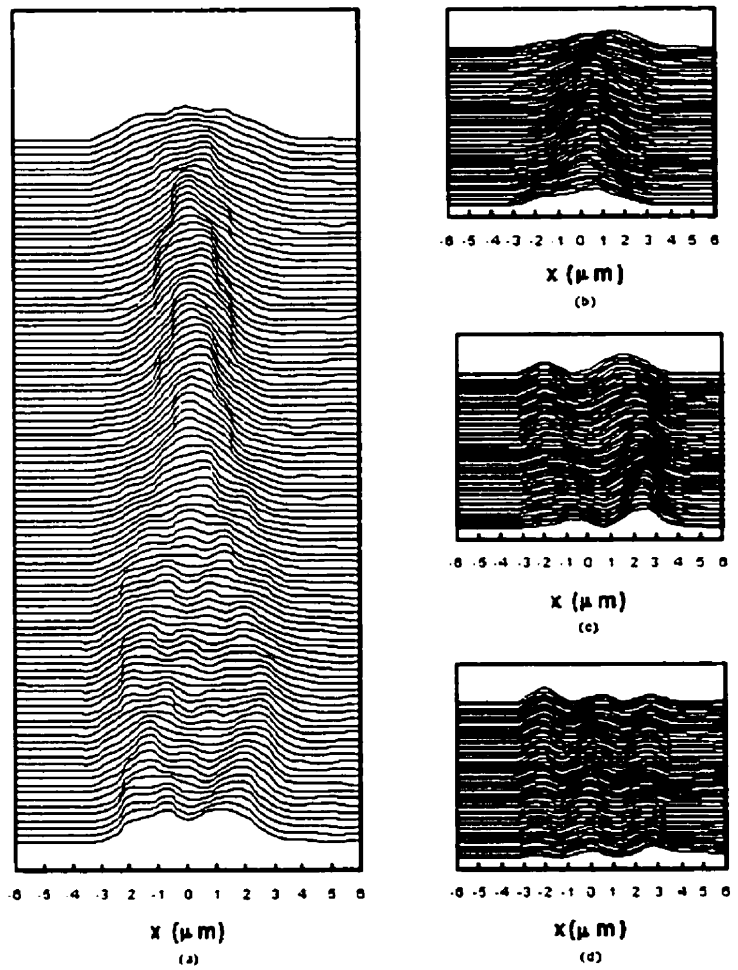

Figure B-2: A plane wave entering a 6 microns slab waveguide perpendicular to the incident excites all possible modes. Far from the perturbations at the entry, the total field is analyzed between the 70-100 microns (a). By varying the incident angle the average mode number within the same 70-100 microns region, becomes an integer for first (b), second (c) and the third mode (d).

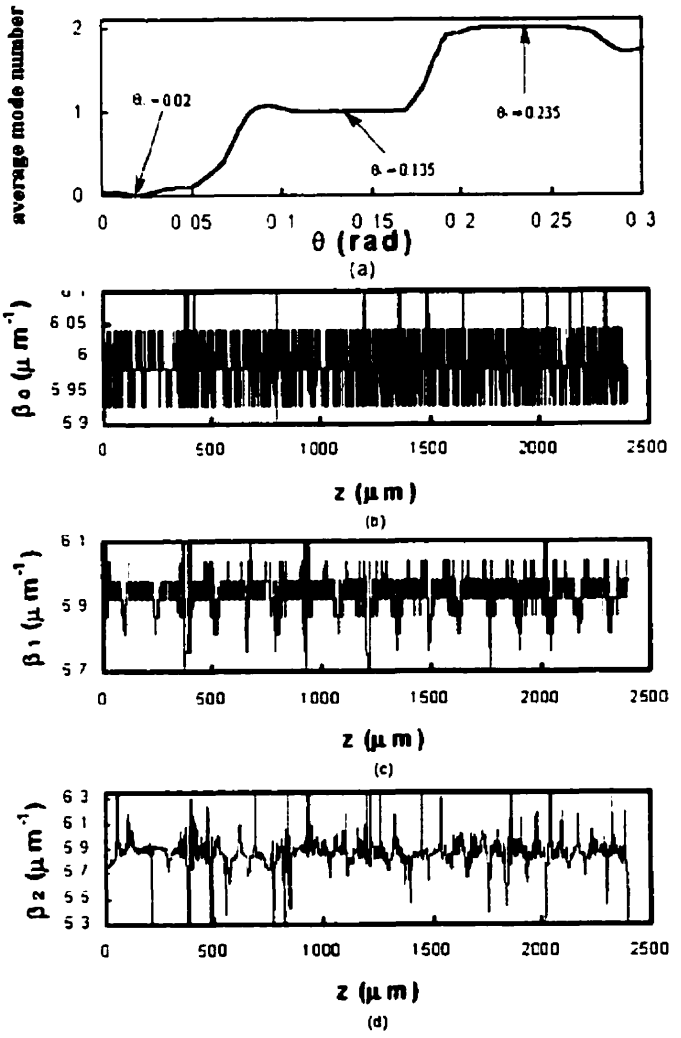

Figure B-3: By varying the angle at the input different modes are excited (a). At $\theta = \theta_m$ the average mode number within the first 70-100 microns becomes a constant integer. The average propagation constant $< \beta_m >$ is measured for the first 2400 microns for first (b), second (c) and the thirs mode by entering a plane wave with the corresponding incident angle. The average $< \beta_m >$ is then found to be 5.988, 5.942 and 5.875 $(\mu m)^{-1}$, respectively.

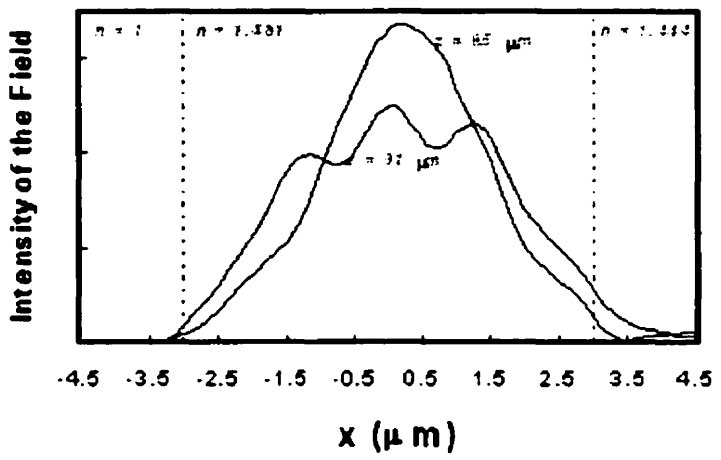

Figure B-4: When more than one mode are propagating, the total intensity along the waveguide is optical path dependent. The different intensity profiles of the slab waveguide at 81 and 85 microns is shown.

For the case of a 3 microns slab waveguide along a path described by a circle with the radius r_0, n is defined as

$$n(r,\phi) = \begin{cases} 1.5, & r < r_0 - 1.5 \\ 1.52, & r_0 - 1.5 \leq r \leq r_0 + 1.5 \\ 1.5, & r > r_0 + 1.5 \end{cases} \tag{B.16}$$

One can now apply the polar WPM to obtain the output intensity profile without needing to obtain the propagation constants. Whenever the displacement vector of the waveguide makes a none-zero angle with the mode propagation vector locally (figure B-5), the angle should be taken into account. For the above case, the angle between the two vectors is equal to the incrementing angle ϕ. At each point the field's phaser itself approximated to ϕ^4 is assumed to be

$$\exp(-jn\mathbf{k}\cdot\mathbf{l}) \approx \exp(-jnkl)\exp(+jnkr\frac{\phi^3}{2}) \tag{B.17}$$

where $\mathbf{l}$ is the displacement vector or the infinitesimal variation of the position vector $\mathbf{r_0}$ of the waveguide. The first term describes the field propagating parallel to the local displacement vector of the waveguide. The second term is the correction for the angle between $\mathbf{l}$ and $\mathbf{k}$. The second exponential term on the right hand side is then multiplied to the local propagating field as a correcting factor. For this simulation, r is considered from 120 microns from each side of the center of the slab's cross-section and it is divided into 300 grids. The parameter ϕ ranged from 0 to π with incrementing steps of $\frac{0.1}{r_0}$. Figure B-6 shows the different output intensity profiles for different radii confirming that the amount of power radiated out of the waveguide is the most for the smallest radius.

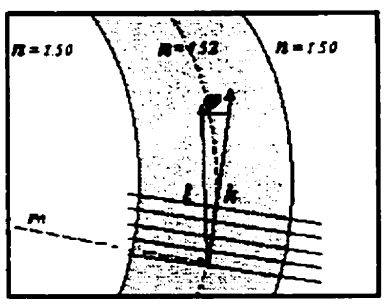

Figure B-5: along the curviture of the waveguide, the displacement vector $\mathbf{l}$ makes a non-zero angle with the propagation vector, $\mathbf{k}$, of the local field.

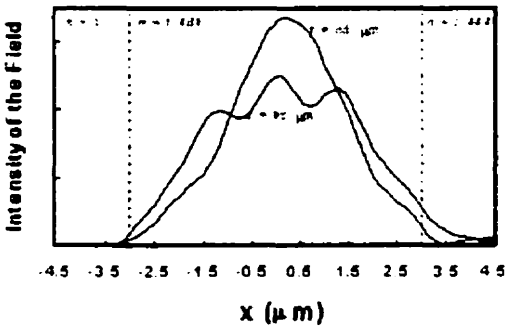

Figure B-6: For the same [plane wave] input profile, different output intensity profiles are illustrated for different radii for the case of a full π circular roatation of a single mode slab waveguide of 3 microns. The center of the circle is towards the decreasing r for each case of r_0.

B.5 Conclusion

Wave Propagation Method was presented as a novel propagation method to obtain propagation constants and the total output profile of an integrated photonics device without solving the wave equation. This method was applied to the case of a planar sol-gel waveguide and the results were compared with those obtained from the analytical method. The algorithm may also be conveniently used in polar representation. The case of a full pi circular rotation of a single mode slab waveguide was also considered in polar co-ordinate system. Since the algorithm does not require one to solve the wave equation, the complexity of the refractive index profile becomes less bothersome. Therefore, for future studies, one may consider the application of this method for the case of the exact differential wave equation of the field obtained from the Maxwell's equations instead of its approximated version used in this paper. Finally, it is difficult not to wonder if this method could also use the same exact wave equation of the field at the presence of charge and current

densities. Such an analysis would indeed have great and immediate contributions in integrated micro wave circuits studies.

Bibliography

[1] D. Wisely, 32 channel wdm demultiplexer with 1 nm channel and 0.7 nm bandwidth, *Electronic Letters* 24 (1991), no. 7, 520–521.

[2] M. K. Smit, New focusing and dispersive planar componant based on an optical phased array, *Electronics Letters* 24 (1988), no. 7, 385–386.

[3] A. R. Vellekoop and M. K. Smit, Low-loss planner optical polarization splitter with small dimensions, *Electronics Letters* 25 (1989) 946–947.

[4] A. R. Vellekoop and M. K. Smit, A polarizaion indepenedent planner wavelength demultiplexer with small dimensions, in *Proc. Euro. conf.*

[5] K. Okamoto, K. Syuto, H. Takahashi, and Y. Ohmori, Fabrication of 128-channel arrayed-waveguide grating multiplexer with 25 ghz channel spaceing, *Electronics Letters* 32 (1996), no. 16, 1474–1475.

[6] H. Takahashi, I. nishi, and Y. Hibino, 10 ghz spacing optical frequency division multiplexer based on arrayed waveguide grating, *elctronics Letters* 28 (1992), no. 4, 380–382.

[7] H. Takahashi, S. suzuki, K. Kato, and I. Nishi, Arrayed-waveguide grating for wavelength division multiplexer/demultiplexer with nanometer resolution, *electronics Letters* 26 (1990), no. 2, 87–88.

[8] J. B. D. Soole, M. R. Amersfoort, H. P. Leblanc, N. Andreadakis, A. Rajhel, C. Caneau, M. A. Koza, R. Bhat, C. Youtsey, and I. Adesida, Polarization-independent inp arrayed waveguide filter using square cross section waveguides, *electronics Letter* 32 (1996), no. 4, 323–324.

[9] H. Bissessur, p. Pagnod-Rossssiaux, R. Mestric, and B. Martin, Extremely small polarization independent phasd array demultiplexers on inp, *IEEE Photon. Technol. Lett* 8 (1996) 554–556.

[10] L. H. Spiekman, F. P. G. M. van Ham, A. Kuntze, J. W. Pedersen, P. Deemester, and M. K. Smit, Polarization-independent inp-based phased array wavelengtth demultiplexer with flatten wavelength response, in *Proc. 20th Euro. Conf. Optical Communication, Firenze, Italy*, 25-29, pp. 759–762. (Sept, 1994).

[11] L. H. Spiekman, M. R. Amersfort, A. H. de vreede, A. K. F. P. G. M. van Ham, J. W. Pedersen, P. Demeester, and M. K. Smit, Design and realization of polarization independent phased array wavelength demultplexers using different array orders for te and tm, *J. Lightwave Technologies* 14 (1996) 991–995.

[12] A. R. Vellekoop and M. K. .smit, Four channel integrated optic wavelength demultiplexer with weak polarization dependence, *J. Lightwave technologies.* 9 (1991), no. 3, 310–314.

[13] H. Yamada, K. Takahashi, Y. Inue, Y. Hibino, and M. Hroiiguchi, 10 ghz spaced arrayed waveguide grating multiplexer with phase errorocompensating thin film heaters, *electronics. Letters* 31 (1995), no. 5, 360–361.

[14] Y. Innoue, Y. Ohmori, M. Kawachi, S. Ando, T. Sawada, and H. Takahashi, Polarization mode converter with polymide halfwave plate in silica-based planar lightwave circuits, *IEEE Photon. Technol. Lett* 6 (1994) 626–628.

[15] K. Okamoto, M. Ishii, Y. Hibino, and H. Toba, Fabrication of un equal channel spacing arrayed waveguide grating multiplexer modules, *Electronics Letters* 31 (1995), no. 17, 1464–1465.

[16] C. A. Msteenberger, C. van Dam, A. H. de Vreede, L. Shi, J. W. Pedersen, P. Demeester, and M. K. Smit, Integrated 1 ghz 4-channel inp phasar based wdm-receiver with si bi-polar frontend array, in *Proc. euro. Conf. Opt. Coomunication, Brussels*, 17-21, pp. 211-214. (1995).

[17] A. Rigny, A. Bruno, and H. Sik, Multigrating method for flattened spectral response wavelength multi/demultiplexer, *electronics Letters* 33 (1997), no. 20, 1701–1702.

[18] K. Okamoto and A. Sugita, Flat spectral response arrayed-waveguide grating multipplexer with parabolic waveguide horns, *Electronics Letters* 32 (1996), no. 18, 1661–1662.

[19] L. L. Hench, J. K. West, J. K. Zhu, and B. F. Ochoa, Gel-silica hybrid glass, in *Proc. SPIE*, vol. 1328, pp. 230–240.

[20] D. R. Ulrich, Prospects for sol-gel process, *J. Non-Cryst. solids* 121 (1990) 465–479.

[21] C. J. Brinker and G. W. Scherer, *Sol-gel Science.* (1990).

[22] I. Sorek, R. Reisfeld, I. finkelstein, and S. Ruschin, Active glass waveguides prepared by the sol-gel mehod, *Optical Materials* 4 (1994) 99–101.

[23] L. Yang, S. S. saavedra, N. R. Armstrong, and J. Hayes, Fabrication and characterization of low-loss sol-gel planer waveguides, *Anal. Chem.* 66 (1994) 1254–1263.

[24] R. R. A. Syms and A. S. Holmes, Deposition of thick silica-titania sol-gel films on si substrate, *J. Non-Cryst. Solids* 170 (1994) 223–233.

[25] Z. Zhang and H. C. Zeng, Catalyst free approach for sol-gel synthesis of highly mixed zr2-sio2 oxides, *J. Non-Cryst. Solids* 243 no. 1999, 26–38.

[26] B. T. Stone and K. L. Bray, Fluorescence properties of er3+ doped sol-gel glasses, *J. Non-Cryst. Solids* 197 (1996) 136–144.

[27] R. M. Almeida, Spectroscopy and strucutre of sol-gel systems, *J. Sol-gel Science and Tech.* 13 (1998) 51–59.

[28] P. Coudray, J. Chisham, M. P. Andrews, and S. I. Najafi, Ultraviolet light imprinted sol-gel silica glass low-loss waveguide for use at 1.55 μ m, *Optical Engineering* 36 (1997), no. 4, 1234–1240.

[29] M. A. Fardad, T. Touam, P. Coudray, R. Sara, X. M. Du, M. P. Andrews, and S. I. Najafi, Uv-light imprintined bragg grating in sol-gel ridge glass waveguide with almost 100(1997), no. 12, 1069–1070.

[30] A. Elshabini-Riad and F. D. B. III, *Thin film technology handbook.* McGraw-Hill, (1997).

[31] J. H. Harris, R. Shubert, and J. N. Polky, Beam coupling to films, *J. Opt. Soc. Amer.* 60 (1970), no. 8, 1007.

[32] P. K. Tien and R. Ulrich, Theory of prism-film coupler and thin-film light guides, *J. Opt. Soc. Amer.* 60 (1970), no. 10, 1325.

[33] R. Ulrich, Thoery of the prism-film coupler by plane wave analysis, *J. Opt. Soc. Amer.* 60 (1970), no. 10, 1337.

[34] H. Nishihara, M. Haruna, and T. Suhara, *Optical integrated circuits.* McGraw-Hill Optical and Electro-optical Engineering Series, (1987).

[35] B. E. A. Saleh and M. C. Teich, *Fundamental of optics.* John wiley and sons, wiley series in pure and applied optics ed.

[36] H. Takahashi and H. Toba, tranmission characteristics of arrayed waveguide nxn wavelength multiplexer, *J. Lightwave Tech.* 13 (1995), no. 3, 447-454.

[37] C. Dragon, Efficient nxn start couplers using fourier optics, *J. Lightwave Tech.* 7 (1989), no. 3, 479-488.

[38] L. L. Hench and J. K. West *Chem. Rev* 90 (1990) 33-72.

[39] D. R. Ulrich *Non-Cryst. Solids* 121 (1990) 465-479.

[40] N. Itomo, N. Shimizu, H. Mori, and M. Ikeda *J. Lightwave Technology* LT-1 (1983) 289-293.

[41] J. T. Boyd, R. W. Wu, D. E. Zelmon, A. Naumaan, H. A. Timlin, and H. E. Jackson *Opt. Eng.* 24 (1985) 230-234.

[42] G. Grand, J. P. Jadot, H. Denis, S. Valette, A. Fournier, and A. M. Grouillet *Electron. Lett.* 26 (1990) 2135-2137.

[43] M. Kawachi, M. Yasu, and T. Edahiro *Electronic Lett.* 19 (1983) 583-584.

[44] R. M. Almeida, X. Orignac, and D. Barbier *J. Sol-gel, Technol.* 2 (1994) 465.

[45] Y. Slek, R. Reisfeld, I. Finkelstein, and S. Ruschin *Appl. Phys. Letters* 63 (1993) 3256.

[46] R. R. A. Syms and A. S. Holmes *J. Non-Cryst. Solids* 170 (1994) 223–233.

[47] Z. Zhang and H. C. Zeng *J. Non-Cryst. Solids* 243 (1999) 26–38.

[48] B. T. Stone and K. L. Bray *J. Non-Cryst solids* 197 (1996) 136–144.

[49] D. P. Partlow and T. W. O'Keef *Appl. Opt.* 29 (19990) 1526.

[50] A. S. Holmes, R. R. A. Syms, M. Li, and M. Green *Appl. Opt.* 32 (1993) 4916.

[51] S. Alavian, T. Touam, and I. Najafi, Analysis of integrated photonics devices by a new simplified propagation method, *J. Opt.* 21 (2000), no. 2, 60–65.

[52] M. D. Feit and J. A. F. Jr., Mode properties and dispersion for two optical fiber-index profiles by the propagating beam method, *Applied Optics* 25 (1979), no. 8, 514–516.

[53] J. B. D. T. B. Koch and D. Wickramasinghe, Finite element/finite difference propagation algorithm for integrated optical devices, *Electronics Letters* 25 (1989), no. 8, 514–516.

[54] D. Zwillinger, *Standard mathematical tables and formulae.* CRC press Inc., (1996).

[55] M. P. Andrews and S. I. Najafi, *Sol-gel and polymer photonics*, vol. CR68. SPIE, (1997).

[56] T. Touam, G. Milova, Z. Saddiki, M. A. Fardad, M. Andrews, J. Chrostowski, and S. I. Najafi, Organoaluminophosphate sol-gel silica glass thin films for integrated optics, *Thin solid film* 307 (1997) 203–207.

[57] a. D. X. M. Du andT. Touam, J. L. Guilbaut, M. P. Andrews, and S. I. Najafi, Sol-gel waveguide fabrication parameters: an experimental investigation, *Optical Engineering* 27 (1998) 1101–1104.